2012

Cultural Sites as Platforms for Environmental Characterization of Marine Landscapes

Michael Lee Brennan
University of Rhode Island, mlbrennan@mail.uri.edu

CULTURAL SITES AS PLATFORMS FOR ENVIRONMENTAL CHARACTERIZATION OF MARINE LANDSCAPES

BY

MICHAEL LEE BRENNAN

A DISSERTATION SUBMITTED IN PARTIAL FULFILLMENT OF

THE REQUIREMENTS FOR THE DEGREE OF

DOCTOR OF PHILOSOPHY

IN

OCEANOGRAPHY

UNIVERSITY OF RHODE ISLAND
2012

DOCTOR OF PHILOSOPHY DISSERTATION

OF

MICHAEL LEE BRENNAN

APPROVED:

Dissertation Committee:

Major Professor Robert D. Ballard

Katherine Kelley

Ilya V. Buynevich

Nasser H. Zawia

DEAN OF THE GRADUATE SCHOOL

UNIVERSITY OF RHODE ISLAND
2012

ABSTRACT

Our ability to understand and interpret archaeological data collected from the excavation of an archaeological site is constrained by our capacity to investigate it. This is often limited by our understanding of the surrounding environment and the modern landscape. This dissertation is composed of three separate studies, each of which examines the environmental and oceanographic contexts of archaeological sites using geophysical and geochemical analyses. The focus of these case studies is to initiate the process of determining the oceanographic and geological histories of the modern sites. Viewing sites from their abandonment to the present day provides an understanding of the ways these sites have changed and come into equilibrium with the surrounding environment over time. By establishing such environmental parameters for each of these regions, this research provides a framework from which future overall site interpretations can be based. Two of these studies focus on the documentation and characterization of shipwreck sites, while the Belize chapter examines the geochemical composition of marine limestone formations at a Maya site.

This dissertation addresses the following research:

1. The issue of damage to shipwreck sites caused by the operation of mobile fishing gear has only recently begun to be addressed by the archaeological community. However, the nature, extent, and intensity of this damage has yet to be quantified. Acoustic and video surveys conducted between 2008 and 2010 located and imaged sixteen ancient shipwrecks around the Bodrum and Datça Peninsulas, Turkey, many of which were heavily damaged by trawling activity. The results of this research illustrate the unfortunate reality that many wreck sites in the Aegean Sea are heavily damaged by

modern fishing activities. Quantifying the extent and intensity of trawl scars on the seabed further reveals the geographic spread of damage in these areas. The results of these mapping projects call attention to the dismantling of cultural sites by the use of mobile fishing gear on the seabed. By comparing the number of broken artifacts on these wreck sites to other sites that have escaped the effects of trawling, such as those in the Black Sea, we demonstrate that shipwrecks that are or were at one time in areas of trawling activity show a considerable amount of damage. The location and condition of these wreck sites helps map and quantify past and recent trawling activity, and pinpoint areas on the shallow coastal shelf where additional trawling restrictions or protected zones may be able to help the preservation of archaeological material.

2. A continuation of exploration of the coastal area of the southern Black Sea off Sinop and Ereğli, Turkey in 2011 documented additional areas at the transition zone along the oxic/anoxic interface. Push cores collected with an ROV from sediments underlying the oxic, suboxic, and anoxic waters were analyzed for geochemistry, meiofauna, and microbiology to help characterize this transition zone. During the course of side-scan sonar surveys, nine shipwrecks were located at various states of preservation, all within 100-115 m depth and ranging from the 4th century BC to the early 20th century. Many of these wrecks have wooden components well preserved due to the influences of the anoxic waters being washed up along the shelf by internal waves. However, many of these sites have also been heavily damaged by bottom trawling along the seabed up to the shelf break, highlighting the drastic threat such activities present to archaeological sites.

3. The carbonate bedrock of northwestern Belize is poorly understood both geochemically and from the standpoint of the use of stone as the building blocks of ancient Maya sites and monuments. This research analyzed 67 limestone samples collected from sites in the Three Rivers Region of Belize with ICP-MS and ICP-AES to characterize the major, minor, and trace element chemistry of the bedrock of the region. Bedrock, quarry, and possible monuments were sampled for this study for the purposes of tracing the movement of monument stone to either the local bedrock or quarries, or to determine if it was imported from outside of the sites' core. At Chawak But'o'ob along the flank of the Rio Bravo, changes downslope in Mg concentration suggest a leaching of the bedrock by meteoric waters based on differences in porosity. However, at Maax Na, a hilltop site, such leaching is not as apparent. Many monuments were found to be composed of stone with the same trace element chemistry as the bedrock, although this does not preclude them from being monuments. A few monuments were shown to be composed of material with a different chemical composition than the local bedrock, which included some of the stelae at Maax Na, and appear to have been made of stone imported from outside the site.

ACKNOWLEDGMENTS

First and foremost, I want to thank Robert Ballard for recruiting me into his program at URI and giving me one of the best opportunities in the world, his steadfast support and trust in me over the past eight years. From snowball fights in Yellowstone to sharing a glass of wine on *Nautilus*, it has truly been an adventure.

Sincere thanks also to my committee - Katie Kelley, Ilya Buynevich, Dennis Piechota, Jim Delgado, Steve Carey, and Nasser Zawia - for giving me the support and freedom to craft this research. Also to my non-committee professors Art Trembanis, Jamie Austin, Steve D'Hondt, and Larry Mayer for their help and support.

To quote Jonathan Kent in Superman: Earth One, "When we say 'I won't take this anymore', that's when we know who we are and what we'll tolerate. Until we're tested, we don't know those things. And that's when people will show up and take your side, when you decide what it is you stand for, when standing is the hardest." I feel truly honored that when I encountered a situation where I faced the unbelievable choice of starting over or leaving GSO, Bob, my committee, the Deans of URI, and the entire GSO community stepped up to the plate for me.

Thanks to Mom, Dad, Kyle, Kelly, Matthew, Jeannie; my grandparents, Mimi and PP, and the rest of my family for their constant support. My colleagues at COE/IFE Katy, Sandra, Dwight, Laurie, Chris, Brennan, Ian, Bob, Alex, Derek, Janice. To Dan G, and to all of my friends in RI: Matt, Chris, Brooke, Jason, Emily, Charlie, Alex, Adam, Josh, Brian, Heather, Marion, David, Julie. Thanks also to everyone at GSO and URI: Meredith, David, April, Amy, Kathy, Jane, Dr. Procopio, Roberta, Joyce.

To all my coauthors and colleagues at sea: Dan, Alexis, Roderick, Sarah, Nicole, Orkan, Jamie, Gabrielle, Ian, Eric, Matt, Gregg, Mary, Brian, Steph, Adam, Art, Meko, Maureen, Bridget, Muhammet, Derya, Rhonda, Kat, Webb, Catalina, Captains and crew of *E/V Nautilus*. Andrei Opait for helping with amphora IDs. And to Tufan Turanli and his constant support, encouragement, and help in all matters.

I am also grateful to Eleanor King and Leslie Shaw for continuing to drag me into the jungle in Belize, and also Chrissy, Darcie, Claire, Fred, Iasha, Dana, Stan and Robyn.

The processing of sediment core samples collected by the author aboard *E/V Nautilus* in the Black Sea for meiofauna and microbiology was done by Derya Urkmez at Sinop University and Gulsen Altug at Istanbul University. Image processing from ROV surveys of shipwreck sites and the production of microbathymetry and photomosaic maps was done by Chris Roman, Gabrielle Inglis, and Ian Vaughn.

DEDICATION

To Mom and Dad

From a field trip to Woods Hole in 1991 to today

For unwavering support, belief, and encouragement

And for going above and beyond to teach and guide me down this road

PREFACE

In accordance with the URI Graduate School's guidelines for thesis formatting, this dissertation follows manuscript format, presenting three papers written for publication in journals. The manuscripts in this dissertation are unified by the common methodology of viewing an archaeological site as a feature of the modern landscape, whether this be a shipwreck or a population center, and using oceanographic and geochemical methods to characterize the modern environment before interpreting the history of the site. In essence, I am looking at the history of each archaeological site from the time of its abandonment to the present day to provide a framework about each site's formation process before the interpretation of the cultural aspects of the sites are undertaken. Chapter 1 on trawl damage to shipwreck sites in the Aegean Sea has been accepted for publication at *Continental Shelf Research*. Chapter 2 on the effects of the suboxic zone and trawling on shipwrecks in the southern Black Sea is in preparation for submission also to *Continental Shelf Research*. The last chapter on sourcing limestone monuments to bedrock and quarry samples at a Maya site in northwestern Belize is in preparation for submission to the *Journal of Archaeological Science*.

TABLE OF CONTENTS

LIST OF TABLES

LIST OF FIGURES

CHAPTER 1

Evaluation of the modern submarine landscape off southwestern Turkey through the documentation of ancient shipwreck sites

Accepted for publication in *Continental Shelf Research*, April 2012

Michael L. Brennan[a], Robert D. Ballard[a], Chris Roman[a,c], Katherine L. Croff Bell[a], Bridget Buxton[b], Dwight F. Coleman[a], Gabrielle Inglis[c], Orkan Köyağasıoğlu[d], Tufan Turanlı[e]

[a]Graduate School of Oceanography, University of Rhode Island, Narragansett, RI 02882, USA
[b]Department of History, University of Rhode Island, Kingston, RI 02881, USA
[c]Department of Ocean Engineering, University of Rhode Island, Narragansett, RI 02882, USA
[d]Institute of Nautical Archaeology, Bodrum, Turkey
[e]BOSAV Foundation, Bodrum, Turkey

Corresponding Author:
Michael L. Brennan
Graduate School of Oceanography
University of Rhode Island
South Ferry Road, Box 200
Narragansett, RI 02882
mlbrennan@gso.uri.edu
(401) 874-6186 office
(860) 777-6181 cell

1.1 Abstract

The issue of damage to shipwreck sites caused by the operation of mobile fishing gear has only recently begun to be addressed by the archaeological community. However, the nature, extent, and intensity of this damage has yet to be quantified. Acoustic and video surveys conducted between 2008 and 2010 located and imaged sixteen ancient shipwrecks around the Bodrum and Datça Peninsulas, Turkey, many of which were heavily damaged by trawling activity. The results of this research illustrate the unfortunate reality that many wreck sites in the Aegean Sea are heavily damaged by modern fishing activities. Quantifying the extent and intensity of trawl scars on the seabed further reveals the geographic spread of damage in these areas. The results of these mapping projects call attention to the dismantling of cultural sites by the use of mobile fishing gear on the seabed. By comparing the number of broken artifacts on these wreck sites to other sites that have escaped the effects of trawling, such as those in the Black Sea, we see that shipwrecks that are or were at one time in areas of trawling activity show a considerable amount of damage. The location and condition of these wreck sites helps map and quantify past and recent trawling activity, and pinpoint areas on the shallow coastal shelf where additional trawling restrictions or protected zones may be able to help the preservation of archaeological material.

1.2 Introduction

The observation of damage to shipwrecks caused by mobile fishing gear, especially ancient sites in the Mediterranean region, has recently begun to draw the attention of the archaeological community (e.g., Atkinson, 2010; Brennan, 2010; Foley, 2008; Royal, 2008, 2009; Sakellariou et al., 2007). A clear understanding of the dismantling of wreck sites by bottom trawls is important in order to document and interpret these shipwrecks effectively, as well as the submarine landscape of which they are a part. The Aegean Sea is not an unaltered ancient landscape because the seafloor rarely lies below depths that trawling vessels can reach (Jones, 1992). Therefore, in order to understand and interpret archaeological materials that remain on the seabed, it is essential to develop an understanding of the extent and intensity of trawling activities in these areas. This paper discusses the recent acoustic and visual documentation of wreck sites in waters below diving depth (50-600 m) off the southwestern coast of Turkey as well as the surrounding seabed in order to quantify the damage to the shipwrecks. These data will be used in plans for future acoustic surveys as we work toward a more comprehensive view of the region. We also assess the potential for locations that could benefit from the establishment of additional marine protected areas and the restriction of bottom trawling activities.

This research was conducted off the Bodrum and Datça Peninsulas in southwestern Turkey (Figure 1.1). These two points straddle a transitional area between the central and southern Aegean Sea (Poulos, 2009; Stanley and Perissoratis, 1977). The coastal region between Bodrum and the island of Samos to the north is characterized as a shelf <100 m deep (Aksu et al., 1987; Poulos, 2009), whereas the Gulf of Gökova south

of Bodrum lies within a graben formed along the E-W trending normal Datça Fault and drops off to depths >700 m (Kurt et al., 1999). The shelf north of Bodrum is influenced by the input of terrigenous material from the Büyük Menderes River delta (Aksu et al., 1987; Ergin et al., 2007). Sediments in the basins, such as Gökova, consist almost entirely of muds (Aksu et al., 1995; Ergin and Yemenicioglu, 1997). The general circulation in this region is governed by the north-moving part of the counter-clockwise current pattern of Aegean surface waters (Pickard and Emery, 1990). These currents are primarily composed of warm and saline waters from the eastern Mediterranean: the Levantine Surface Waters in the upper 50-100 m, and the Levantine Intermediate Waters to depths of 250-300 m in the south Aegean (Malanotte-Rizzoli et al., 1999; Poulos, 2009; Poulos et al., 1997; Robinson et al., 2001; Theocharis et al., 1993, 1999; Wust, 1961). Mesoscale circulation is driven by the interaction of the Asia Minor Current with the coast that causes anticyclonic eddies to develop, moving Levantine waters into the southeast Aegean through the Rhodes Strait toward the Datça Peninsula (Malanotte-Rizzoli et al., 1999; Theocharis et al., 1993, 1999). The surface waters in this region are strongly influenced in the summer by the northerly Etesian winds, causing a southward movement and upwelling along the eastern coast (Hopkins, 1978; Metaxas, 1973).

These oceanographic properties and geological characteristics of the Aegean Sea heavily influenced seafaring in ancient times. Promontories along the west coast of Asia Minor, such as the Datça Peninsula, are primarily oriented E-W. Such physical geography creates areas of shelter from the Etesian winds but also increases the dangers of sailing around such headlands, where winds are stronger (Morton, 2001; Murray, 1987). The ancient site of Knidos on the western end of the Datça Peninsula was one such area where

ships often had to take refuge before continuing north against both winds and currents around the headland (Newton and Pullan, 1863). Sites along the Anatolian coast of the Aegean, such as Halikarnassos (modern Bodrum), which is nestled within a bay along the southern coast of the Bodrum Peninsula, were positioned as havens from the northerly winds for sailing ships. As such, Halikarnassos was one of the primary coastal cities along the route between Knidos and Miletos (Bean and Cook, 1955). Other natural harbors along the Bodrum Peninsula, such as Yalıkavak on the northwest coast, were inferior for shelter as a result of their exposure to the winds (Bean and Cook, 1955). Ancient shipwrecks have been commonly found in this region, which sank due to the hazards of winds, currents, and shallow reefs around the promontories of Asia Minor, such as those found off Yassı Ada (Bass and Van Doorninck, 1982). A survey of the coastal regions around the Bodrum and Datça Peninsulas by the Institute of Nautical Archaeology (INA) in 1973 found 17 ancient wrecks in depths ranging from 5-46 m (Gifford, 1974). However, little of the submarine landscape in this area has been explored below recreational diving depth (~50 m). Whereas the majority of located shipwreck sites are in shallow waters near the shore, ancient mariners did not necessarily hug the coast as, especially during periods of strong winds, doing so increased the dangers of navigating rocky coastlines (Davis, 2009; Morton, 2001). Therefore, documenting the landscape >50 m deep is important to developing a broader understanding of ancient maritime activity. While wrecks in these deeper waters are out of reach of recreational divers and looters, they are in more open waters and therefore susceptible to dredges, trawls, and other types of mobile fishing gear.

Advances in mobile fishing technology have allowed fishermen to work at greater depths and expand the areas within reach of their gear. The operation of modern trawling gear has a direct effect on the seabed environment to depths reaching 1000 m (Jones, 1992). The use of trawls on muddy or sandy seabeds results in the smoothing of bedforms, compression and resuspension of sediments, and the displacement of buried objects (Durrieu de Madron et al., 2005; NRC, 2002). Figure 1.2 shows a trawl scar on a muddy bottom in the Aegean Sea. Additionally, trawl doors can plough furrows in the seabed as deep as 15 cm, which causes advection, resuspension, and oxygenation of surface sediments (Friedlander et al., 1999). Side-scan sonar imaging of seabed regions have been able to observe that trawl scars often run parallel to isobaths, showing that such imaging is an effective method for evaluating the extent of recent trawling activity and the disturbance of the seabed (Smith et al., 2003). Numerous studies have been conducted on the effects of trawling on the benthic biology and sediment morphology, and have documented the damaging effects of these activities (e.g., Collie et al., 2000; Friedlander et al., 1999; Lampadariou et al., 2005; Pusceddu et al., 2005). These results suggest that the recovery time for the seabed of regions in deeper water is on the order of decades, due to lower sedimentation rates compared to shallower environments (Jones, 1992).

Turkish fisheries have been minimally studied, and little data exist about their operations. However, it is estimated that industrial trawlers and purse seiners have drastically overexploited fish stocks both in the Black and Aegean Seas, including species such as red mullet and hake (Pitcher, 2006; Ünal, 2004). Less than 10% of Turkey's fish catch is from the Aegean, with the majority coming from the Black Sea, where large

trawling vessels started working before moving into the Aegean region in the 1940s (Ünal, 2004). Bottom trawling has been specifically regulated in the coastal waters of southwestern Turkey, which prohibits the activity within 2.5 km of shore, although some illegal trawling occurs (Lok et al., 2002). The Fisheries Law of 1971 and its subsequent amendments enacted more specific prohibitions for the coastal waters of Turkey. In addition to the 2.5 km limit off the coast along the Aegean Sea, bottom trawling is prohibited within 100 m to either side of submarine cables, and at depths >1000 m (KKGM, 2006; Figure 1.1). However, compliance with such regulations is limited because of a lack of enforcement, which has caused an encroachment over time into coastal shelf areas where bottom trawling is banned (Pitcher, 2006).

The effects of the fishing industry on submerged cultural material is only beginning to be documented. Over the past few decades, many shipwrecks have been discovered through the actions of trawlers, which have raised statues, ceramics, and cannons in their nets (e.g., Beltrame and Gaddi, 2002; Sakellariou et al., 2007). The 1988 ancient shipwreck survey around Skerki Bank in the Mediterranean Sea documented extensive trawl marks throughout the region, although no recent trawl scars were apparent around the discovered wrecks themselves (Ballard et al., 2000; Foley, 2008). Some of the wrecks, however, showed some evidence of being scattered or damaged, possibly by past trawling activity (Oleson and Adams, 1997). More recent archaeological research has noted damage from mobile fishing gear on shipwrecks in both the Mediterranean and Aegean Seas (Royal, 2008; Sakellariou et al., 2007). Recent surveys in the Adriatic Sea have discovered a number of ancient wrecks that consist of disarticulated mounds with fragments of amphora scattered by drag nets (Royal, 2009).

With the exception of wrecks discovered by trawlers, most of the observations of trawling damage on ancient wrecks to date consist of broken or scattered ceramic cargos (e.g., Royal, 2008; 2009). Currently, such evidence of trawl damage to shipwreck sites is being used by commercial salvage companies to justify the removal of artifacts from the seabed (see Atkinson, 2010; Greene et al., 2011: 115 n. 25). Our work illustrates a different approach to responding to this threat in an effort to evaluate the extent of the damage to archaeological sites. We found a number of shipwrecks in the Aegean Sea that have remained well-preserved due to their proximity to areas where bottom-trawling is prohibited, which allow us to suggest appropriate marine policy changes that can do much to further protect these sites *in situ*.

The objective of this research is to develop an understanding of the effects of trawling on the seabed in the waters around the Bodrum and Datça Peninsulas in southwestern Turkey through the development and refining of our acoustic and visual imaging surveys (Figure 1.1). The mapped areas of scarred seabed indicate the extent and intensity of recent trawling activity in these areas, which is also represented by the location and conditions of ancient shipwreck sites. During the course of these imaging surveys, 16 ancient shipwrecks were located, exhibiting varied states of disarticulation by bottom trawling. Quantification of the damage to these wreck sites and incorporation of these data into the mapped landscape broadens our understanding of the destructive effects of mobile fishing on the seabed. Our secondary objective is to establish a baseline for documenting shipwreck sites that are threatened by trawling. Quantifying the effects of trawls on both the seabed and on ancient wreck sites is essential to being able to locate and interpret these sites as components of both the ancient and modern submarine

landscapes. In this study we show that severe damage to many of these ancient wrecks highlights the need for comprehensive surveys of these areas before the wrecks are damaged to the point that such sites can no longer be found.

1.3 Methods

1.3.1 Yalıkavak

In October 2008, acoustic survey operations were conducted in the immediate area off Yalıkavak, Turkey (Figure 1.1) with a small dive vessel, *Atlantis Ege*. An EdgeTech 4200-MP dual frequency side-scan sonar, *Diana*, and a small ROV, *Hylas*, were used to locate and identify targets. The sonar towfish was systematically towed along tracklines running approximately SW-NE along the western and northwestern coast of the Bodrum Peninsula (Brennan, 2009; Figure 1.1). *Diana*, a dual-frequency (300/600 kHz) high-resolution side-scan sonar system, was towed at 10-20 m altitude and covered a swath of seabed 300 m wide. The survey strategy focused on waters > 50 m and covered a range of depths down to 85 m in areas around which shallow-water wreck sites have been found. Two of the wrecks imaged in 2008, named Yalıkavak I and II, were discovered by INA in 1967 and 1990, respectively, in the vicinity of Yalıkavak harbor (Parker, 1992). Off the island of Yassı Ada to the south, two Byzantine wrecks were also excavated by INA in the 1960s (Bass and van Doorninck, 1971; 1982). Our efforts focused on the area between Yalıkavak and Yassı Ada in order to document this submarine landscape.

1.3.2 Knidos

In September 2009 and July 2010, we conducted video and side-scan sonar imaging surveys in select areas around the Datça Peninsula, in order to document the extent of trawling activities and pinpoint regions of the submarine landscape unaffected by fishing operations. First, we towed the camera sled *Argus* along a survey line in the deeper waters of the Gulf of Gökova to look for trawl marks and determine if they were limited to a certain depth (Figure 1.1). This acoustic and video survey in the deeper waters northwest and south of the Datça Peninsula was exploratory, in contrast to the near-complete coverage of the region off Yalıkavak. Operations began near the boundary between Turkish and Greek territorial waters, then moved inward from deep (~600 m) to shallower waters. Surveys were also conducted along the 200 m contour south of Datça, an area of rocky slumps near the coast, as well as along the submarine cable route between Knidos and Kos (Figure 1.1). These surveys were conducted from the Exploration Vessel *Nautilus*, using *Diana* for shallower waters and *Echo*, a lower resolution dual-frequency (100/400 kHz) side-scan sonar, for waters > 400 m, together covering depths ranging from 150-600 m. Both sonar systems were towed at an altitude of 30 m with a swath width of 300 m, which was optimal for imaging the low profiles of ancient shipwrecks and associated debris.

1.3.3 Remotely operated vehicle systems

The *Hercules* and *Argus* remotely operated vehicle (ROV) systems were developed by the Institute for Exploration in the early 2000s (Coleman et al., 2003; Newman et al., 2008). Having an operating depth of 4000 m, *Argus* was designed as an

imaging vehicle and can be used alone or as part of a dual-body vehicle system with *Hercules*. *Argus* is equipped with multiple video cameras, including one high-definition camera used to oversee *Hercules* and image the seafloor. *Argus* illuminates the seafloor with two 1200 Watt lights. Sensors include a magnetic compass, altimeter, and depth sensor. Thrusters mounted on either end of the vehicle control heading while *Argus* is being towed or overlooking *Hercules*.

Hercules has more maneuverability and is used for precise operations, such as high-resolution mapping of the seafloor. Its imaging and mapping tools include a high-definition camera, several standard-definition cameras, a 12-bit stereo camera system, a 2250 kHz multibeam sonar, and a 532 nm sheet laser structured light system. For navigation, *Hercules* is equipped with an Octans fiberoptic gyrocompass, a TrackLink ultrashort baseline navigation system, an RDI Workhorse doppler velocity log, a Benthos PSA-916 altitude sensor, and a Paroscientific depth sensor. Other sensors include an Aanderaa optode for dissolved oxygen and a Falmouth Scientific CTD for conductivity, temperature, and depth measurements. *Hercules* is also equipped with a 675 kHz Simrad 1071 scanning sonar, which is used to help locate targets found during side-scan sonar operations.

1.3.4 Imaging

We used several different survey tools to map and characterize the wreck sites, including a stereo camera system, high frequency multibeam sonar, and laser structured light system. The overall goal of the mapping surveys was to document the wreck sites and evaluate the relative merits of these systems. The baseline site maps were made by

assembling the multiple downward-looking images into a single photomosaic (Pizarro and Singh, 2003) and producing three-dimensional (3D) stereo reconstructions (Figure 1.3; Johnson-Roberson et al., 2010). The large photomosaics convey the overall texture and layout of the wreck sites, but often contain distortions related to projecting the 3D sites onto a single two-dimensional plane. As such, photomosaics generally cannot be used for precise scale-accurate measurements. The fully 3D stereo vision techniques however produce composite terrain and texture images with true scaling properties. These surveys require collecting simultaneous stereo image pairs with two cameras mounted to a fixed and calibrated rig.

Several of the sites mapped during the expedition are in shallow water (50-80 m) and require low, 3 m constant altitude surveys to obtain clear images. The deeper wrecks (200-600 m) are located where the bottom waters have better visibility, allowing us to collect images from a higher altitude, up to 5 m. The higher imaging altitude reduces the distortions due to 3D effects and makes the mosaics easier to construct. The vehicle surveys to produce these products were done in an auto-piloted closed loop control manner. This ensures that the images are collected with generally more than 30% overlap along a trackline and between adjacent tracklines (Figure 1.4). This level of overlap aids the detection of common image features between images and increases the quality of the reconstructions. The use of 12-bit 1360x1024 cameras allows for high-resolution imaging and sufficient dynamic range. A color correction step was applied to all the images, which flattens out the consistent but uneven illumination pattern created by the ROV's strobe lighting, prior to building the composite image. Stereo processing was also performed using individual image pairs and a technique that can additionally incorporate the

multibeam bathymetry when generating the triangulated stereo points. This method uses the acoustic range information to help guide the search for common features between the paired images, which is often difficult in images with low-contrast features (Figure 1.5; Inglis and Roman, 2009).

High frequency multibeam data were also used to create true scale 3D representations of the wreck sites (Figure 1.4). The bathymetry data were processed using a Simultaneous Localization and Mapping (SLAM) refinement technique that combats the potential artifacts related to navigation errors and drift (Roman and Singh, 2007). This technique automatically registers small overlapping sections of the bathymetry and makes adjustments to the map within a navigation filtering framework. The algorithms use the vehicle velocity, depth and attitude measurements from the ROV's Doppler Velocity Log (DVL), depth sensor and fiber optic gyro, respectively. Relative vehicle positioning information was obtained using an Ultra Short Baseline (USBL) system, calibrated to a GPS location. The high frequency multibeam sonar had a maximum range of 10 m and was able to obtain resolutions down to centimeter scale.

Three-dimensional maps were also produced with fine scale definition with a structured light laser sheet (Figure 1.6). This imaging technique derives the 3D profile of the seafloor, analogous to a single multibeam sonar ping, by identifying the visible line produced by an inclined laser sheet where it hits the bottom. The method requires viewing the visible laser line with a calibrated camera and knowledge of the laser sheet's orientation relative to the camera (Roman et al., 2010). Our system uses a 532 nm 100 milliwatt laser inclined approximately 11° relative to the camera axis. During our surveys we obtained greater than sub-centimeter range resolution from imaging altitudes up to 3

m. The resulting data sets were gridded with a 2.5 millimeter grid size to produce the 3D maps. The laser system worked equally well at wrecks in the deeper clearer water and in the shallower, more turbid water.

1.3.5 Acoustic data

Side-scan sonar data were collected over the course of three expeditions between 2008 and 2010. Sonar and navigation data were processed and filtered with CARIS HIPS and SIPS software. The data were then viewed in 300x300 m blocks; trawl scars were counted by area in order to develop a trawl intensity map for both regions (Figures 1.7b and 1.8b; after DeAlteris et al., 1999). QTC Swathview software (Quester Tangent Corp., Sidney, BC, Canada) was used to process the side-scan data sets and classify the mapped seabed regions based on acoustic properties, such as seabed reflectivity and backscatter intensity (Michaels, 2007; Preston 2008). This software creates rectangular patches of the side-scan data images and uses 132 acoustic features for principal component analysis clustering for classification (Michaels, 2007; Preston et al., 2004). The generated classes can be linked to differences in sediment grain size, roughness, and seabed morphology (e.g., Shumchenia and King, 2010). Data collected with the *Diana* towfish were processed as two sets, one for the Knidos region, and one for the area off Yalıkavak; data collected with *Echo* could not be used for classification. Rectangles with estimated dimensions of 5 x 60 m were generated for both data sets. Fifteen acoustic classes were identified for the Yalıkavak area, and 23 for the Knidos area. However, many of these classes covered only small fragments of the mapped regions and were incorporated into larger classes during the interpolation process with QTC CLAMS (Classification

Mapping Suite, Quester Tangent Corp.). This software produced maps of both the acoustic classes (Figures 1.7c and 1.8c) and feature complexity of the side-scan data (Figures 1.7d and 1.8d). Feature complexity is a measure of variance over the area of each rectangle with white indicating a higher level of complexity (QTC, 2010). However, due to the nature of our imaging permit, these acoustic classes could not be ground-truthed.

1.3.6 Artifacts

Dating of the shipwrecks was based on the predominant ceramic artifact type on each wreck, although in some instances, the wreck sites contained multiple artifact types. Diagnostic features of these artifacts were photographed *in situ* at each wreck site (see Table 1). Dimensions of each site were measured based on the photomosaics and bathymetry generated by *Hercules'* mapped data. The photomosaics were also used to count the number of artifacts on the surface of each site (Table 2). These counts are not an estimate of the total cargo, as they do not take into account buried artifacts or objects that may have been dragged off-site. In addition, the numbers of visible broken and unbroken artifacts were counted to determine the relative percentage of broken artifacts for each shipwreck site (Table 2). Artifacts counted as broken were those where the body of the vessel was in visible pieces, rather than just cracked or chipped. These data were plotted against distance from shore for each wreck. To serve as a comparison to the Aegean wrecks, we also conducted artifact counts using photomosaics of wrecks from the Black and Mediterranean Seas that do not appear to have been damaged by trawling.

1.4 Results

1.4.1 Ancient shipwreck sites

A total of 16 shipwrecks were located in waters below ~50 m, six off Yalıkavak, and ten off Knidos (Table 1). In addition to the previously known Yalıkavak I and II late Hellenistic shipwrecks (Figure 1.9h), four other ancient wrecks were discovered in 2008 in the vicinity of this harbor. Yalıkavak III consists of a scatter of Roman terracotta plumbing pipes spread over an area of 20 m^2 at 80 m depth, accompanied by fragments of Byzantine amphoras (Figure 1.7a). Büyükkiremit I, a heavily damaged amphora wreck south of the harbor at 70 m depth, consists of a scatter of large amorphous concretions and at least three different types of amphora. Çavuş Adası II and III were discovered in 2008 to the north and south of that island (Figure 1.7a). Both of these wrecks consist of piles of rounded rocks that are extensive enough to suggest that they formed part of the cargo of these vessels and did not serve merely as ballast. A scatter of broken amphora sherds and a flat-bottomed jar were observed among the rocks, but there was little information to yield dates and origins of these ships. Both Yalıkavak I and Büyükkiremit I exhibit extensive damage to their ceramic cargo. At these depths of <100 m, the observed damage may be the result of a combination of small-scale trawling and the effects of heavy wave action from storms that could have impacted the sites.

Nine ancient shipwrecks and one possible 16th century wreck were discovered between 2009 and 2010, all within a 20 km radius around the ancient site of Knidos, a promontory already known for numerous shallow-water wrecks (Parker, 1992). Three amphora wrecks were located to the north of Knidos, between the Datça Peninsula and Kos (Figure 1.8a). Knidos A (Figure 1.9a) and F (Figure 1.9d) are large Byzantine

shipwrecks, each about 140 m^2 area, and dating to the 6th and 11th centuries AD, respectively (Table 1). Knidos B is a smaller wreck, with an area of 76 m^2, dating to the Greek Archaic period (Figure 1.9b). This wreck has a lower relief on the seabed than the Byzantine wrecks because it has been more heavily buried by sediment, given its age, which is approximately a thousand years older than Knidos A. Seven wrecks were found southeast of Knidos, of which four are amphora wrecks (Figure 1.8a). Knidos G is a somewhat scattered pile of amphoras, while Knidos H is a more consolidated pile of amphoras with a higher relief (Figure 1.9e). Knidos C, a Byzantine amphora wreck (Figure 1.3), and Knidos J (Figure 1.9f), a Roman-era wreck, both exhibit the most direct evidence of trawl damage, with a clear trawl scar running through each site. In the case of Knidos J, this damage exposed portions of the heavily-sedimented wreck, including preserved wooden planking.

The other three wrecks located southeast of Knidos have little observed cargo. Knidos D and I are primarily stone ballast piles with scattered artifacts. These wrecks are much smaller than the amphora wrecks, covering areas of 20 and 30 m^2, respectively. Knidos E is a premodern wreck dated to the 16th century AD based on the form of its cannon and anchors (Figure 1.9c). This wreck is also the only wreck off Knidos that lies within 2.5 km of shore, within which bottom trawling is prohibited. The pronged anchors on this wreck, which would catch any trawl nets that pass overhead, remain near the wreck with no evidence of fishing gear caught up on them. Nevertheless, these three wreck sites cannot be used to discuss damage from trawling because there are few visible artifacts that exhibit damage. Additionally, the smaller nature of these sites make it impossible to determine if more cargo was part of the sites that has since either

decomposed or been dragged away. Therefore, like Yalıkavak III and the two wrecks off Çavuş Adası, we did not use these wrecks for the purpose of quantifying trawl damage.

1.4.2 Seabed classification

The *Argus* video survey in the western Gulf of Gökova observed trawl scars at depths ranging from 200 m to > 400 m (Figure 1.1). The only scars observed during *Hercules* dives were around the Knidos C and J wreck sites, which are also the only wrecks where trawl scars are visible running through the sites themselves (Figure 1.3 and 1.9f). Further acoustic surveys in the region between Knidos and Kos during 2009 and 2010 documented only occasional trawl marks in addition to the visual survey, which was conducted just to the east of the sonar surveys (Figure 1.8b). The side-scan sonar did, however, indicate a landscape of steep slopes, ridges, and rocky slumps, especially in proximity to the Datça Peninsula. The only trawl marks in this area were close to the basin east of Kos where the visual survey was conducted and where bottom topography is relatively flat. The acoustic surveys south of the Datça Peninsula also documented areas of slumps and rocky seabed along the 200 m contour near the coast, but smoother bathymetry in the deeper waters to the south. More extensive trawl scarring was observed in the side-scan data in this area south of Knidos in water depths between 300-500 m, with the marks generally following the bathymetric contours. The heaviest scarring in this region was observed along the easternmost survey line between 150 and 200 m depth, parallel to the submarine cable (Figure 1.8b). Another area of heavy trawl scarring was documented north of Yalıkavak harbor during the 2008 survey (Figure 1.7b).

Figures 1.7 and 1.8 show the results of the side-scan sonar and image processing, including trawl scar intensity, percentages of broken artifacts, and the Swathview seabed classification for the Yalıkavak and Knidos regions, respectively. The pie charts indicating percentages of broken artifacts for each amphora wreck (from data in Table 2) illustrate the relationship between artifact damage and trawl intensity, including areas where bottom trawling is prohibited, i.e. within 2.5 km of shore and along the submarine cables (Figures 1.7b, 1.8b). All six of the Yalıkavak wrecks are located within 2.5 km of shore. A large majority of the seabed surveyed outside this zone has been heavily trawled (Figure 1.7b). The cessation of heavy scarring was apparent each time the sonar towfish crossed the 2.5 km boundary. By contrast, the area south of Datça exhibits the heaviest intensity of trawl scars along the submarine cables, all running parallel to the cable to avoid catching it with trawl doors. The area along the easternmost survey line shows the most trawl scars, which end at the 200 m depth contour. Other scars in this area follow the cable along the southernmost survey lines and also along the 300 m isobath. Of the shipwrecks south of Knidos, the two most heavily damaged, Knidos C and J (Figures 1.3and 1.9f), lie in areas where trawl scars were observed with side-scan sonar (Figure 1.8b). The better-preserved amphora wrecks Knidos H and G (Figures 1.9d and 1.9e) are closer to the 2.5 km zone near the coast where no trawl scars were observed on the seabed. South of Knidos, trawl intensity appears to increase with distance from shore, a phenomenon that is also reflected by the damage to the shipwreck sites. Figure 1.10 shows the percentage of broken artifacts plotted in relation to distance from the coast. The four amphora wrecks south of Knidos (C, G, H, J) are plotted separately to indicate the correlation for the group of sites in this localized area.

The acoustic classes identified with Swathview are illustrated in Figures 1.7c and 1.8c. The data from the Yalıkavak and Knidos surveys were processed separately, and they represent different sedimentary environments, so the identified acoustic classes exhibit no correlation with each other. The Yalıkavak survey, which was small but more comprehensive in coverage, shows a distinct change in acoustic class west of the Bodrum Peninsula, away from the coast, represented by class YI in Figure 1.7c by a light blue color. The Knidos data do not show as distinct a change; further acoustic survey will obtain more complete coverage of this area. There is, however, a noticeable change in acoustic class with depth off Knidos, represented by classes K4 and K5 between the 300 and 400 m contours (Figure 1.8c). While these acoustic classes have not yet been ground-truthed, they indicate possible changes in the seabed. Class YI off Yalıkavak correlates with depths ranging between 70 and 90 m. The northern- and southern-most reaches of the survey moved into shallower waters, between 50 and 60 m depth. Shallower areas off Yalıkavak and those closer to shore and islands comprise different acoustic classes. Class YI likely represents a finer-grained sediment in a lower-energy environment characteristic of the deeper waters of the area(Aksu et al., 1998; Duman et al., 2004, Ergin et al., 2007).

The large size of the rectangles (~5 x 60 m) selected for processing with Swathview allowed enough area of seabed to be included so that trawl scarring could be detected with the software. The feature complexity plots made with CLAMS indicate (as shades of gray, Figure 1.8d) the variability of the seabed for each rectangle, darker shades representing flatter, more featureless seafloor (QTC, 2010). An area of higher seabed complexity is visible north of Yalıkavak harbor (Figure 1.7d), which corresponds with the area of greatest trawl intensity (Figure 1.7b). The scarring of the seabed in this area by

bottom trawls has increased the variability of the seabed, thereby increasing its feature complexity. Changes in surficial sediment characteristics and increased roughness caused by intensive trawling has been previously observed and acoustically classified by Humborstad et al. (2004) in the Barents Sea. The intensity of the trawl scars north of Yalıkavak is great enough that Swathview also identified this area as a separate acoustic class (class Y2, Figure 1.7c). The majority of the higher feature complexity in the Yalıkavak survey is due to trawl intensity. This is not the case, however, for the Knidos region. The survey line along the 200 m contour south of Knidos contains areas of high complexity, presumably as a result of the distal parts of rocky slumps observed along the coastline (Figure 1.8d). One area of high complexity that correlates with trawl intensity is that just inshore of the 200 m contour along the easternmost survey line. The heavy trawl scarring is illustrated in Figure 1.8b. This area of the heaviest trawl intensity south of Knidos is also characterized as an acoustic class separate from the rest of that survey line, although it is not as distinct as the Yalıkavak acoustic class designations due to the greater variability of the seafloor south of Knidos and larger area of coverage.

1.5 Discussion

Results of three years of imaging surveys in the southeast Aegean Sea have identified areas of the seabed where archaeological material may be better preserved and areas where the existence of such sites are threatened or where they may already be eradicated. This study draws attention to the fact that trawling operations have continued in some areas after restrictions have been put in place, and adds both acoustic and video image evidence of this activity. Damage to both the seabed and shipwreck sites as a result

of trawling activity could be used by policy-makers and enforcement officials. These data from our surveys show that ancient shipwreck sites can be used as indicators of past trawling activity. However, before damage to wreck sites can be quantified, an understanding of the effect of trawling on the seabed is needed. Changes in fishing grounds and areas where bottom trawling is prohibited, areas of illegal trawling, and variability in sedimentation rates are among some of the challenges associated with evaluating the intensity and extent of trawling over time. This study presents the evidence of trawling on the seabed and uses wreck sites as indicators of potential areas of past trawling.

1.5.1 Age of trawl scars on the seabed

A major component in understanding the submarine landscape of the Aegean Sea includes quantifying the extent of trawling effects. However, damage from mobile fishing gear on the seabed is difficult to both quantify and date. Side-scan sonar is an effective tool for documenting recent scarring, such as that observed north of Yalıkavak, where past damage is less pronounced as the scars are slowly filled in over time (e.g. Smith et al., 2007). However, trawling operations in this area have been expanding into deeper waters for more than a century (Sakellariou et al., 2007). In addition to the ephemeral nature of trawl marks over long periods of time, the effect and scale of the fishing gear damage depends greatly on environmental conditions, such as sedimentation rate, seabed lithology, and the intensity of biological activity (Caddy, 1973). In the Aegean Sea, sedimentation rates vary greatly from > 1 m/kyr in areas near mouths of rivers to regions with sedimentation as low as a few cm/kyr in deep basins such as the Sea of Crete (e.g.,

Aksu et al., 1995; Poulos, 2009). Substrate lithology and bed flow intensityalso affect how long trawl scars will remain visible on the seabed; muddy bottoms in low-energy environments will permit scars to remain intact longer (DeAlteris et al., 1999; Jones, 1992; NRC, 2002).

There are important questions related to quantifying trawl scars - how old are visible scars on the seabed, and for areas clear of trawl marks, how long ago could the area have been trawled for the evidence to have since been erased? Estimates of recent trawling by analysis of side-scan sonar data are problematic due to variability in sonar data resolution, bioturbation, smoothing of past trawl scars by more recent activity, and burial by sedimentation (Smith et al., 2003; Friedlander et al., 1999). An experimental study of the effect of trawling on the seabed in the Bay of Fundy, Canada, a high-energy environment, showed that trawl scars lasted between 2 and 7 months (Brylinsky et al., 1994). In deeper waters and low-energy environments, trawl marks will be deeper, up to 15 cm, and will persist longer due to lower sedimentation rates, potentially in the range of 50-75 years (Caddy, 1973; DeAlteris et al., 1999; Friedlander et al., 1999). A surface sample taken between Knidos and Kos has shown that the sediment composition was 98% silt and clay, indicative of a low-energy deposition environment (Ergin and Yemenicioglu, 1997). Additionally, cores taken between Kos and the Datça Peninsula indicate an average Holocene-modern sedimentation rate of 10 cm/kyr (Aksu et al., 1995; Piper and Perissoratis, 2003). In this area, trawl doors will make furrows deeper than in coarser-grained or harder sediments and the furrows will remain visible longer in the low-energy environment. Given these data from the region off Knidos, we estimate that trawl scars could remain visible on the seabed for decades.

1.5.2 Assessment of trawl damage to ancient shipwreck sites

Trawl damage to ancient shipwreck sites differs from that on the seabed. On muddy bottoms, trawl doors leave long troughs in the range of 10-15 cm deep. Spoil heaps and small piles of mud lie adjacent to the furrows (NRC, 2002; Smith et al., 2003). On amphora wrecks, this damage translates to broken artifacts. There are other processes that can disturb ceramic cargos, such as the violence of the wrecking event itself, but this can be quantified thanks to the high-resolution imaging capabilities of our ROV systems, as discussed above. Four additional ancient wrecks from the Mediterranean and Black Seas that have been similarly documented and photomosaicked were used as a comparison for the Aegean wreck sites. For all of these shipwrecks, the artifact counts generated a percentage of broken artifacts per wreck site (Table 2). These values are not estimates of the total artifact count, but include only those exposed at the surface of the sites. Büyükkiremit I is the only amphora wreck not included, as we could not survey it due to poor visibility. Additionally, this does not account for any artifacts that may have been dragged off-site by trawl nets and have since been buried.

The percentages of broken artifacts, represented as pie charts over the wrecks' locations in Figures 1.7b and 1.8b, illustrate the degree of damage for the amphora wrecks located off southwest Turkey. Of the six wrecks located off Yalıkavak, only Yalıkavak I and II have been photomosaicked. Less than 1% of the cargo of Yalıkavak II is broken, protected as it is by its location in the harbor where it is sheltered from both trawling and storm events. Yalıkavak I exhibits more damage (see Table 2), possibly from small-scale trawling, as it lies on the edge of the 2.5 km from shore restricted zone, or

from storm events. Our assessment of trawl damage is more precise for wrecks below 100 m depth and away from the effects of large storms. The Knidos wrecks exhibit damage ranging between 5-10% for wrecks F, G, and H to between 25-40% for wrecks A, C, and J (Table 2). Knidos C and J are in areas where trawl scars have been observed, indicating the nature of the damage. Knidos G and H are located just outside the 2.5 km restricted zone (Figure 1.8b); the light damage to these sites and lack of recent trawl marks in the side-scan data suggest that there is little trawling in the area, as opposed to further south near the Knidos J and C wrecks. We found an additional amphora wreck, Marmaris B, in 2010 during a survey south of Marmaris, Turkey (Figure 1.9g; Brennan et al., 2011b); while this wreck lies outside the regional scope of this paper, a photomosaic of the site shows that 62.5% of its artifacts have been broken and scattered. Its damage is the heaviest among the ancient wrecks documented in this larger region.

In order to characterize the extent of damage exhibited by the wrecks located off Knidos, we analyzed photomosaics of four other amphora wrecks that have escaped the reach of trawlers to serve as a proxy for damage associated with bottom trawling. Chersonesos A, a Byzantine wreck located off the Crimean coast of Ukraine, is protected by its location in an area where trawling and dredging are prohibited due to the proximity of an explosives dumping ground. This wreck also lies within the suboxic water layer (Ballard et al., 2008; Brennan et al., 2011a). Skerki D, an amphora wreck found in 1997 at 850 m depth on Skerki Bank between Sicily, Sardinia, and Tunisia, lies in an area where trawl scars have been observed, but not on the wreck sites on the Bank (Ballard, 2008; Ballard et al., 2000). Finally, Tanit and Elissa are two Iron Age Phoenician wrecks found in 1999 off the coast of Ashkelon, Israel near a series of cold hydrocarbon seeps at

400 m depth (Ballard et al., 2002; Coleman and Ballard, 2001). Bottom trawling was not regulated in the area of these wrecks until the establishment of a fisheries restricted area around the cold hydrocarbon seeps east of the Nile Delta in 2006 (FAO, 2006). However, other factors have contributed to the preservation of these Iron Age wrecks, including the collapse of fish stocks in the 1970's caused by the effects of the Aswan High Dam on the Nile discharge, and changes in Egyptian and Israeli fishing grounds due to security constraints (Aleem, 1972; Halim et al., 1995). The Ashkelon wrecks' location in the waters between Egypt and Israel, the effects of the Nile's reduced discharge, and their depth have aided in their preservation, illustrating the benefit of fishing prohibitions to the preservation of shipwreck sites.

These wrecks help illustrate the damage from trawling on shipwrecks from a range of depths in areas of seafloor out of reach of the effects of both storms and trawlers. The wreck sites discussed above from outside the Aegean Sea exhibit a breakage rate of < 5% (Table 2), which we interpret to be the damage associated with their original sinking events. All of these wrecks have escaped the reach of trawlers for various reasons and show that the heavier damage exhibited by the Aegean wrecks is greater than that caused by the ship-wrecking process. Some of the wrecks exhibiting heavy damage (> 20% broken artifacts), such as Knidos A and C, lie near a submarine cable. Recent trawl scars were documented with sonar on the eastern edge of the acoustic survey around the Datça Peninsula where trawlers have operated parallel to the cable. This appears also to be the case for Knidos C and J, although to a lesser degree, and explains why these two sites are more heavily damaged than Knidos G and H. Knidos A and B lie in an area of steeper topography and rocky slumps, so trawling along isobaths is more difficult. Knidos A,

however, which is closer to the cable than Knidos B and F, is the most heavily damaged of these three wrecks; it may have suffered from the effects of trawlers operating parallel to the cable in the past, and the scars have since been erased. Knidos B shows light damage, but it appears to have been less recent, like Knidos A, evident here by the burial of the site and biota overgrowth on the wreck (Figure 1.9b). The quantification of damage to these wreck sites helps evaluate the extent of trawling damage on the shipwrecks in the Aegean and allows a better understanding of the damage to a ship's ceramic cargo that should be expected from the shipwreck event itself and its subsequent deposition and residence on the seabed.

1.5.3 Evaluation of the modern submarine landscape

Ancient shipwrecks have been affected by trawling activity since the development of mobile fishing gear, and fluctuating fish stocks and the implementation of regulations have changed the locations of trawlers' operations over time (Berkes, 1986). Because only the most recent trawl scars are visible, it is difficult to document the total extent of past damage to the seabed. Shipwrecks that have been damaged to different degrees, such as the set of wrecks off Knidos, can be used as indicators of past trawling activity because damage to shipwrecks is permanent while scars on the seabed are erased over time. The only wrecks that have visible trawl scars in the area are Knidos C and J (Figures 1.3 and 1.9f). Although many of these wrecks exhibit damage typical of trawling gear, despite legislation that has been passed to regulate the operation of trawling vessels along the Aegean coast, illegal fishing activity, such as we observed along the cable south of Knidos, continues to damage these sites. In fact, based on the observed damage to these

sites and the intensity and extent of trawling documented in the region, it appears that the most damaged sites are those closest to the submarine cables. Observations of the long-term effects of trawling on shipwreck sites - damage that is still visible after the trawling furrows have disappeared - provide a potential measure of human impacts on the submarine landscape.

Imaging surveys of landscapes off southwestern Turkey from 2008-2010 have illustrated the intensity and extent of bottom trawling operations in these areas. Trawl scars have been observed with side-scan sonar on the seabed primarily running parallel to isobaths or along submarine cables, and trawling along the latter is illegal. In contrast, a stronger adherence to regulations in areas where bottom trawling is prohibited has been observed with proximity to the 2.5 km distance from the coast, as illustrated by the absence of trawl scars within this zone off Yalıkavak (Figure 1.7b). While the survey south of Knidos focused on areas further offshore, a similar trend is apparent there. We show a correlation between the damage to the four shipwreck sites south of Knidos and distance from shore (Figure 1.10). This illustrates that the 2.5 km zone here is generally observed by trawlers and that the majority of trawling in these areas increases with distance from the restricted zone. This is visible both in the increasing damage to shipwrecks south of Knidos, as well as in the increased extent of trawl scars to the south (Figure 1.8b); this correlation is confirmed by the heavily damaged Knidos C and J wreck sites farthest from shore. However, while these wrecks exhibit the heaviest damage of all wrecks observed, they lie in areas of medium trawl intensity. Areas of more intense trawling, such as those documented north of Yalıkavak and east of Knidos, may be where

wrecks either are no longer preserved or have been damaged beyond the point at which they can be detected with sonar.

The geographic extent of observed trawl scars also indicates certain patterns to modern trawling operations. Figure 1.11 shows histograms of the occurrence of trawl scar numbers by area (1.11a) and by depth (1.11b). The three areas where trawl scars have been observed - northwest of Yalıkavak, south of Knidos, and southeast of Knidos - represent different modes of operation for trawling vessels. The first set of data (Figure 1.11b) represents the depths <100 m off Yalıkavak. The second shows depths of 100-200 m southeast of Knidos (see Figures 1.7b and 1.8b). The third set representing greater depths, 300-450 m, is the area south of Knidos. The greatest intensity of trawl scars is in the first two sets. The majority of Turkish trawling vessels working in the coastal waters of the Aegean are 15-24 m in length (Ünal, 2004). Vessels up to 50 m in length in US waters are known to trawl the bottom down to 400 m depth (NRC, 2002). Those smaller vessels operating off Turkey are therefore more likely to operate in shallower waters. The heavy trawl intensity observed east of Knidos ends abruptly at the 200 m contour (Figure 1.8b), suggesting that that is the maximum depth for fishing vessels that trawl off Yalıkavak and Knidos. Deeper waters, 300-500 m, where trawl scars were observed south of Knidos are worked by larger, industrial trawling vessels, indicating two modes of trawl operations in this area.

The region surveyed between Datça and Kos is the only area where little evidence of trawling was observed. We documented ridges, slumps, and steep bathymetry in this area, each of which makes trawling more difficult than operating along isobaths. Most of the scars in this region were only observed during the video survey in the basin of the

Gulf of Gökova. However, both Knidos A and B (Figures 1.9a and 1.9b) exhibit damage interpreted to be from trawling. Knidos B lies at a depth of 595 m, which is the deepest wreck found during these surveys. Larger trawling vessels that work along the Aegean coast of Turkey have the capability to work down to depths of 700 m, but the demand and expense of working at those depths limits that ability so they tend to work in depths <500 m (pers. comm., Mehmet Turguttekin). The damage to these sites may have been caused by past trawling operations, the scars from which have since been erased, but such operations in this area have been abandoned due to the depth and complex bathymetry that make them difficult. Additionally, of the three wrecks found in this area, Knidos A lies closest to the submarine cable, but it is the most heavily damaged (Figure 1.8b). As Knidos C and J illustrate, trawlers often work illegally along submarine cables, and this may have been the cause of the damage to Knidos A.

This set of amphora wrecks off southwestern Turkey, based on their location on the seabed, establishes a baseline for the damage that may be be expected from trawling on such sites. Figure 1.10 shows the correlation between increasing damage to shipwreck sites with distance from the coast, resulting from governmental restrictions on bottom trawling there, which we have demonstrated are generally observed. The plot also includes Yalıkavak II as a control for a close-to-shore and undamaged wreck, and Marmaris B as the most heavily damage shipwreck found in relatively flat terrain and in deep water (Brennan et al., 2011b). The wreck sites in this model represent those in areas where trawling is frequent, due to flat bathymetry and depths within reasonable reach of Turkish trawl gear. Wreck sites that plot to the right of this line that were not included in the model, such as the three wrecks between Knidos and Kos (Knidos A, B, and F),

indicate areas where trawling has been less intense, due to steep slopes and deeper waters, thereby preserving these sites more than would be expected considering their distance from shore. Sites that plot to the left of the line, such as Yalıkavak I, exhibit damage greater than is expected given their proximity to shore. This indicates either some amount of illegal trawling close to shore or damage caused by the effects of storms. The left of the line is where shallow-water wrecks in reach of storms, divers, and wave action would be expected to plot. This plot illustrates the benefit of trawling prohibitions in coastal zones. Enforcement of such regulations can only improve the preservation of these shipwrecks, and those yet to be discovered off the coast of Turkey.

1.6 Conclusions

The establishment of remote methods for documenting and quantifying the conditions of both ancient shipwreck sites and the surrounding seabed off-shore southwestern Turkey illustrates the need for continued imaging surveys in this important region of ancient commerce. We must not only understand the transformative impact of human activity on the modern submarine landscape in order to interpret the remnants of the ancient one, but also to assess the ongoing potential threats to these cultural resources. Continued monitoring of previously discovered shipwrecks can also help document the frequency and intensity of damage to these sites. In subsequent years, we will return to these sites and conduct additional photomosaic surveys to evaluate recent damage to them since their discovery. The results of these imaging surveys suggest that, while shipwrecks in the Aegean Sea have been and continue to be threatened by modern fishing operations, the creation of protected areas and regions where bottom trawling is

prohibited increases the chances that cultural sites will be preserved to the point that they can be found and properly documented. The adherence of local trawlers to the prohibition against trawling in the 2.5 km coastal zone shows that increased enforcement of such boundaries could greatly increase the preservation of these cultural sites. Some marine protected areas already exist in the area. For example, the Datça-Bozburun Specially Protected Area (e.g., Almac, 2005; Okuş et al., 2007) could be expanded to include areas with high concentrations of threatened shipwreck sites are now known to exist, such as the area south of Knidos. Previous research has shown that such protected areas around submerged cultural sites in the Mediterranean have been effective, particularly in Italian and Spanish waters (e.g., Davidde, 2002; Negueruela, 2000). The non-invasive imaging technologies used in this research illustrate a standard for a baseline level of remote investigation that can be accomplished quickly and effectively in order to characterize and document ancient wrecks in the deeper waters of the Aegean Sea, and elsewhere in the Mediterranean Sea. It is essential to continue to conduct rapid comprehensive surveys of such threatened areas before these sites are damaged further, potentially beyond the point at which they can be detected.

References

Aksu, A.E., Yaşar, D., Mudie, P.J., 1995. Origin of late glacial-Holocene hemipelagic sediments in the Aegean Sea: clay mineralogy and carbonate cementation. *Marine Geology* 123, 33–59.

Aksu, A.E., Yaşar, D., Uslu, O., 1998. Assessment of marine pollution in Gulf of İzmir: heavy metal and organic compound concentrations in surficial sediments. *TUBITAK Translations and Journal of Engineering and Environmental Science* 22, 387-415.

Aksu, A.E., Piper, D.J.W., Konuk, T., 1987. Quaternary growth patterns of Büyük Menderes and Kucuk Menderes deltas, western Turkey. *Sedimentary Geology* 52, 227-250.

Aleem, A.A., 1972. Effect of river outflow management on marine life. *Marine Biology* 15, 200-208.

Almaç, Ö., 2005. Problems caused by coastal law and decision making mechanism in small coastal settlements: case study Mugla-Bozburun. Unpublished Masters thesis. Middle East Technical University.

Atkinson, C., 2010. From the bottom up: further discussion of bottom trawling. *INA Quarterly* 37(1), 10-11.

Ballard, R.D., 2008. Searching for ancient shipwrecks in the deep sea, in: Ballard, R.D., (ed.), Archaeological Oceanography. Princeton University Press, Princeton, pp. 131-147.

Ballard, R., Buxton, B., Brennan, M., Coleman, D., Croff, K., Davis, D., Piechota, D., Voronov, S., 2008. Byzantium beneath the Black Sea. Poster presented at the 2008 Meeting of the Archaeological Institute of America, Chicago.

Ballard, R.D., McCann, A.M., Yoerger, D., Whitcomb, L., Mindell, D., Oleson, J., Singh, H., Foley, B., Adams, J., Piechota, D., Giangrande, C., 2000. The discovery of ancient history in the deep sea using advanced deep submergence technology. *Deep-Sea Research I* 47, 1591-1620.

Ballard, R.D., Stager, L.E., Master, D., Yoerger, D., Mindell, D., Whitcomb, L., Singh, H., Piechota, D., 2002. Iron Age shipwrecks in deep water off Ashkelon, Israel. *Journal of American Archaeology* 106, 151-168.

Bass, G. and van Doorninck Jr., F.H., 1971. A fourth-century shipwreck at Yassı Ada. *Journal of American Archaeology* 75, 27-37.

Bass, G.F. and van Doorninck Jr., F.H., 1982. Yassı Ada Volume I: A seventh-century Byzantine shipwreck. Texas A&M University Press, College Station.

Bean, G.E. and Cook, J.M., 1955. The Halicarnassus Peninsula. *The Annual of the British School at Athens* 50, 85-171.

Beltrame, C. and Gaddi, D., 2002. Report on the first research campaign on the Napoleonic brick, Mercure, wrecked off Lignano, Udine, Italy in 1812. *International Journal of Nautical Archaeology* 31, 60-73.

Berkes, F., 1986. Local-level management and the commons problem: A comparative study of Turkish fisheries. *Marine Policy* 10, 215-229.

Brennan, M.L., 2009. Ancient shipwreck survey and the modern submarine landscape off Yalıkavak, Turkey. *Marine Technology Society Journal* 43, 47-49.

Brennan, M.L., 2010. The disarticulation of ancient shipwreck sites by mobile fishing gear: A case study from the southeast Aegean Sea. *INA Quarterly* 36(4), 6-7.

Brennan, M.L., Ballard, R.D., Croff Bell, K.L., and Piechota, D., 2011a. Archaeological oceanography and environmental characterization of shipwrecks in the Black Sea, in Buynevich, I., Yanko-Hombach, V., Gilbert, A., and Martin, R.E., eds., Geology and Geoarchaeology of the Black Sea Region: Beyond the Flood Hypothesis. Geological Society of America Special Paper 473, pp. 179-188, doi: 10.1130/2011.2473(11).

Brennan, M.L., Turanli, T., Buxton, B., Bell, K.L.C., Roman, C.N., Kofahl, M., Koyagasioglu, O., Whitesell, D., Chamberlain, T., Sullivan, R., Ballard, R., 2011b. Landscape imaging of the southeast Aegean Sea, in: Bell, K.L.C. and Fuller, S.A., eds. New Frontiers in Ocean Exploration: The *E/V Nautilus* 2010 Field Season. *Oceanography* 24(1), supplement, p. 18-19.

Brylinsky, M., Gibson, J., Gordon, D.C., 1994. Impacts of flounder trawls on the intertidal habitat and community of the Minas Basin, Bay of Fundy. *Canadian Journal of Fisheries and Aquatic Sciences* 51, 650-661.

Caddy, J.F., 1973. Underwater observations on tracks of dredges and trawls and some effects of dredging on scallop ground. *Journal of the Fisheries Research Board of Canada* 30(2), 173-180.

Coleman, D.F. and Ballard, R.D., 2001. A highly concentrated region of cold hydrocarbon seeps in the southeastern Mediterranean Sea. *Geo-Marine Letters* 21, 162-167.

Coleman, D.F., Ballard, R.D., Gregory, T., 2003. Marine archaeological exploration of the Black Sea. *OCEANS 2003 MTS/IEEE Conference Proceedings* 2, 1287-1295.

Collie, J.S., Escanerol G.A., Valentine, P.C., 2000. Photographic evaluation of the impacts of bottom fishing on benthic epifauna. *ICES Journal of Marine Science* 57: 987-1001.

Davidde, B., 2002. Underwater archaeological parks: a new perspective and a challenge for conservation - the Italian panorama. *International Journal of Underwater Archaeology* 31, 83-88.

Davis, D.L., 2009. Commercial Navigation in the Greek and Roman World. Unpublished Ph.D. diss. University of Texas at Austin.

DeAlteris, J., Skrobe, L., Lipsky, C., 1999. The significance of seabed disturbance by mobile fishing gear relative to natural processes: A case study in Narragansett Bay, Rhode Island. *American Fisheries Society Symposium* 22, 224-237.

Duman, M., Avcı, M., Duman, Ş., Demirkurt, E., Düzbastılar, M.K., 2004. Surficial sediment distribution and net sediment transport pattern in İzmir Bay, western Turkey. *Continental Shelf Research* 24, 965-981.

Durrieu de Madron, X., Ferre, B., Le Corre, G., Grenz, C., Conan, P., Pujo-Pay, M., Buscail, R., Bodoit, O., 2005. Trawling-induced resuspension and dispersal of muddy sediments and dissolved elements in the Gulf of Lion (NW Mediterranean). *Continental Shelf Research* 25, 2387-2409.

Ergin, M. and Yemenicioglu, S., 1997. Geologic assessment of environmental impact in bottom sediments of the eastern Aegean Sea. *International Journal of Environmental Studies* 51, 323-334.

Ergin, M., Kadir, S., Keskin, Ş., Turhan-Akyüz, N., Yaşar, D., 2007. Late Quaternary climate and sea-level changes recorded in sediment composition off the Büyük Menderes River delta (eastern Aegean Sea, Turkey). *Quaternary International* 167-168, 162-176.

FAO General Fisheries Commission for the Mediterranean, 2006. Report of the thirtieth session. Istanbul, Turkey, 24–27 January 2006. GFCM Report 30.

Foley, B., 2008. Archaeology in deep water: Impact of fishing on shipwrecks. Woods Hole Oceanographic Institution. <http://www.whoi.edu/sbl/liteSite.do?litesiteid=2740&articleId=4965>. Accessed December 2009.

Friedlander, A.M., Boehlert, G.W., Field, M.E., Mason, J.E., Gardner, J.V., Dartnell, P., 1999. Sidescan-sonar mapping of benthic trawl marks on the shelf and slope off Eureka, *California*. *Fishery Bulletin* 97, 786-801.

Gifford, J.A., 1974. A survey of shipwreck sites off the southwestern coast of Turkey. *Journal of Field Archaeology* 1, 23-25.

Greene, E.S., Leidwanger, J., Leventhal, R.M., Daniels, B.I., 2011. Mare nostrum? Ethics and archaeology in Mediterranean waters. *American Journal of Archaeology* 115, 311-319.

Halim, Y., Morcos, S.A., Rizkalla, S., El-Sayed, M.K., 1995. The impact of the Nile and the Suez Canal on the living marine resources of the Egyptian Mediterranean waters (1958-1986), in: FAO Marine Resource Services (ed.) Effects of riverine inputs on coastal ecosystems and fisheries resources. FAO Fisheries Technical Paper no. 349, FAO, Rome.

Hopkins, T. S., 1978. Physical processes in the Mediterranean basins, in: B. Kjerfve (ed.) Estuarine Transport Processes. University of South Carolina Press, pp. 269–310.

Humborstad, O.-B., Nottestad, L., Lokkeborg, S., Rapp, H.T., 2004. RoxAnn bottom classification system, sidescan sonar and video-sledge: spatial resolution and their use in assessing trawling impacts. *ICES Journal of Marine Science* 61, 53-63.

Inglis, G. and Roman, C., 2009. Terrain constrained stereo correspondence. Paper presented at the 2009 OCEANS conference, Biloxi, Mississippi.

Johnson-Roberson, M., Pizarro, O., Williams, S.B., Mahon, I.J., 2010. Generation and Visualization of Large-Scale Three-Dimensional Reconstructions from Underwater Robotic Surveys. *Journal of Field Robotics*, 27, p. 21-51.

Jones, J.B. 1992. Environmental impact of trawling on the seabed: a review. *New Zealand Journal of Marine and Freshwater Research* 26, 59-67.

Koruma ve Kontrol Genel Müdürlüğü (KKGM), 2006. Circular No. 37/1 of 2006-2008 Fishing Year Regulating Commercial Fishing in Seas and Inland Waters. Koruma ve Kontrol Genel Müdürlüğü, Ankara, Turkey. <http://www.kkgm.gov.tr/regulation/circular/37-1.html>. Accessed December 2009.

Kurt, H., Demirbag, E., Kuscu, I., 1999. Investigation of the submarine active tectonism in the Gulf of Gökova, southwest Anatolia - southeast Aegean Sea, by multi-channel seismic reflection data. *Tectonophysics* 305, 477-496.

Lampadariou, N., Hatziyanni, E., Tselepides, A., 2005. Meiofaunal community structure in Thermaikos Gulf: Response to intense trawling pressure. *Continental Shelf Research* 25, 2554-2569.

Lok, A., Metin, C., Ulas, A., Duzbastilar, F.O., Tokac, A., 2002. Artificial reefs in Turkey. *ICES Journal of Marine Science* 59, S192-S195.

Malanotte-Rizzoli, P., Manca, B.B., d'Alcala, M.R., Theocharis, A., Brenner, S., Budillon, G., Ozsoy, E., 1999. The Eastern Mediterranean in the 80s and in the 90s: the big transition in the intermediate and deep circulations. *Dynamics of Atmospheres and Oceans* 29, 365-395.

Metaxas, D.A., 1973. Air-sea interaction in the Greek seas and resulted Etesian wind characteristics. Univ. Ioannina Tech. Rep. 5.

Michaels, W.L., 2007. Review of acoustic seabed classification systems, in: Anderson, J.T., Holliday, D.V., Kloser, R., Reid, D., Simard, Y., (eds.) Acoustic seabed classification of marine physical and biological landscapes. ICES Cooperative Research Report, no. 286, 94-115.

Morton, J., 2001. The Role of the Physical Environment in Ancient Greek Seafaring. Brill Academic Publishers, Boston.

Murray, William M., 1987. Do modern winds equal ancient winds? *Mediterranean Historical Review* 2, 139-167.

National Research Council (NRC), 2002. Effects of Trawling & Dredging on Seafloor Habitat. National Academy Press, Washington, D.C.

Negueruela, I., 2000. Managing the maritime heritage: the National Maritime Archaeological Museum and National Centre for Underwater Research, Cartagena, Spain. *International Journal of Nautical Archaeology* 29, 179-198.

Newman, J.B., Gregory, T.S., Howland, J., 2008. The development of towed optical and acoustical vehicle systems and remotely operated vehicles in support of archaeological oceanography, in: Ballard, R.D., (ed.), Archaeological Oceanography. Princeton University Press, Princeton, pp. 15-29.

Newton, C.T. and Pullan, R.P., 1863. A history of discoveries at Halicarnassus, Cnidus, and Branchidae. Day and Son, London.

Okuş, E., Yüksek, A., Yılmaz, İ.N., Yılmaz, A.A., Karhan, S.Ü., Öz, M.İ., Demirel, N., Taş, S., Demir, V., Zeki, S., Koç, E.M., Tural, U., Yokeş, B., Kalkan, E., Deniz, N., Çaylarbaşı, Z., Savut, E., Murat, E., 2007. Marine biodiversity of Datça-Bozburun specially protected area (Southeastern Aegean Sea, Turkey). *Journal of the Black Sea / Mediterranean Environment* 13, 39-49.

Oleson, J.P. and Adams, J., 1997. Formation, survey, and sampling of the wreck sites, in: McCann, A.M. and Oleson, J.P. (eds.) Deep-Water Shipwrecks off Skerki Bank: The 1997 Survey. *Journal of Roman Archaeology* (Suppl.) Ser. 58.

Parker, A.J., 1992. Ancient shipwrecks of the Mediterranean and the Roman provinces. British Archaeological Reports International Series 580.

Pickard, G.L., and Emery, W.J., 1990. Descriptive Physical Oceanography. Pergamon, Oxford.

Piper, D.J.W. and Perissoratis, C., 2003. Quaternary neotectonics of the South Aegean arc. *Marine Geology* 198, 259-288.

Pitcher, T.J., 2006. An estimation of compliance of the fisheries of Turkey with Article 7 (Fisheries Management) of the UN Code of Conduct for responsible fishing. <ftp://aerl03.aerl.ubc.ca/CodeConduct/CountriesCodePDF/Turkey-CCRF.pdf>. Accessed Januray 2011.

Pizarro, O. and Singh, H., 2003. Toward large-area mosaicing for underwater scientific applications. *Journal of Oceanic Exploration* 28(4), 651-672.

Poulos, S.E., 2009. Origin and distribution of the terrigenous component of the unconsolidated surface sediment of the Aegean floor: A synthesis. *Continental Shelf Research* 29, 2045-2060.

Poulos, S.E., Drakopoulos, P.G., Collins, M.B., 1997. Seasonal variability in sea surface oceanographic conditions in the Aegean Sea (Eastern Mediterranean): an overview. *Journal of Marine Systems* 13, 225-244.

Preston, J., 2008. Automated acoustic seabed classification of multibeam images of Stanton Banks. *Applied Acoustics* 70, 1277-1287.

Preston, J.M., Christney, A.C., Collins, W.T., Bloomer, S., 2004. Automated acoustic classification of sidescan images. OCEANS 2004 MTS/IEEE Conference Proceedings 4, 2060-2065.

Pusceddu, A., Fiordelmondo, C., Polymenakou, P., Polychronaki, T., Tselepides, A., Danovaro, R., 2005. Effects of bottom trawling on the quantity and biochemical composition of organic matter in coastal marine sediments (Thermaikos Gulf, northwestern Aegean Sea). *Continental Shelf Research* 25, 2491-2505.

Quester Tangent Corp. (QTC), 2010. QTC CLAMS visualization and mapping tools user manual and reference. Sidney, B.C.

Robinson, A.R., Leslie, W.G., Theocharis, A., Lascaratos, A., 2001. Mediterranean Sea circulation. *Encyclopedia of Ocean Sciences*, Academic Press, pp. 1689-1706.

Roman, C., Inglis, G., Rutter, J., 2010. Application of structured light imaging for high resolution mapping of underwater archaeological sites. IEEE OCEANS, Sydney.

Roman, C. and Singh, H., 2007. A Self Consistent Bathymetric Mapping Algorithm. *Journal of Field Robotics* 24(1-2), 23-50.

Royal, J.G., 2008. Description and analysis of finds from the 2006 Turkish coastal survey: Marmaris and Bodrum. *International Journal of Nautical Archaeology* 37, 88-97.

Royal, J., 2009. Albanian coastal survey project: 2008 field season. *The INA Annual 2008*, 21-25.

Sakellariou, D., Georgiou, P., Mallios, A., Kapsimalis, V., Kourkoumelis, D., Micha, P., Theodoulou, T., Dellaporta, K., 2007. Searching for ancient shipwrecks in the Aegean Sea: The discovery of Chios and Kythnos Hellenistic wrecks with the use of marine geological-geophysical methods. *International Journal of Nautical Archaeology* 36, 365-381.

Shumchenia, E.J. and King, J.W., 2010. Comparison of methods for integrating biological and physical data for marine habitat mapping and classification. *Continental Shelf Research* 30, 1717-1729.

Smith, C. J., Banks, A. C., Papadopoulou, K.-N., 2007. Improving the quantitative estimation of trawling impacts from sidescan-sonar and underwater-video imagery. *ICES Journal of Marine Science* 64, 1692–1701.

Smith, C.J., Rumohr, H., Karakassis, I., Papadopoulou, K.-N., 2003. Analysing the impact of bottom trawls on sedimentary seabeds with sediment profile imagery. *Journal of Experimental Marine Biology and Ecology* 285-286, 479-496.

Stanley, D.J., and Perissoratis, C., 1977. Aegean ridge barrier-and-basin sedimentation patterns. *Marine Geology* 24, 97-107.

Theocharis, A., Georgopoulos, D., Lascaratos, A., Nittis, K., 1993. Water masses and circulation in the central region of the Eastern Mediterranean: Eastern Ionian, South Aegean and Northwest Levantine, 1986-1987. *Deep-Sea Research II* 40(6), 1121-1142.

Theocharis, A., Balopoulos, E., Kioroglou, S., Kontoyiannis, H., Iona, A., 1999. A synthesis of the circulation and hydrography of the South Aegean Sea and the Straits of the Cretan Arc (March 1994-January 1995). *Progress in Oceanography* 44, 469-509.

Ünal, V., 2004. Viability of trawl fishing fleet Foca (the Aegean Sea), Turkey and some advices to central management authority. *Turkish Journal of Fisheries and Aquatic Sciences* 4, 93-97.

Wust, G., 1961. On the vertical circulation of the Mediterranean Sea. *Journal of Geophysical Research* 66, 3261–3271.

Wreck Name	Depth (m)	Length (m)	Width (m)	Area (m2)	Height (m)	Surface Artifacts	Example artifacts	Dates
Yalıkavak I	82	26.6	12.5	333	1.45	544	Lamboglia II	1st c. BC
Yalıkavak II	50	19.4	8.1	157	1.4	365	Lamboglia II	1st c. BC
Yalıkavak III	81	19.1	10.2	195	0.31	586	terracotta water pipes	2nd c. AD
Büyükkiremit I	70	-	-	-	-	-	LR 5, LR 6	5-7 c. AD
Çavuş Adası II	86	-	-	-	-	-	stone cargo	Byzantine
Çavuş Adası III	78	-	-	-	-	-	stone cargo	Byzantine
Knidos A	460	16.8	8.6	145	0.73	708	LR 1	6-7 c. AD
Knidos B	595	12.9	5.9	76.1	0.43	298	Samian	late Archaic
Knidos C	435	19.4	8.4	163	1.14	557	LR 1	6-7 c. AD
Knidos D	497	6.8	3	20.4	-	7	Koan	2nd c. BC
Knidos E	268	20	6	120	-	12	stave-build iron cannon	16th c. AD
Knidos F*	370	12.7	10.7	136	0.52	506	Günsenin 1 (Ganos)	11th-12th c. AD
Knidos G	372	11.5	9.6	110	0.11	153	Knidian	4th c. BC
Knidos H*	372	16.5	9.7	160	1.7	459	Agora M 54/Nea Paphos 8	1-2nd c. AD
Knidos I**	370	6	5	30.0	0.34	38	Zemer 57	2-4 c. AD
Knidos J**	410	-	-	-	-	112	Rhodian	2nd c. AD

Table 1.1. List of shipwrecks located below recreational diving depth, 2008-2010, including primary artifact type and estimated date-range. Artifact dating was done by Bridget Buxton except where noted.
*Artifact identification and dating by Cemal Pulak, Texas A&M University, 2010.
**Artifact identification and dating by Meko Kofahl and Cemal Pulak, Texas A&M University, 2010.

Wreck Name	Location	Depth (m)	Broken	Unbroken	Total	% Broken
Yalikavak I	SE Aegean Sea	82	131	413	544	24.1
Yalikavak II	SE Aegean Sea	50	2	363	365	0.6
Knidos A	SE Aegean Sea	460	184	524	708	25.9
Knidos B	SE Aegean Sea	595	32	266	298	10.7
Knidos C	SE Aegean Sea	435	223	334	557	40.0
Knidos F	SE Aegean Sea	370	26	480	506	5.1
Knidos G	SE Aegean Sea	372	11	142	153	7.2
Knidos H	SE Aegean Sea	372	39	420	459	8.5
Knidos J	SE Aegean Sea	410	28	84	112	25.0
Chersonesos A	N Black Sea	135	2	64	66	3.0
Skerki D	SW Mediterranean	850	3	72	75	4.0
Elissa	SE Mediterranean	400	14	382	396	3.5
Tanit	SE Mediterranean	400	4	381	385	1.0
Marmaris B	NE Mediterranean	520	472	283	755	62.5

Table 1.2. Counts of artifacts visible at the surface of amphora shipwreck sites in the Aegean, Black, and Mediterranean Seas, including the percentages of broken artifacts for each wreck.

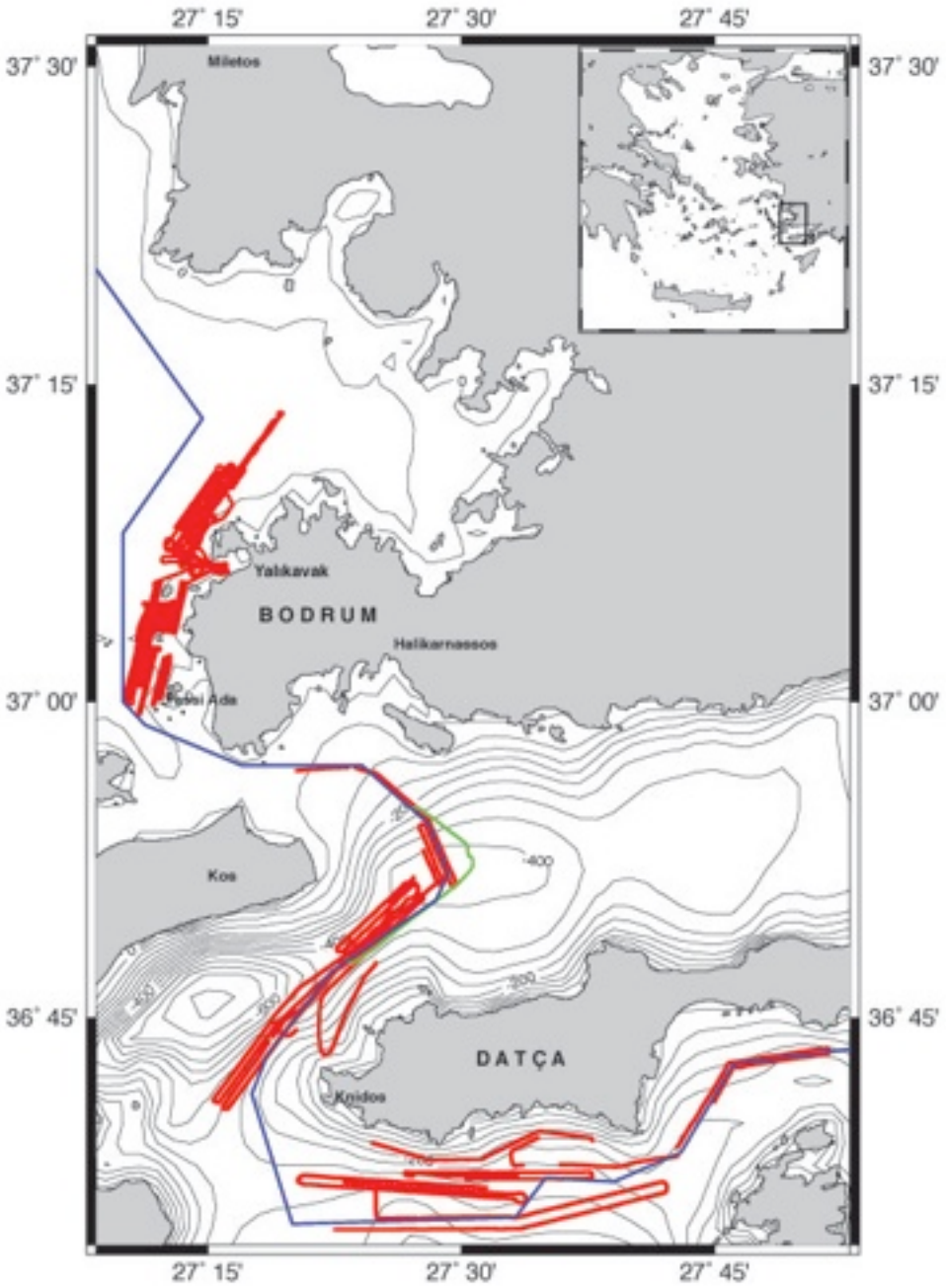

Figure 1.1. Map of Bodrum and Datça Peninsulas showing the 2008-2010 side-scan sonar survey coverage (red lines). The green line indicates a video transect with the camera sled *Argus*. The blue line indicates the location of a submarine cable. Bathymetry data (in m) from the GEBCO_08 Grid, version 20091120, http://www.gebco.net.

Figure 1.2. HD video capture of a trawl scar on the muddy bottom of the Aegean Sea.

Figure 1.3. Composite 3D texture maps of the Knidos C wreck site made with the stereo cameras. Red line indicates trawl scars.

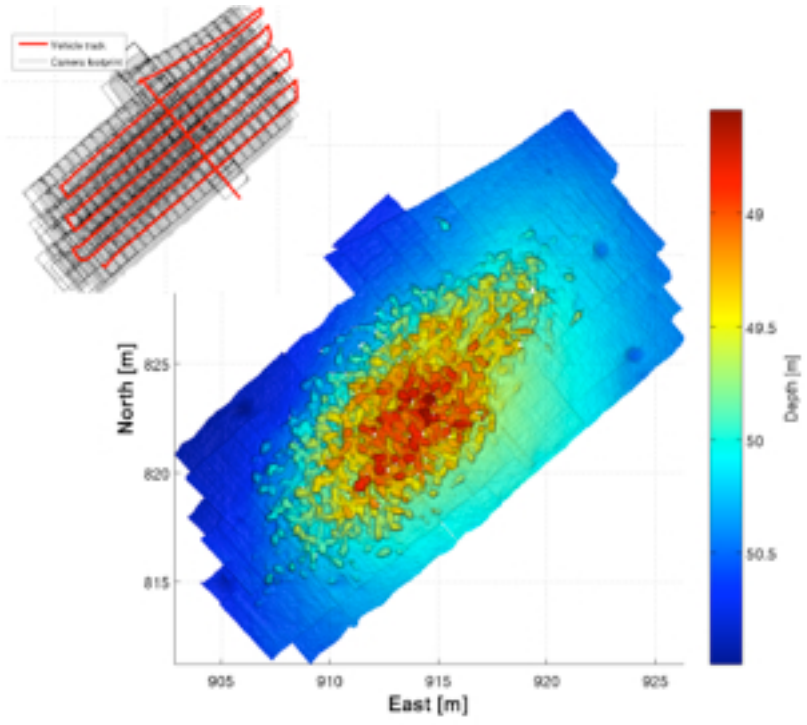

Figure 1.4. Complete bathymetric map of the Yalıkavak II wreck site made with the 2250 kHz multbeam data taken during the survey shown in the inset. The vehicle speed along the lines was 0.15 cm/sec, which ensured at least a 30% overlap between images and sonar swaths along track. All tracklines were run with the vehicle maintaining a constant heading and altitude.

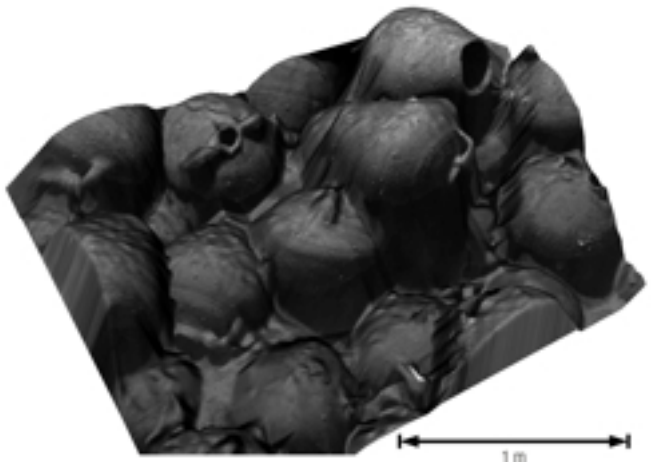

Figure 1.5. Small section of the Knidos F wreck site showing texture mapped stereo data.

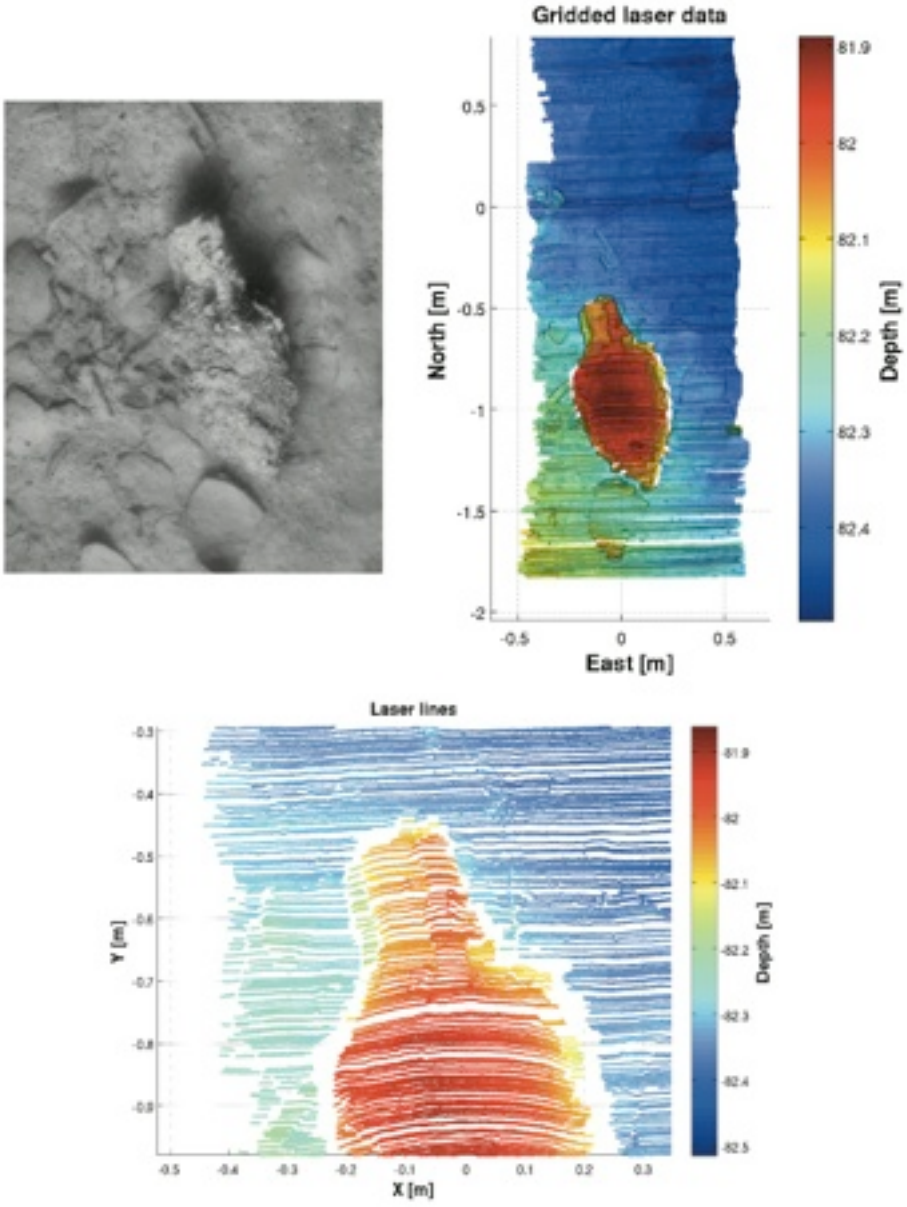

Figure 1.6. Close up of a single amphora from the Yalıkavak I wreck site mapped with the sheet laser structured light imaging. The individual linear lines correspond to points generated from the single images of the laser projected into three dimensions. The gridded image was produced with a Gaussian weighted average over a 2x2 cm window area on a mesh with 2.5 mm spacing.

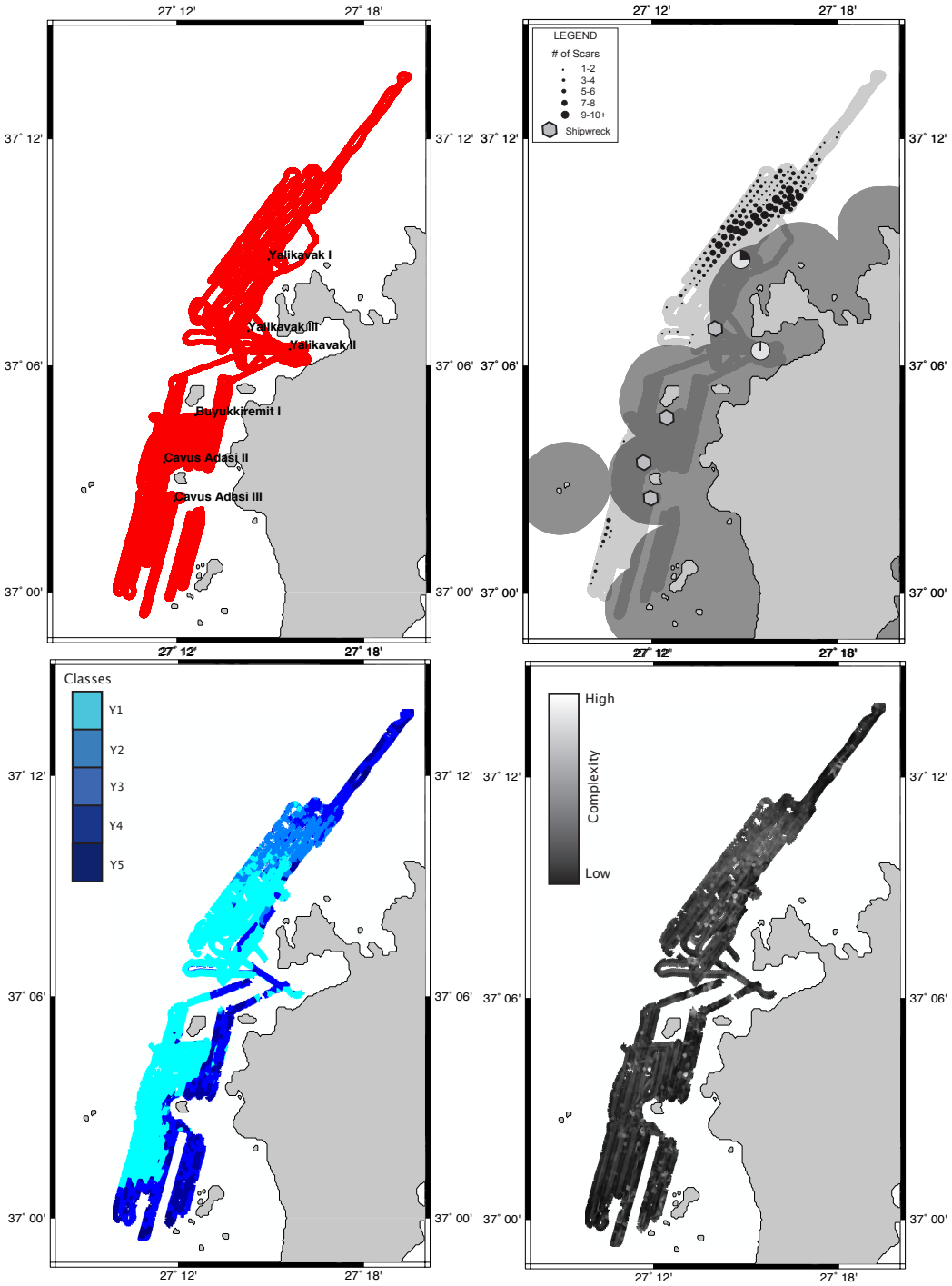

Figure 1.7. Results of side-scan sonar analysis for the Yalıkavak survey, showing (a) side-scan coverage and shipwreck locations; (b) 2.5 km area around the coast where bottom trawling is prohibited, trawl extent and intensity, pie charts indicating percentage of broken artifacts for amphora wrecks, and grey hexagons representing non-amphora wrecks; (c) results of Swathview seabed classification showing acoustic classes; and (d) feature complexity map generated by QTC CLAMS with lighter colors indicating higher complexity.

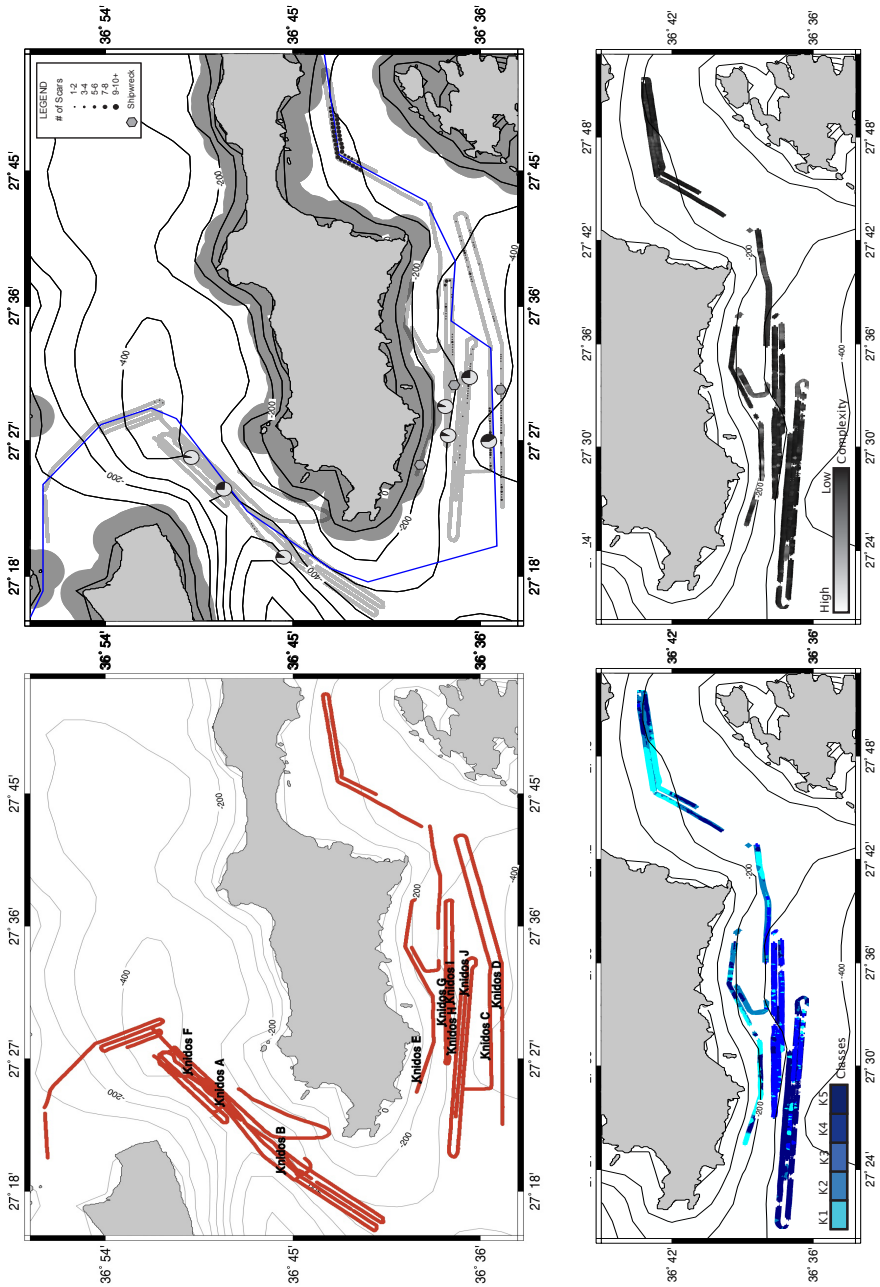

Figure 1.8. Results of side-scan sonar analysis for the Knidos survey, showing (a) side-scan coverage and shipwreck locations; (b) 2.5 km area around the coast where bottom trawling is prohibited, location of submarine cable, trawl extent and intensity, pie charts indicating percentage of broken artifacts for amphora wrecks, and grey hexagons representing non-amphora wrecks; (c) results of Swathview seabed classification showing acoustic classes; and (d) feature complexity map generated by QTC CLAMS with lighter colors indicating higher complexity.

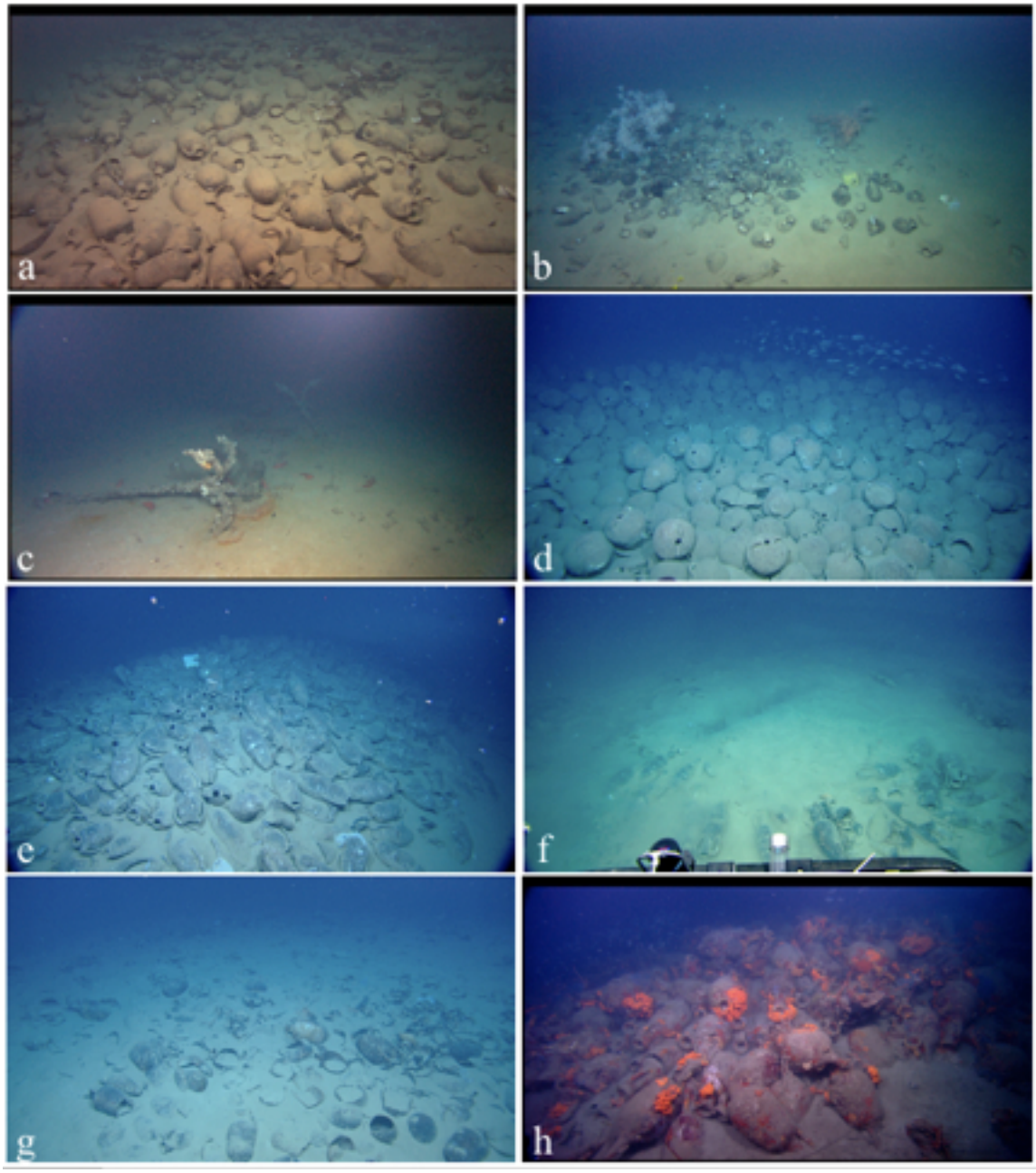

Figure 1.9. High definition video captures of wreck sites (a) Knidos A; (b) Knidos B; (c) Knidos E; (d) Knidos F; (e) Knidos H; (f) Knidos J; (g) Marmaris B; and (h) Yalıkavak II. ©IFE/COE

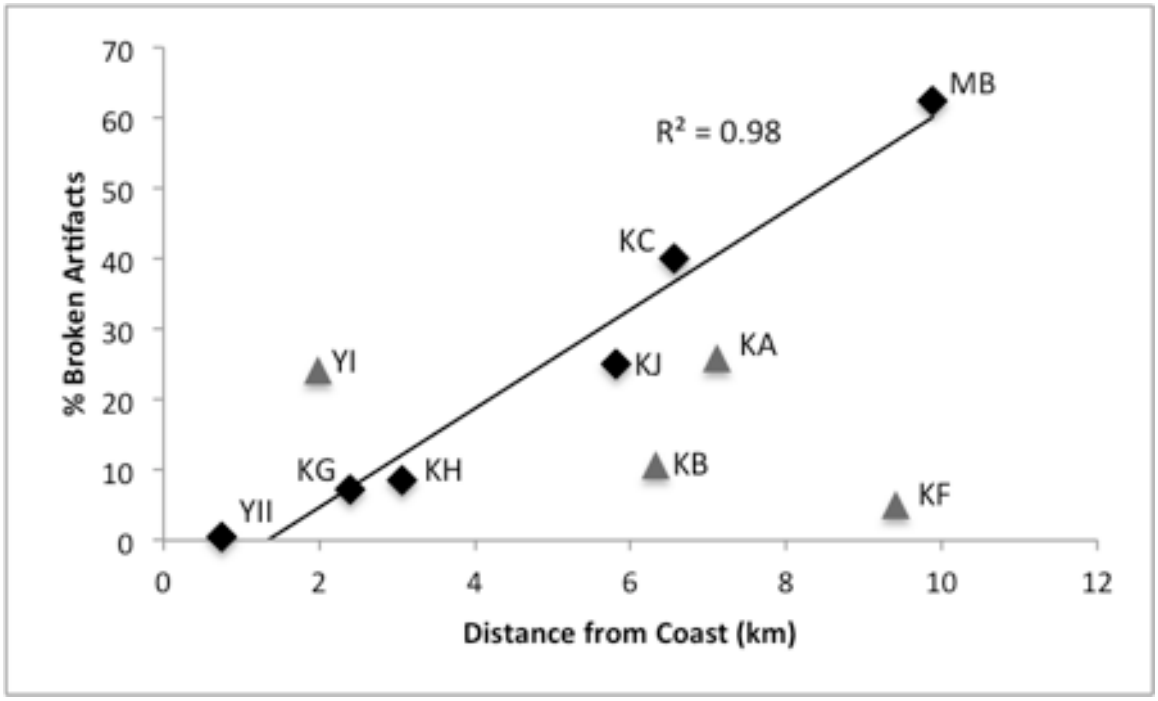

Figure 1.10. Percentage of broken artifacts for each wreck site compared against distance from shore. Linear regression is significant at p = 0.0002. KA = Knidos A; KB = Knidos B; KC = Knidos C; KF = Knidos F; KG = Knidos G; KH = Knidos H; KJ = Knidos J; MB = Marmaris B; YI = Yalıkavak I; YII = Yalıkavak II.

Figure 1.11. Histograms of (a) trawl intensity and (b) water depth of trawl scars.

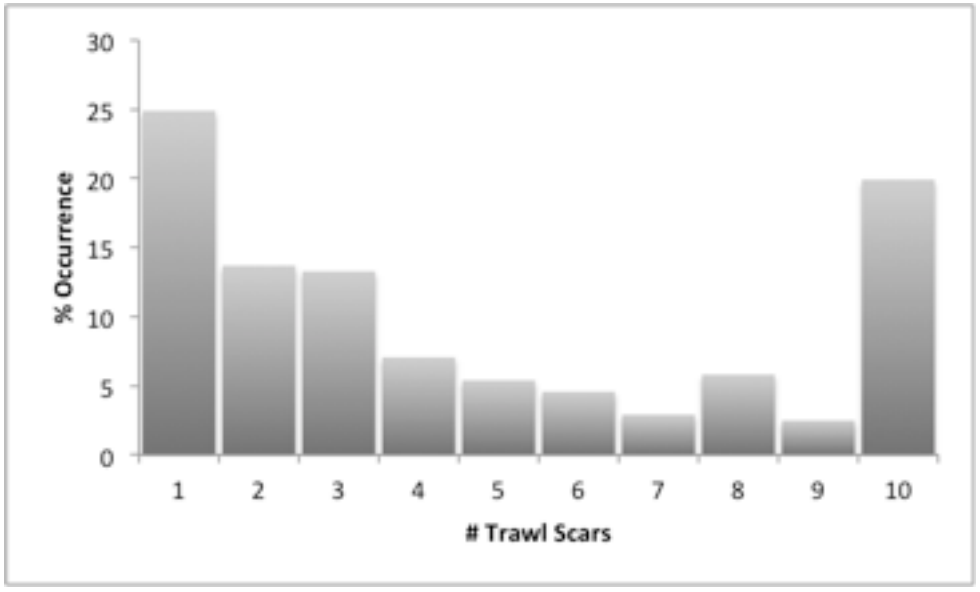

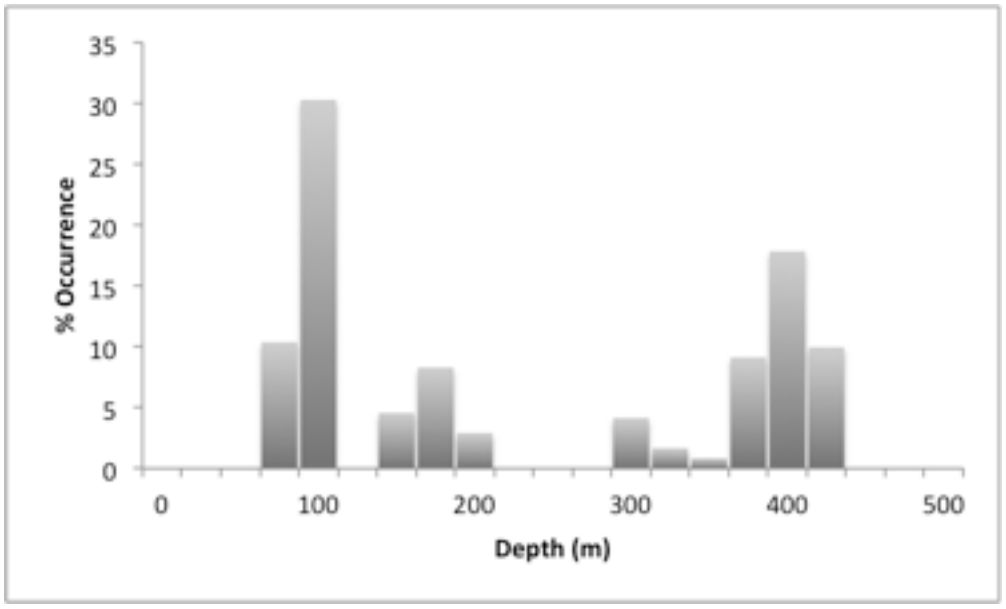

CHAPTER 2

Ocean dynamics and anthropogenic impacts along the southern Black Sea shelf examined by the preservation of premodern shipwrecks

Prepared for submission to *Continental Shelf Research*, March 2012

Michael L. Brennan[a], Dan Davis[b], Chris Roman[a,c], Ilya Buynevich[d], Alexis Catsambis[e], Meko Kofahl[e], Derya Urkmez[f], Ian Vaughn[c], Maureen Merrigan[e], Muhammet Duman[g]

[a]Graduate School of Oceanography, University of Rhode Island, Narragansett, RI 02882, USA
[b]Department of Classics, Luther College, Decorah, IA 52101, USA
[c]Department of Ocean Engineering, University of Rhode Island, Narragansett, RI 02882, USA
[d]Department of Earth and Environmental Science, Temple University, Philadelphia, PA 19122, USA
[e]Department of Anthropology, Texas A&M University, College Station, TX 77843, USA
[f]Department of Hydrobiology, University of Sinop, Turkey
[g]Institute of Marine Science and Technology, Dokuz Eylul University, Izmir, Turkey

Corresponding Author:
Michael L. Brennan
Graduate School of Oceanography
University of Rhode Island
South Ferry Road, Box 200
Narragansett, RI 02882
mlbrennan@gso.uri.edu
(401) 874-6186 office
(860) 777-6181 cell

2.1 Abstract

Continued exploration of the coastal area of the southern Black Sea off Sinop and Ereğli, Turkey in 2011 further documented the transition zone along the oxic/anoxic interface. Push cores collected with an ROV from sediments underlying the oxic, suboxic, and anoxic waters were analyzed for geochemistry, meiofauna, and microbiology to help characterize this transition zone. During the course of side-scan sonar surveys, nine shipwrecks were located at various states of preservation, all within 100-115 m depth and ranging from the 4th century BC to the early 20th century. Many of these wrecks have wooden components well preserved due to the influences of the anoxic waters being washed up along the shelf by internal waves. However, a number of these sites have also been heavily damaged by bottom trawling along the seabed up to the shelf break, highlighting the drastic threat such activities pose to archaeological sites.

2.2 Introduction

The Black Sea has long been hypothesized to be a repository of well-preserved cultural material due to anoxic conditions below ~155 m depth (e.g., Bascom, 1976). The discovery and subsequent investigations of Sinop D, a well-preserved Byzantine shipwreck, in 2000, 2003 and 2007 illustrated the potential for wreck preservation in the deep waters of the Black Sea (Ballard et al., 2001; Ward and Ballard, 2004; Brennan et al., 2011). Further acoustic mapping and exploration of the Turkish continental shelf of the southern Black Sea in 2011 was aimed at documenting the landscape across the oxic/ anoxic interface between 100-300 m depth and to acoustically map the extent and intensity of bottom trawling in the region. Push cores were collected from the sediments underlying the oxic, suboxic, and anoxic waters to evaluate these differing environments for geochemical and biological processes. The survey also resulted in the discovery of nine pre-modern shipwrecks at depths ranging from 100 to 115 m, several of which exhibit better than expected preservation at this shallow depth (Figure 2.1). The location of these shipwreck sites provides for an additional perspective to our current understanding of the dynamics of this interface. The preservation of the wood timbers in oxic waters suggests that density currents may be episodically introducing anoxic water up and onto the shelf to depths shallower than previously expected. Additionally, the various states of damage and disarticulation of wooden timbers on some of these wrecks illustrate past and present operations of bottom trawlers right up to and below the chemocline.

The suboxic zone of the Black Sea is a recent discovery and the dynamics of this mixed layer are poorly understood. The low-salinity surface water from riverine input

that overlies the dense, higher-salinity deep water from the Mediterranean creates a strong stratification in the Black Sea. A series of cruises on *R/V Knorr* in 1988 studied the oxic/anoxic interface and found a gap between the depletion of dissolved oxygen (O_2) and the onset of hydrogen sulfide (H_2S), instead of a layer where these overlap as noted during cruises in 1969 and 1975 (Murray et al., 1989). These earlier cruises found a constant density along which oxygen was depleted to zero, creating a dome-shaped layer ranging from 115 m depth in the middle of the basin and down to 275 m near the continental shelf. Observations in 1988 described a gap of 10-40 m between the oxic and anoxic layers, and a rise in the boundary of the anoxic zone (Murray et al., 1989). More recent research has shown that, prior to 1988, results suggesting a coexistence of O_2 and H_2S were an artifact of atmospheric contamination of the instruments, and that the transitional suboxic zone is a permanent feature in the vertical hydrological structure of the Black Sea (Glazer et al., 2006b). Furthermore, not only is the suboxic zone a barrier between the coexistence of O_2 and H_2S, but O_2 cannot be the oxidant for sulfide during the cycling through the water column, as they do not interact. Therefore, the mechanism for sulfide oxidation may instead be ferromanganese-oxides that transport oxygen across the suboxic gap (e.g. Glazer et al., 2006a, 2006b; Murray et al., 2007; Trouwborst et al., 2006).

This research is a continuation of work begun in 1998 by the Institute for Exploration. Ryan et al. (1997) proposed a catastrophic flood of the Black Sea's isolated Quaternary freshwater lake 9000 years ago, beginning the transformation of the Black Sea into a euxinic basin. The restricted outflow at the shallow Bosporus sill has since caused the stratification of the Black Sea by keeping the dense, saline Mediterranean

waters within the basin, and creating a stagnant, anoxic layer below 155 m depth. The first expeditions in 1998 and 1999 surveyed the shelf area east of Sinop, Turkey (Figure 2.1) and documented what was interpreted as the paleoshoreline at the 155 m isobath (Ballard et al., 2001; Coleman and Ballard, 2004). This relict beach was characterized by rocks rounded by beach erosional processes as well as Holocene freshwater mollusk shells (Ballard et al., 2001). Further work in 2000 continued these surveys west of Sinop and resulted in the discovery of four early Byzantine shipwrecks, three at ~100 m depth, and Sinop D at 325 m, which was investigated further with test excavations in 2003 and 2007 (Ward and Ballard, 2004; Ward and Horlings, 2008; Brennan et al., 2011). Sinop A, B, and C consist of mounds of exposed carrot-shaped amphoras, which are a type commonly found at kiln sites near Sinop (Ward and Ballard, 2004). Sinop A and C are smaller sites, consisting of two and three piles of artifacts respectively, while Sinop B is a single, larger and consolidated site. Also, B contains a variety of ceramic types, whereas A and C contain only the carrot-shaped amphoras. A small amount of wooden timbers was also found preserved on each wreck, but the majority of the ships' structural elements are gone. These wrecks, however, have more preserved wood than on contemporary amphora wrecks in the Mediterranean and Aegean Seas, which were thought to be due to fluctuations in anoxic waters moving up onto the shelf (Ward and Horlings, 2008).

Ballard et al. (2001) initially pointed to internal waves moving anoxic waters up along the shelf as helping preserve some wooden components of the Sinop A, B, and C wrecks because of the layered structure of the Black Sea water column. The density gradient between the oxic and anoxic water layers is great enough to support the propagation of internal waves (Trembanis et al., 2011). The thermohaline structure of the

Black Sea is affected by oceanographic processes, such as storms and thermic fronts caused by surges at river mouths and the Bosporus outflow, all of which transmit energy through the halocline in the form of density currents, or internal waves (Filonov, 2000). These events are poorly understood, although they have been observed off the Crimean peninsula (Filonov, 2000). The dynamics of this interface in the Black Sea is of particular interest with respect to the preservation potential of cultural sites and has been hypothesized that the effects of these waves may help preserve wrecks at shallower depths than previously thought (Ballard et al., 2001; Trembanis et al., 2011). The depth of the anoxic layer varies, but is generally in the range of the paleoshoreline at 155 m. When waves traveling through the interface between water layers of different densities interact with the continental shelf, they break across it similarly to a surface wave on a beach (Trembanis et al., 2011), which likely has a drastic effect on the benthic ecology including wood-boring organisms (e.g. teredinid bivalves) that destroy the wooden components of shipwrecks. The slope of the continental shelf will also affect how far the waves will wash anoxic water; the slope in the area west of Sinop is more gradual than off Crimea, for example. In this shelf region, Duman et al. (2006) show that the permanent halocline exists at 100-110 m depth, while the transitional suboxic layer extends down from 100 m to ~200 m, at which point the anoxic layer begins. It is expected, therefore, that within this transitional zone from 100-200 m depth, and possibly even shallower, shipwrecks should be found better preserved than those in normal oxic waters. Two such areas are found along the southern Black Sea coast near two cities that thrived as maritime powers during antiquity and the Byzantine period, Heraclea Pontica (modern Ereğli) and Sinope (modern Sinop).

Between their foundations in the Archaic period until the Middle Ages, Sinope and Heraclea Pontica ranked among the Black Sea's most active trading powers. Both cities possessed rich fishing grounds, fertile coastal plains, and abundant forests. Sinope with its twin natural harbors lies midway along the southern coast from the entrance to the Black Sea and at the closest crossing point to the northern shore. The city was founded by Greeks from the Ionian city of Miletus in the late 7th century B.C. (Strabo, 12.3.11; Hind, 1988; Doonan, 2004; Avram, Hind and Tsetskhladze, 2004). Early on the city itself founded three colonies on this shore and became one of the region's major trading powers, serving as an important node in a dense network of seaborne trade. The soil on the promontory encouraged the production of wine and olive oil, which it exported for centuries in large quantities in distinctive amphorae, and the densely-forested hinterland produced timber perfectly suited to ship-building. Throughout the Roman and Byzantine periods the city's fortunes waxed and waned, depending on military and political movements in and outside the Black Sea region. Evidence of Sinope's prosperity is difficult to detect in the archaeological record because the ancient city lies directly below the modern one. Based on the quantities of Sinopean amphorae found at sites around the Black Sea, however, the city exported goods extensively during the Hellenistic, Roman and Early Byzantine periods (Doonan, 2004; Opaiţ, 2010b).

Heraclea Pontica, located on a bay near a projecting headland midway between the Bosporus and Sinop, was founded by Greek settlers around the mid-6th century B.C. (Saprykin, 1997; Avram, Hind and Tsetskhladze, 2004). Like Sinope, Heraclea's vast hinterland produced olive oil and wine for export, and thick forests furnished timber for ship construction. The city lies just a long day's sail from the Bosporus (Xenophon,

Anabasis 6.4.2) and near the southern end of a natural maritime corridor that spanned the shortest distance across the open sea between Cape Carambis (halfway between Heraclea and Sinope) and Criumetopon, the southernmost point of the Crimea, near to which Heraclean settlers founded Chersonesos in the 5th century B.C. Although archaeological of the city is been minimal (as in the case of Sinop, Ereğli lies atop its ancient counterpart), numerous literary sources attest to Heraclea's commercial prosperity during the Classical and Hellenistic periods (Burstein, 1976; Saprykin, 1997; Avram, Hind and Tsetskhladze, 2004). The city and its rulers grew wealthy from harbor and market tolls exacted from the grain ships that touched this coast en route to the Bosporus and beyond to other Aegean centers, most notably Athens (Isager and Hansen, 1975; Burstein, 1976). Heraclean amphoras have been discovered in coastal and inland sites all over the Black Sea region, particularly at Chersonesos. Heraclea waned during the Roman period, losing territory and power to its neighbors to the east and west, but the city maintained some level of influence and regional connections into medieval times.

In addition to the four shipwrecks discovered off Sinop in 2000, another four were found in the vicinity in 2011, and five were located west of Ereğli at 100-115 m depth (except Sinop D). The investigation of the twelve shipwrecks found within this transitional suboxic zone between 2000 and 2011 is indicative of the thermohaline dynamics that have affected the sites since the time of the ships' sinking. The Black Sea presents a good example of archaeological oceanography, as the investigation of shipwrecks gives us the opportunity to use these sites as platforms from which to learn about the oceanographic environment (Brennan and Ballard, in review; Brennan et al., 2011). The objectives of this research off the Turkish Black Sea coast were to document

the dynamics of the oxic/anoxic interface on the coastal shelf and those of anthropogenic impacts, especially bottom trawl fishing. Further investigations of these two aspects of the submarine landscape will in turn allow us to understand the effects of both internal waves and trawl damage on the preservation and degradation of shipwreck sites. The twelve wrecks located in this zone are disarticulated to varying degrees and in most cases this relates to the extent and intensity of trawling activities in the region. Additionally, based on the preservation state of these shipwrecks at such shallow depths, we postulate that internal wave action washes water from the sulfidic zone up across shallow-gradient shelves, such as that along the coastal zone off Sinop, frequently enough to impede the degradation of wooden ships by wood-boring organisms.

2.3. Methods

2.3.1 Side-scan sonar

A series of grids were surveyed off Ereğli and Sinop, Turkey in July-August 2011 on *E/V Nautilus* (Figure 2.1). These survey areas were placed along regions of the Turkish continental shelf where either the slope was gentle enough to effectively conduct sonar operations, such as off Sinop, or where the shelf formed a plateau, such as west of Ereğli. The goal of placing these surveys here was to document the seabed morphology of areas of the shelf between 100-300 m depth, which cross the oxic/anoxic interface. An EdgeTech 4200-MP dual frequency (300/600 kHz) high resolution side-scan sonar, *Diana*, was towed behind *Nautilus* along systematic survey lines with a 300 m swath width. Slope failures, slumps, bedforms, trawl scars, and other targets were logged during the surveys. As these areas are in close proximity to the ancient sites of Heraclea and

Sinop, we also expected that some of the targets located with sonar would be shipwrecks, the investigation of which would allow for the evaluation of the effects of both the water column dynamics and trawl damage to these sites. The side-scan sonar data was imported into and processed with CARIS HIPS and SIPS. The lines were viewed in 300x300 m patches and trawl scars on the seabed were counted per unit area. These were used to create trawl intensity maps for both regions (e.g. DeAlteris et al., 1999; Brennan et al., in press).

2.3.2 ROV Operations

Target identification, side-scan sonar ground-truthing, and sediment core collection was conducted with remotely operate vehicles (ROVs) *Hercules* and *Argus* (see Newman et al., 2008; Brennan et al., in press). *Hercules* is equipped with a suite of sensors, including an Aanderaa optode for dissolved oxygen and a Falmouth Scientific CTD for conductivity, temperature, and depth measurements. These sensor data were processed with Matlab to create water column profiles for temperature, salinity, and dissolved oxygen. The front of the vehicle is equipped with push core tubes with which the manipulator arm can collect sediment samples. Ten push cores were collected from three locations off Sinop. Six cores were collected at 203 m depth in the anoxic layer for grain size, microbiology, meiofaunal, and porewater geochemistry analyses. Two cores were collected at 90 m in the oxic layer and another two from 120 m in the suboxic layer for microbiology and meiofaunal analyses. The location for the suboxic cores was determined by monitoring the dissolved oxygen readings on the sensor on Hercules,

which dropped below 5 μM at 120 m depth. These analyses are currently ongoing, and only preliminary results are discussed below.

2.3.3 Imaging

Three methods were used to document wreck sites. All sites were surveyed with a BlueView MB1350-90 1.35MHz multibeam sonar system mounted on the ROV *Hercules*. Most sites were also surveyed with two AVT/Prosilica GC-1380 1.3 Megapixel cameras configured as a stereo pair taking one image pair every 7 seconds to produce photomosaics (Figure 2.2). Survey navigation data was obtained from an Ixsea Fiber Optic Gyrocompass (FOG), an RDI Doppler Velocity Log (DVL), and a Paroscientific depth sensor. The optical surveys were conducted at an altitude of 2.0-4.5 m, a speed of 10-12 cm/s, and a trackline spacing of 1.0-1.2 m. Multibeam surveys were conducted concurrently with all optical surveys. Additional multibeam surveys were conducted at altitudes from 2.0-10.0 m and speeds up to 25 cm/s. High levels of water turbidity made optical surveys impractical at several locations, in which case only the multibeam sonar was used. Stereo survey data were processed using the featureless Simultaneous Localization and Mapping (SLAM) implementation of Johnson-Roberson et al. (2010); multibeam data were processed using the Submap-SLAM algorithm presented in Roman and Singh (2007). Both SLAM algorithms use the optical and/or bathymetric data to constrain drift in the dead-reckoning solution from the FOG and DVL.

The high relief of some of the wooden sites complicated ROV operations within the effective range of the cameras. Ereğli D, in particular, included wooded structure extending some 6 m from the seafloor (Figure 2.3). An initial optical survey at 4.0 m was

conducted over those portions of the wreck close to the seafloor, and a supplemental multibeam-only survey at an altitude of 8.5 m was necessary to fill in the portions of the site with higher relief. This range of scene relief led to occlusions that produced some large holes in the final stereo map.

2.3.4 Sample Processing

Meiofauna

Meiofauna samples were taken during three dives at three different depths chosen from anoxic (203 m), suboxic (120.5 m) and oxic (90 m) areas off Sinop Peninsula. Samples were collected in sediment corer plastic tubes (surface area of 32 cm^2) pushed into the sediment by ROVs. Obtained material was put into 500 ml glass jars and fixed on board with 75% ethanol. Meiofaunal examination was carried out at the benthos laboratory of Sinop University Fisheries Faculty. Mesh nets of 500, 250, 125, and 63 μm screens and filtered water were used to wash and obtain the necessary material. The sample retained on 63 μm mesh was transferred into glass containers and stained with Rose Bengal. Stained material was examined using Modified Bogorov counting chambers under a Olympus SX61 stereomicroscope. Organisms were sorted into main taxonomic groups, counted for quantitative analysis, and stored in 2 ml cryo-tubes. Glass pipets and several specialized needles were used for sorting the material. For quantitative analysis, the number of meiofauna in each sample was converted into individuals per m^2 by multiplying the numbers with the coefficient *k* which was found to be 311 based on the cross-sectional area of sediment corers (32.15 cm^2).

Microbiology

Each of the cores collected from sediments underlying the three water layers were sealed and stored in a -80° C freezer on board. Following the expedition, the frozen cores were transported to Istanbul University in dry ice. There, the total bacteria were tested in each sediment sample and pure isolates were screened with anaerobic cards in a VITEK 2 Compact 30 automated micro identification system. Finally, isolated 16S rDNA was analyzed with Roche High Pure Polymerase Chain Reaction (PCR) template kit (pers. communication, Gulsen Altug).

2.4. Results

2.4.1 Acoustic Mapping

The side-scan sonar surveys documented a series of morphological features of the seabed downslope toward the shelf break. The survey of the shelf plateau west of Ereğli covered depths ranging from 95 down to 190 m, at which point the slope dropped off steeply. Along the northern and eastern edges of the plateau, large-scale slope failures were observed with side-scan sonar. Recent slumps are known in this area of both steep slopes and active seismicity (e.g. Kuscu et al., 2004). A high density of trawl scars was also observed across the plateau, intensifying near the shelf edge and in some cases leading off the edge. The force of bottom trawling activities may have triggered some of the slope failures. Such slumping was not as evident off Sinop, where the shelf break and slope is more gradual. The survey there extended from 80 m down to 270 m, well below the oxic/anoxic interface and along the upper part of the slope. During the 2000 survey bedforms were noted below 170 m and were interpreted to be the result of internal wave

action (Ballard et al., 2001). In 2011, we observed extensive bedforms at and below 200 m (Figure 2.4). A transect conducted with *Hercules* over these features with the BlueView multibeam system showed the spacing of these bedforms as 4-5 m, classifying them as megaripples. Areas of heavy trawl scarring were also observed off Sinop, with the highest density near the shelf break.

2.4.2 Chemical Profiles

Much work has been done documenting the profiles of temperature, salinity, and especially dissolved oxygen through the water column of the Black Sea (e.g., Murray et al., 1989; Oguz et al., 1992; Glazer et al., 2006b). However, the dynamics of the water structure, which include shoaling of the oxic/anoxic interface and differences between coastal and basin regions of the sea, cause the depths at which certain features exist to vary (e.g., Anderson et al., 1994; Murray et al., 1989; 2007). The profiles for dissolved oxygen, salinity, and temperature recorded during descents with the ROVs reflect summer conditions along the Turkish coast during the time of the expedition. The temperature profile shows a strong thermocline in the upper 50 m, but a more gradual halocline, although both are within the expected range of values (Figure 2.5). The O_2 profile also shows the expected increase just below the photic zone, before dropping to zero at 120 m depth. The center of the Black Sea basin features a shallower depth of the top of the suboxic gap, reported at ~70 m by Glazer et al. (2006a), and deeper along the coast, reported at 100 m at the NW shelf break. At this depth of the suboxic zone, salinity evens out before increasing again into the anoxic layer (Figure 2.5). For this specific area west of Sinop, Duman et al. (2006) report a permanent halocline at 100-110 m depth,

followed by the transitional suboxic zone down to ~200 m. A steep slope in salinity is apparent in Figure 2.5 as O_2 drops to zero between 100-120 m, followed by more stable conditions downward into the anoxic layer. It was at this depth that bedforms in the sediment became apparent.

2.4.3 Biological Analyses

Meiofauna

This component of sampling was aimed at comparing the meiobenthic community composition of the oxic, suboxic, and anoxic waters of the Black Sea off Sinop. Some research has been conducted on the meiofauna of the sediments underlying the suboxic and anoxic waters, primarily in the northern Black Sea offshore Crimea (e.g. Luth and Luth, 1998; Sergeeva, 2003; Sergeeva and Gulin, 2007). The results presented here are preliminary, including only general taxa. Nematode composition is being analyzed and is beyond the scope of this paper.

The total abundance of meiofauna shows a sharp increase from 1,140 indiv./m^2 to 217,078 indiv./m^2 with the highest abundance at the oxic station and the lowest at the anoxic station. The taxa composition of meiobenthos from three sites ranged between 5 and 9 major groups. Total abundance of all groups significantly decreased with increasing water depth, and therefore decreasing O_2 levels. The total number of individuals in the oxic zone was approximately 200 times higher than the number of individuals found in the anoxic zone (Figure 2.6). The oxic and suboxic samples showed relatively comparable results whereas the anoxic zone revealed a very small density. Meiofauna of anoxic sample was determined to include representatives of only *Nematoda*, *Acarina*,

Harpacticoida and hard shelled *Foraminifera*. *Nematoda* dominated all three zones, followed by *Harpacticoida* in the oxic and suboxic zones. The third dominating group was *Polychaeta* in the oxic zone and *Hydrozoa* in the suboxic zone. *Kinorhyncha* was recruited only from the oxic and suboxic zones. *Turbellaria*, *Ostracoda* and *Echinodermata* was only detected in the oxic sample. These preliminary results correspond with similar studies in the northern Black Sea. Luth and Luth (1998) also show a significant decrease in meiofauna biomass in anoxic sediments compared to oxic and suboxic samples and a similar meiobenthic composition from three depths (60m, 110m, 190m). Sergeeva (2003) found certain benthic fauna present at depths of 130-150 m that had adapted to limited oxygen concentrations and reported typical groups live under anaerobic conditions as also found in our samples. Our results show that the most abundant main taxon in all three zones was *Nematoda* with its highest contribution (90%) within the suboxic sample (Figure 2.6).

Microbiology

The VITEK 2 identification system noted *Propionibacterium acnes* as one of the 25 isolates analyzed, the rest were unknown (pers. communication, Gulsen Altug). While additional 16S rDNA studies are ongoing to identify the unknown species, counts of colony forming units (CFU) from each of the three cores show expected differences between the oxic core and the two from zero-oxygen environments. Counts were conducted on cultures in aerobic and anaerobic conditions for each of the three sediment cores. The highest aerobic bacteria counts were found in the oxic sample, while the suboxic and anoxic samples each had slightly higher counts of anaerobic bacteria

compared to the oxic sample. Many of these CFUs are likely facultative anaerobes and grew in both aerobic and anaerobic conditions, but the expected presence of more aerobic bacteria in the oxic sample was observed. Further identification of bacteria in these cores will provide more data about the microbial communities within this coastal transition zone.

2.4.4 Sinop Shipwrecks

During the course of the survey northwest of Sinop, four shipwrecks in addition to those found in 2000 were located. With the exception of Sinop D, which lies at 325 m in the anoxic layer, all of these wrecks were found in a band along the shelf between 100-115 m depth. Ward and Horlings (2008) suggested that the proximity of Sinop A, B, and C represented a pattern of loss possibly caused by weather conditions related to the Sinop peninsula. The discovery of four additional wreck sites in this area further support this, however, their location along this 15 m depth interval also speaks to the presence of a zone where the combination of oceanographic and anthropogenic conditions and effects have preserved these wrecks to differing degrees (Table 1).

Sinop F

The first shipwreck located in 2011, Sinop F, was found during a side-scan sonar reconnaissance of the A, B, and C wreck sites. The wreck is located only 500 m SE of Sinop B. The mound of amphoras measures 7 x 4 m and about 1 m in height. The site has been heavily damaged by trawls, and the mound has the appearance of a flattened top caused by the dragging of weighted fishing nets over the site. A displaced timber lies at

the west end of the site, composed of multiple joined pieces and resembles the stern post of an ancient ship. The ceramic cargo is composed of three types of amphora, including two widespread types, LRA 3 and LRA 4 (Late Roman Amphora), dating to the 1st c. BC to 6th c. AD, and the second half of the 5th c. AD, respectively. The third type is a North African amphora, likely the predecessor of the Keay 62 Q/Bonifay 45 type, known in the Black Sea area at Tomi and dating to the second half of the 5th c. AD (Opaiţ, 1997-1998). The combination of these types provides a date for the ship of the late 5th or early 6th century.

Sinop G

Sinop G appears to be a more recent wreck, although no diagnostic artifacts were visible on the site. The wreck is a small wooden ship, 11 x 4.5 m, with a deck platform and lies upright, partially buried up to its upper sides on a semi-hard bottom (Figure 2.7b). A stem post, frames, shelf clamps, and deck beams remain, outlining the extent of the ship, but no deck planks or strakes remain. The preserved articulation of the ship suggests that it has escaped damage from trawlers.

Sinop H

Like Sinop G, this wreck is the preserved skeleton of a large wooden ship, although larger, measuring 26 x 9 m and listed to the south, or starboard. This site contains a series of intact regularly spaced frames, with at least 55 along the north side and measuring up to 2.8 m in height (Figure 2.7c). The south side appears disturbed from the sinking event as the vessel settled onto the seabed, although here too the frames

remain in place. The mast of the ship lies adjacent to the wreck, and is mostly buried in the sediment. The exposed end widens to accommodate a deep mortise along the centerline. Also like Sinop G, the preserved articulation of the ship's structure shows that the site has escaped damage from trawls. No cargo was visible, though three ceramic artifacts were located near the frames along the southeastern part of the site. A single anchor was observed standing upright on the southwestern end of the wreck, complete with a concreted iron ring and anchor eye lead fixed to the stock near the shaft. The anchor together with the lack of any machinery, place this wreck tentatively in the 18th or early 19th centuries.

Sinop I

The last wreck located off Sinop in 2011, Sinop I, is an amphora wreck measuring 12.5 x 5 m, and consisting of three small mounds of amphoras oriented on an E-W axis. Unlike the other amphora wrecks, Sinop A, B, C, and F, this site exhibits no discernible damage from trawls and the amphoras comprising the southeast mound remain in an *in situ* vertical orientation. Visibility was poor at the site due to high turbidity, but three types of Sinopean amphoras were observed, all dating to the 1st century AD. These include Zeest 31/Vnukov Sin II (Zeest, 1960), Vnukov Sin II and Ib (Vnukov, 2003), the latter of which is usually dated to the second quarter of the 1st century BC. All are ubiquitous in the northern Black Sea region, particularly in Chersonesos and its extended chora (Vnukov, 2003).

2.4.5 Ereğli Shipwrecks

The side-scan sonar surveys on a shelf plateau west of Ereğli were conducted at the start of the cruise, and logged targets were identified with ROV dives on the return to Istanbul following the work off Sinop. Five shipwrecks were located, one in a coastal zone just west of Ereğli, and four on the plateau further west. Like the area surveyed off Sinop, these locations are along western approaches to an ancient harbor situated on a peninsula. Also like the wrecks off Sinop, these five are all located in depths ranging from 100-115 m, and have more exposed wood preserved than temporally equivalent wrecks in the Mediterranean and Aegean Seas.

Ereğli A

Ereğli A was the only site located during the survey just west of Ereğli. It is a small wooden ship with no discernible cargo (Figure 2.8a). Extremely poor visibility made visual inspection difficult; the extreme state of disarticulation of the wooden components of the wreck by trawl damage hindered the inspection of this wreck even more. The ship's structural elements are thoroughly displaced to such a degree that it appears as if there are no two timbers remaining fastened together. No diagnostic artifacts were visible. Notches and other preserved cuttings on the timbers suggest the ship post-dates the 13th century, whereas the lack of machinery suggests it pre-dates the early 20th century.

Ereğli B

Like Ereğli A, this is the wreck of a small wooden ship with no visible or diagnostic cargo. Clear damage from bottom trawls has ripped apart the site, with two deep scars visible running directly through the center of the wreck mound (Figure 2.8b). The ship appears to have settled into the seabed off-axis, leaving a perimeter of frames outlining the wreck's location prior to its dismantling by trawls. Dating of this site remains inconclusive.

Ereğli C

Ereğli C is the wreck of a small Byzantine ship that has also been subjected to heavy trawl damage like A and B. The majority of the timbers lie in a jumble of unconnected fragments atop the wreck mound, although individual timbers lie scattered about the perimeter of the site for several dozen meters off site, with a few located over 200 m from the main mound. Four visible LRA 1 amphoras were discerned in the middle of the site; the shape of their bodies point towards a date in the 6th century (Opaiţ, 2010). While most of the timbers of the ship have been displaced from their *in situ* positions, a small central area of the site appears better preserved and includes a series of four regularly-spaced frames set between 15-20 cm apart (center to center). What seems to be a plank edge rises out of the mud on the outer face of these frames. It shows no evidence of edge joinery along its 1.5-2.0 m of exposed length. No further evidence of the ship's original form was discernible.

Ereğli D

The remains of an immense wooden ship measuring ca. 30 x 14 m were found near the steep slope off the edge of the shelf, and therefore away from bottom trawl activity. This location has help to preserve this wreck in a notably better condition. The site consists of large amounts of preserved wooden timbers in situ and undisturbed in two lobes (Figure 2.8d). The ship seems to have split open upon impact with the seabed at the stern area and fallen over in two parts to create these two sections. The higher relief area (Figure 2.3), which appears to be the stern, also has what may be a cargo of stacked wooden planks (Figure 2.8e). The absence of additional visible cargo or other diagnostic artifacts have hindered the dating of this ship.

Ereğli E

The only ancient wreck found in this area, Ereğli E, is a relatively large wreck of a merchant ship of the Late Classical/Early Hellenistic period. The wreck site measures 23 x 8 m and is composed of amphorae and displaced wood fragments. The ship was carrying at least nine different types of amphoras, almost none of which remain wholly intact. Three types originate from Pontic production centers, including Chersonesos (type IБ) from the late 4th century B.C. (Monachov, 1989; Kac et al., 2002), Sinop from the mid-4th to early 3rd century B.C. (Monachov, 1992), and an unknown South Pontic center, perhaps from the late 4th or early 3rd century B.C. (Monachov, 1999). Four other types were produced in Aegean centers: Thasos in the late 4th and early 3rd century B.C.; Knidos in the late 4th or early 3rd century B.C. (Monachov 1999; Empereur and Tuma 1988); and Rhodes in the late 4th century B.C. The date ranges of these identifiable types

help pinpoint the wreck to the last quarter of the 4th century (pers. communication, Andrei Opaiţ). The timbers of the ship have also suffered violent displacement as a result of trawling damage, the scars from which are evident on the surrounding seabed. Some timbers appear to lie *in situ*, while others lie scattered around the site. From these timbers, it is evident that the ship employed at least two types of joinery, mortise and tenon, and sewn construction.

2.5. Discussion

2.5.1 Shipwreck Sites

Deep-water surveys typically consist of concentrated sampling over a large area. This is one of the first large-area, comprehensive acoustic and video surveys of the seabed, particularly in this region of the Black Sea and across the oxic/anoxic interface. As such, the combined data sets collected in 2000 and 2011 have produced good documentation of the number of shipwrecks in the area. While it is unlikely that these are the only ships that sank in the region, these surveys afford a complete view of the detected wrecks that have been preserved and of their varying states of preservation. As such, the research permits an examination of the processes and events that have both preserved and impacted the sites over time. The investigation of these wrecks also allows for a more comprehensive picture of ancient and medieval seafaring along what is believed to be a heavily-trafficked maritime corridor near the south coast between the Bosporus and ancient and medieval Trabzon (Davis, 2009). The discovery of a high density of wrecks lying on the seabed west of both Heraclea Pontica and Sinope helps support this hypothesis.

The history and economy of Sinop in the Early Byzantine period is becoming better known owing to the discovery of five Byzantine shipwrecks in 2000 and 2011. Sinop A, B, and C, discovered in 2000, and reinvestigated in 2003 and 2011, all contained cargoes of carrot-shaped amphoras manufactured in or around Sinop in the 5th century A.D. (Ballard et al., 2001; Ward and Ballard, 2004; Ward and Horlings, 2008). Wrecks A, B, and C lie very near each other: Sinop A and C lie just 150 m apart, and about 1.7 km away from Sinop B. Sinop D, also located in 2000, and the other four wrecks found in 2011, suggest this area was the crossroads of two well-traveled routes, a maritime corridor that skirted the coast of the entire southern shore, and an open-sea corridor that leads northward from the peninsula to the Crimea (Maximova 1959; Gajdukevich 1969; Davis, 2009). The carrot-shaped amphoras of Sinop A, B, and C exhibit uniformity in their dimensions and shapes with slight variations, which are characteristic of industrial production (pers. communication, Andrei Opaiţ). Therefore, given their proximity, it appears that all three ships, and perhaps others similarly laden, departed Sinop under convoy for points west or north before sinking very close to each other as a result of a violent squall. That merchant vessels sailed in convoys, and that harbors often emptied on the same day in spring when the sailing season began, is well documented in antiquity and the Middle Ages (e.g. Goitein, 1999; Casson, 1995; Davis, 2009). Such was hypothesized for the two Phoenician wrecks found in deep water off Ashkelon, Israel, both carrying nearly identical amphorae, with only minor variations, which likely sank at the same time in a storm or sudden squall (Ballard et al., 2002).

Sinop F, dated to the late 5th or early 6th century A.D., was found just 500 m from Sinop B. This wreck is slightly later in date than Sinop A, B and C; more importantly, this

vessel was clearly headed toward Sinop, unlike the others. Its cargo of goods stored in containers that hail from the Aegean, Gaza/Ashkelon, and North Africa suggest that Sinop was well connected to the trading networks of the Early Byzantine Empire. It and the other Sinop wrecks add depth to our view of Sinop as a vibrant trading center long after the city's heyday in the Greek and Roman periods (Robinson, 1906; Doonan, 2004). Sinop I, the earliest of the wrecks so far located off Sinop, dating to the 1st century A.D., sank with its cargo of Sinopean wine shortly after its departure. Given its location, the ship may have been headed westward, possibly to Heraclea, the Bosporus, or points beyond. On the other hand, these specific amphora types turn up in large numbers in the northern Black Sea, particularly in the Crimea (e.g. Zeest 1960). The ship, then, may have been about to make the open-sea passage before sinking.

Unlike most of the shipwrecks found off Sinop, the five shipwrecks found off Ereğli show no obvious connection to this important trading center. Nevertheless, they provide insights into the kinds of ships that were active along this stretch of coast between antiquity and the pre-modern period. Ereğli E is among the earliest shipwrecks found to date in the Black Sea. The variety of late 4th-century B.C. amphora types found on the wreck suggests that the ship called at several Aegean ports, including Rhodes, Knidos and Thasos, before transiting the Bosporus. Based on the north Pontic amphoras discovered on the wreck, the ship then sailed north, probably along the west Pontic coast. At some point, perhaps at the mouth of the Danube, the ship made the open-water crossing to western Crimea, a well-attested route in this period (*Periplus* of Pseudo-Scylax, 68; Gajdukevich, 1969; Davis, 2009). After picking up a small cargo of wine at Chersonesos, the ship headed south across the open sea to Sinop, where it picked up more

cargo, then headed west before sinking off of Heraclea Pontica, the next likely stop on its circuitous voyage. The other four wrecks off Ereğli have few diagnostic artifacts, hindering further conclusions about their origins or destinations.

2.5.2 Trawl Damage

Unlike the Mediterranean and Aegean Seas, where a large percentage of the seabed is within reach of trawl fishers, the Black Sea's water structure confines operations to <200 m depth before anoxia sets in. Such limitations isolate bottom trawling to a small band along the coastline, consequently intensifying the operations in these coastal regions. Brennan et al. (in press) showed the extent and intensity of trawl scarring on the seabed of the southwestern Aegean coast and the placement of shipwrecks on the seabed based on the amount of resulting damage to each. In the Aegean, trawling areas are limited by inshore restrictions and the proximity of Greek islands. Trawling is also generally conducted by smaller vessels in comparison to the larger and more powerful trawling vessels that operate in the Black Sea (Unal, 2004). The amount of scarring on the seabed off both Sinop and Ereğli is extensive and running in multiple directions, except for near the shelf break, where the scars tend to run parallel to the isobath. In the region off Knidos, trawl scars were estimated to last on the seabed on the scale of decades due to low sedimentation rates and the low energy environment (Brennan et al., in press). Along the southern Black Sea coast off Turkey, however, sedimentation is greater, ranging from 55-110 cm/1000 years, or 6-11 cm/100 years (Duman et al., 2006; Anderson et al., 1994). Additionally, longshore currents move west to east along the Turkish coastline, establishing a net sediment transport vector eastward (Duman et al., 2006).

Both of these sedimentary processes would erase trawl scars faster than those in the Aegean Sea, possibly on the scale of years.

Figures 2.9 and 2.10 show the extent and intensity of trawl scars on the seabed for the areas surveyed off Sinop and Ereğli (after Brennan et al., in press; DeAlteris et al., 1999). Both areas exhibit the most intense scarring along the seafloor just above the shelf break, which has occurred at least within the past decade. While the survey off Ereğli did not cover any of the slope due to its steepness, the survey off Sinop shows no scarring north of the shelf break, as anoxic waters begin to set in. Areas south of the heavily-trawled shelf break show generally less scarring, although the plateau off Ereğli indicates more extensive trawling than Sinop because it is one of the few shallow areas there compared to Sinop's more gradual slope. Regions of the seabed exhibiting little scarring, such as the southwestern part of the survey area for Sinop (Figure 2.9) and the southeast for that off Ereğli (Figure 2.10), are areas where rocks and other potential snags for fishing nets are prevalent on the seabed. The placement of shipwrecks on these maps clearly illustrates the levels of damage observed at each site. Four of the eleven wrecks show no visible damage from bottom trawls. Sinop G, H, and I plot in areas where no or few trawl scars were observed with side-scan sonar. Sinop H and I are both in rocky areas. Ereğli D, the only untrawled wreck found here, sits very close to the shelf break and has thereby escaped damage. Both wooden wrecks, such as Ereğli B and C, and amphora wrecks, such as Sinop A, B, C, and F, that plot in heavily trawled areas showed extensive damage to the sites. Since trawl scars probably remain visible for less than a decade, in the eleven years since the discovery of Sinop A, B, and C, there has been increased damage to these wrecks.

One of the objectives of the expedition's return to the Black Sea was to revisit the Sinop A, B, and C wreck sites and re-evaluate their condition after eleven years. Only partial photomosaics were produced in 2000, so we also conducted new imaging surveys of A and B. What was immediately apparent in the 2011 photomosaic of Sinop A (Figure 2.2) is the swept appearance of the wreck site by trawls. Scars run across the site in multiple directions, but the dominant orientation of the marks is roughly E-W, which is the observed direction of the scars in side-scan sonar running parallel to the slope. Despite statements to the contrary (Ballard et al., 2001; Ward and Horlings, 2008), a reexamination of still photo imagery from 2000 shows that Sinop A was damaged by trawl fishing at the time of its initial investigation, both in broken artifacts and trawl scars visible in the surrounding sediment. Comparison to data from the 2011 surveys shows that over the course of the intervening eleven years, Sinop A has suffered serious additional damage. An estimate of broken vs. unbroken amphoras (after Brennan et al., in press) from these images in 2000 shows about 21% broken, whereas a count based on the 2011 photomosaic shows 59% broken. This reexamination illustrates that the wrecks are continually threatened by trawling, as they lie in an area of high activity and have been significantly damaged over the past decade.

The new amphora wrecks found in 2011 are also indicative of the localized areas of heavy trawling shown in the intensity maps. The only one found outside of heavily trawled areas is Sinop I, on which only a handful of amphoras appear to be broken, certainly <5% that is expected for the ship wrecking event (Brennan et al., in press), and many are still upright in their original positions. However, photomosaics of Sinop F and Ereğli E indicate even more damage than Sinop A; Sinop F is similar at 60% broken, and

Ereğli E is at 68%, which is damaged to a greater extent than any wreck we have documented in the Aegean Sea. The discovery of preserved wooden planks from the ship featuring evidence of multiple types of joinery is probably due to trawls overturning timbers that had been preserved underneath the sediment. Such uprooting of preserved timbers is also evident at the other trawled Sinop amphora wrecks, especially F and A, including the large timber visible in the Sinop A photomosaic (Figure 2.2) that appears to be part of the mast and was not visible in 2000. In addition to the preserved timbers from the ships, the wrecks act as traps for modern debris, including pieces of wood and brush (e.g. McNinch et al., 2006). This is particularly true in the case of the better-preserved wooden wrecks, which have a higher relief on the seabed and appeared in side-scan sonar as mounds of sediment with linear reflections jutting out.

It is becoming increasingly evident that trawling has a profound impact on the site formation processes leading to the current state of preservation of pre-modern wrecks. This is especially apparent at the sites where the wooden components are still preserved on the seabed. Due to the characteristics of the water column of the Black Sea Ereğli A, B, and C would have likely remained as intact as Sinop G, H, and Ereğli D. Instead, the former are heavily impacted sites that now consist of mounds of trapped sediment with a litter of timbers scattered about the surrounding seabed. These wrecks, with little to no visible cargo, would have likely deteriorated completely if they sank in the Mediterranean, but were preserved and able to be found in the Black Sea due to the suboxic conditions. The addition of trauma to the shipwrecks by trawling over the past century disturbed and destroyed sites that had already been in equilibrium with the surrounding environment for centuries. This interaction of ocean dynamics and

anthropogenic activities has both preserved these wrecks and destroyed the sites, leaving what we see today as nearly unrecognizable wood remnants of ships.

2.5.3 Dynamics of the Oxic/Anoxic Interface

Despite all eleven of these wrecks' being located within 15 m depth of each other, there is a wide range in preservation visible between the sites. The main factor between preserved wooden wrecks (Sinop G, H; Ereğli D) and degraded wooden wrecks (Ereğli A, B, C) is bottom trawl effects. Even with extensive damage to some of the sites, timbers are well-preserved and show little to no evidence of deterioration. However, while the five ancient wrecks contain some preserved timbers, the ships' structures have mostly deteriorated. The degradation of wooden components of ships is caused by wood-boring organisms, such as Teredinidae and pholadidae, such as Xylophaginae, depending on depth, both of which are found in the Black Sea and Sea of Marmara areas (e.g. Culha, 2010; Micu, 2007). While teredinids can survive periods of anoxia (e.g. Richards et al., 1984), the waters of the Black Sea will prevent their settling onto wooden structures and survival, thereby causing the highly preserved condition of wrecks such as Sinop D within the anoxic layer (Ward and Ballard, 2004). Like Sinop D, the timbers of all the wooden ships found in 2011, regardless of trawl damage, appear free of any damage from teredinid boring. This is not, however, the case for the largely destroyed timbers from the amphora wrecks. For example, some of the amphora cargo at Sinop A remained in their original stacked orientation in 2000, but the wooden structure was gone (Ward and Ballard, 2004). Regardless, such artifact orientation in 2011 appeared destroyed eleven years later by trawling.

The differences in preservation of the wood of these wrecks is not related to depth, as they are all within a similar depth range, nor is it merely age, as teredinids have been shown to colonize a wreck site within five years (Bergstrand, 2010). A shift in the depth of the chemocline appears to be the primary cause of the difference in preservation of these sets of wrecks. A core from the region just east of Sinop at 160 m depth indicated a shoaling of the oxic/anoxic interface with a shift from bioturbated sediments to undisturbed laminae above, showing the oxic layer having once been at that depth, about 200 years ago (Anderson et al., 1994). One possible cause of this shoaling event is the opening of canals between tributaries of rivers draining into the Black and Baltic Seas in the early 1800s, which are known to have transported invasive species, such as zebra mussels, between the bodies of water (e.g. Buynevich et al., 2011; Olenin and Leppakoski, 1999). The timing of the canal construction and changes to freshwater discharge into the Black Sea likely had an impact on its physico-chemical structure. Regardless, the ancient wrecks would have been fully within the oxic waters at the time of their sinking up until this shoaling event. The wooden wrecks, which appear later although we do not yet have secure dates for them, likely had little to no time in oxygenated waters, and may give us a rough *terminus post quem* of the late 18th to early 19th centuries for their sinking. Additionally, all of these wrecks lie just above the 120 m depth at which we observed the beginning of the suboxic zone. Internal waves moving across the oxic/anoxic interface must wash anoxic water up across the shelf frequently enough to prevent the settling and survival of wood-boring mollusks. The shoaling event, therefore, raised the chemocline enough that these wrecks came within reach of the waves' effects. The exposure of preserved timbers from the amphora wrecks by trawling

and their subsequent survival also illustrates the effect of the internal waves on the benthic communities.

The preliminary results of the biological analyses reported here from cores of sediments underlying the oxic, suboxic, and anoxic water layers support the premise of varying dissolved oxygen levels in the suboxic zone. The CFU counts of bacteria as well as the counts of meiofauna show similar community populations for the oxic and suboxic cores, and depleted communities in the anoxic core. The anoxic layer has been stable and stagnant, but the results here show a more dynamic layer in the suboxic zone, one that may indicate periods of both anoxic and oxic waters in this region of the continental slope. Present in the suboxic cores were facultative anaerobes that can function in either oxic or anoxic environments, as well as benthic fauna that can withstand low oxygen conditions. While the anoxic layer is stable relative to the conditions for wreck preservation and benthic communities, the internal wave effects on the seabed were also evident in the side-scan sonar as megaripples. Such areas of bedforms, which were observed at around 200 m depth, indicates movement of sediment that would periodically bury and scour any shipwrecks present at these depths, as is seen off the North Carolina coast (e.g. McNinch et al., 2006). The Black Sea wrecks found in 2011 just above the suboxic zone also act as sediment traps causing additional burial and accumulation of modern debris. The culmination of all of these processes creates a dynamic and variable environment in which to study archaeological sites. While the anoxic waters preserve the wooden components of wrecks, other processes in this transitional area can also bury or destroy these sites, regardless of their preservation state.

2.6 Conclusions

The wrecks located along the southern Black Sea coast of Turkey provide evidence for a series of complex processes occurring at the transition between oxic and anoxic waters. The dynamics at this zone from 100-115 m depth show an unstable interface that has not remained at one depth over time, and which responds to events in the form of internal waves, the effects of which are visible in varying states of preservation of pre-modern shipwreck sites. Added to this are the recent effects of bottom trawling, further complicating the formation processes that created the sites we see today, and damaging them to differing degrees based on their location on the bathymetric landscape. Due to the extent of this damage, some of the more heavily impacted wooden wrecks can be identified little more than to say that there is a wreck there. On the other hand, these ships without a ceramic cargo would have little chance of surviving to this day had they sunk in the Mediterranean or Aegean Seas. Taken together, investigations of these wreck sites tell us not only about historic seafaring, but also about both the recent history of the Black Sea's suboxic zone and the recent extent of bottom trawl activities.

The data collected during the 2011 cruise of *E/V Nautilus* introduce more questions than they answer, in particular because such well-preserved shipwrecks were not expected at such shallow depths. The dynamics of the suboxic zone require more investigation, ideally on longer time scales. In 2007, we deployed a sensor package equipped with a CTD, O_2 sensor, and ADCP at 103 m depth off Sinop Turkey, as well as one at 325 m in the anoxic zone. The deeper package was retrieved the following year (results reported in Brennan et al., 2011), but the suboxic package was not recovered. In 2011, the mooring was discovered tangled in fish nets, a long line rising up from the

seabed, and the sensors missing. It appears that the intensity of trawling in the region also presents a substantial challenge for long-term monitoring of the depths at which internal waves through the suboxic zone can be recorded. It raises a question of how such long-term data sets can be collected while avoiding trawling. In addition, the intensity of trawling observed off Sinop and Ereğli clearly presents a continuing threat to the preservation of ancient shipwrecks on the seabed above the anoxic layer as the 2000 and 2011 documentation of Sinop A demonstrates. Efforts in areas of high density of shipwrecks, such as these two regions surveyed in 2011, should be considered for marine protected areas, which would also allow for better environmental monitoring of the suboxic zone. Further surveys and documentation of the cultural sites along the southern Black Sea margin is needed to strengthen the case for sites preservation and the threats posed by bottom trawling.

References

Anderson, R.F., Lyons, T.W., Cowie, G.L., 1994. Sedimentary record of a shoaling of the oxic/anoxic interface in the Black Sea, in: M.I. Scranton (Ed), Variability in Anoxic Systems. *Marine Geology* 116, 373-384.

Avram, A., Hind, J., Tsetskhladze, G, 2004. The Black Sea Area, in Hansen, M.H. and Nielsen, T.H. (eds.), An Inventory of Archaic and Classical Poleis. Oxford: Oxford University Press, pp. 924-973.

Ballard, R.D., Hiebert, F.T., Coleman, D.F., Ward, C., Smith, J.S., Willis, K., Foley, B., Croff, K., Major, C., Torre, F., 2001. Deepwater archaeology of the Black Sea: The 2000 season at Sinop, Turkey. *American Journal of Archaeology* 105, 607-623.

Ballard, R.D., Stager, L.E., Master, D., Yoerger, D., Mindell, D., Whitcomb, L.L., Singh, H., Piechota, D., 2002. Iron Age shipwrecks in deep water off Ashkelon, Israel. *American Journal of Archaeology* 106, 151-168.

Bascom, W., 1976. Deep Water, Ancient Ships. New York: Doubleday & Company, Inc.

Bergstrand, T., 2010. The Danish 7th-century Man-of-War *Stora Sofia*: Documentation and *in situ* preservation. *International Journal of Archaeology* 39, 56-65.

Brennan, M.L. and Ballard, R.D., in press. Archaeological Oceanography. Encyclopedia of Natural Resources.

Brennan, M.L., Ballard, R.D., Croff Bell, K.L., Piechota, D., 2011. Archaeological oceanography and environmental characterization of shipwrecks in the Black Sea, in Buynevich, I., Yanko-Hombach, V., Gilbert, A., and Martin, R.E., eds., Geology and Geoarchaeology of the Black Sea Region: Beyond the Flood Hypothesis. Geological Society of America Special Paper 473, p. 179-188, doi: 10.1130/2011.2473(11).

Brennan, M.L., Ballard, R.D., Roman, C., Bell, K.L.C., Buxton, B., Coleman, D.F., Inglis, G., Koyagasioglu, O., Turanli, T., in press. Evaluation of the modern submarine landscape off southwestern Turkey through the documentation of ancient shipwreck sites. *Continental Shelf Research*.

Burstein, S.M., 1976. Outpost of Hellenism: The Emergence of Heraclea on the Black Sea. University of California Press, Berkley.

Buynevich, I.V., Damusyte, A., Bitinas, A., Olenin, S., Mazeika, J., Petrosius, R., 2011. Pontic-Baltic pathways for invasive aquatic species: Geoarchaeological implications, in Buynevich, I., Yanko-Hombach, V., Gilbert, A., and Martin, R.E., eds., Geology and Geoarchaeology of the Black Sea Region: Beyond the Flood

Hypothesis. Geological Society of America Special Paper 473, p. 189-196, doi: 10.1130/2011.2473(12).

Casson, L., 1995. Ships and Seamanship in the Ancient World. Johns Hopkins University Press, London.

Coleman, D.F. and Ballard, R.D., 2004. Archaeological Oceanography of the Black Sea, in: Akal, T., Ballard, R.D., and Bass, G.F., eds., The Application of Recent Advances in Underwater Detection and Survey Techniques to Underwater Archaeology. Uluburun Publishing, Istanbul.

Culha, M., 2010. The presence of *Teredo navalis* Linnaeus, 1758 (Mollusca, Bivalvia, Teredinidae) in the southern Black Sea, Turkey. *Journal of Animal and Veterinary Advances* 9, 1515-1518.

Davis, D.L., 2009. Commercial Navigation in the Greek and Roman World. Ph.D. Dissertation, University of Texas at Austin.

DeAlteris, J., Skrobe, L., Lipsky, C., 1999. The significance of seabed disturbance by mobile fishing gear relative to natural processes: A case study in Narragansett Bay, Rhode Island. *American Fisheries Society Symposium* 22, 224-237.

Doonan, O.P., 2004. Sinop Landscapes: Exploring Connections in a Black Sea Hinterland. University of Pennsylvania Museum of Archaeology and Anthropology, Philadelphia.

Duman, M., Duman, S., Lyons, T.W., Avci, M., Izdar, E., Demirkurt, E., 2006. Geochemistry and sedimentology of shelf and upper slope sediments of the south-central Black Sea. *Marine Geology* 227: 51-65.

Empereur, J.-Y. and Picon, M., 1986. A la recherché des four d'amphores, in: Empereur, J.-Y., and Y. Garlan, eds., Recherches sur les amphores grecques. Actes du Colloque International organisé par le Centre National de la Recherche Scientifique, L'Université de Rennes II et L'École Française d'Athènes, 10–12 Septembre 1984. BCH Supplement 13. École Française d'Athènes, Athènes.

Empereur, J.-Y. and Tuma, N., 1988. Zénon de Caunos et l'épave de Serçe Limani. *BCH* 112, 341-357.

Filonov, A.E., 2000. Thermic structure and intense internal waves on the narrow continental shelf of the Black Sea. *Journal of Marine Systems* 24, 27–40.

Gajdukevich, V.F., 1969. On How Ancient Greek Ships Sailed Across the Pontus Euxine. *KSIA* 116, 11–19 (in Russian).

Glazer, B.T., Luther, G.W. III, Konovalov, S.K., Friederich, G.E., Nuzzio, D.B., Trouwborst, R.E., Tebo, B.M., Clement, B., Murray, K., Romanov, A.S., 2006a. Documenting the suboxic zone of the Black Sea via high-resolution real-time redox profiling. *Deep-Sea Research II* 53, 1740-1755.

Glazer, B.T., Luther, G.W. III, Konovalov, S.K., Friederich, G.E., Trouwborst, R.E., Romanov, A.S., 2006b, Spatial and temporal variability of the Black Sea suboxic zone. *Deep-Sea Research II* 53, 1756-1768.

Goitein, S.D., 1999. A Mediterranean Society: The Jewish Communities of the World as Portrayed in the Documents of the Cairo Geniza. Vol. 1, Economic Foundations. University of California Press, Berkley.

Hind, J.G.F., 1988. The Colonisation of Sinope and the S.E. Black Sea Area, in: Mestnye etnopoliticheskie obedineniya Prichernomor'ya VII-IV vekakh do n.e., Materialy IV Vsesoyuznogo Sympozyuma po drevnej istorii (Tblisi) 207-23.

Isager, S. and Hansen, M.H., 1975. Aspects of Athenian Society in the Fourth Century B.C. Odense University Press, Odense.

Johnson-Roberson M., Pizarro O., Williams S.B., Mahon I.J., 2010. Generation and Visualization of Large-Scale Three-Dimensional Reconstructions from Underwater Robotic Surveys. *Journal of Field Robotics* 27(1), 21-51.

Kac, V.I., Monachov, S.Y., Stolba, V.F., Shcheglov, A.N., 2002. Tiles and ceramic containers, in: Hannestad, L., V.F. Stolba, and A.N. Shcheglov, eds., Panskoye I. Vol.1. The Monumental Building U6. Aarhus University Press, Aarhus, pp. 101-126.

Kuscu, I., Parke, J.R., White, R.S., McKenzie, D., Anderson, G.A., Minshull, T.A., Gorur, N., Sengor, A.M.C., 2004. Active slumping offshore Amasra (southwest Black Sea) and its relation with regional tectonics. *Bulletin of the Mineral Research and Exploration* 128, 27-47.

Luth U. and Luth, C., 1998. Benthic meiofauna and macrofauna of a methane seep area South-west of the Crimean Peninsula, Black Sea. In: Luth U., Luth C., Thiel H., eds., MEGA-SEEPS- Methane Gas Seeps Exploration in the Black Sea. Berichte aus dem Zentrum fuer Meeres-und Klimatoforsch, Hamburg: 14, 59-77.

Maximova, M.I., 1959. Der Kurze Seeweg über das Schwarze Meer im Altertum. *Klio* 37, 101-118.

McNinch, J.E., Wells, J.T., Trembanis, A.C., 2006. Predicting the fate of artefacts in energetic, shallow marine environments: An approach to site management. *International Journal of Nautical Archaeology* 35, 290-309.

Micu, D., 2007. Recent records of *Pholas dactylus* (Bivalvia: Myoida: Pholadidae) from the Romanian Black Sea, with considerations on its habitat and proposed IUCN regional status. *Acta Zoologica Bulgarica* 59, 267-273.

Monachov, S.Y., 1989. Amfory Chersonesa Tavricheskogo IV-II vv. Do n.e. Opyt sistemnogo analiza. Saratov (in Russian).

Monachov, S.Y., 1992. Dinamika form i standartov sinopskih amfor, in: Grecheskie amfor'. Saratov, (Capatob) pp. 163-204 (in Russian).

Monachov, S.Y., 1999. Grecheskis amfory v Prichernomor'e: kompleksy keramicheskoiy tary VII-II vv. do n.e. Saratov (Capatob) (in Russian).

Murray, J.W., Jannasch, H.W., Honjo, S., Anderson, R.F., Reeburgh, W.S., Top, Z., Friedrich, G.E., Codispoti, L.A., and Izdar, E., 1989, Unexpected changes in the oxic/anoxic interface in the Black Sea *Nature* 338, 411-413.

Murray, J.W., Stewart, K., Kassakian, S., Krynytzky, M., and DiJulio, D., 2007, Oxic, suboxic, and anoxic conditions in the Black Sea, in: Yanko-Hombach, V., Gilbert, A.S., Panin, N., and Dolukhanov, P.M., eds., The Black Sea flood question: Changes in coastline, climate and human settlement: Dordrecht, Springer, p. 1-22.

Newman, J.B., Gregory, T.S., Howland, J., 2008. The development of towed optical and acoustical vehicle systems and remotely operated vehicles in support of archaeological oceanography, in: Ballard, R.D., ed., Archaeological Oceanography. Princeton University Press, Princeton, pp. 15-29.

Oguz, T., La Violette, P.E., Unluata, U., 1992. The upper layer circulation of the Black Sea: Its variability as inferred from hydrographic and satellite observations. *Journal of Geophysical Research* 97, 12569-12584.

Olenin, S. and Leppakoski, E., 1999. Non-native animals in the Baltic Sea: alteration of benthic habitats in coastal inlets and lagoons. *Hydrobiologia* 393, 233-243.

Opaiţ, A., 1997-1998. New pottery from the circular harbour at Carthage. *CEDAC Carthage* 18, 21–35.

Opaiţ, A., 2010. On the origin of Carthage LR Amphora 1, in: Menchelli, S., Santoro, S., Pasquinuci, M., Guiducci, G., eds., LRCW3. Late Roman Coarse Wares, Cooking Wares and Amphorae in the Mediterranean (BAR-IS 2185), 1015-1022.

Opaiţ, A., 2010. Sinopean, Heraklean and Chersonesan "Carrot" Amphorae" *Ancient Civilizations from Scythia to Siberia* 16, 371-401, 552-556.

Richards B.R., Hillman, R.E., and Maciolek, N.J.. 1984. Shipworms, in: Kennish M.J., Lutz, R.A., eds., Lecture Notes on Coastal and Estuarine Studies - Ecology of Barnegat Bay, New Jersey. Springer-Verlag, New York, pp. 201-225.

Robinson, D., 1906. Ancient Sinope. *American Journal of Philology* 27, 125-53, 245-79.

Roman, C. and Singh, H., 2007. A Self-Consistent Bathymetric Mapping Algorithm. *Journal of Field Robotics* 24, 23-50.

Ryan, W.B.F., Pitman, W.C. III, Major, C.O., Shimkus, K., Moskalenko, V., Jones, G.A., Dimitrov, P., Görür, N., Sakınç, M., Yüce, H., 1997. An abrupt drowning of the Black Sea shelf. *Marine Geology* 138, 119–126.

Saprykin, S.J., 1997. Heracleia Pontica and Tauric Chersonesus before Roman Domination: VI-I Centuries B.C. A.M. Hakkert, Amsterdam.

Sergeeva N.G., 2003. Meiobenthos in the region with the methane gas seeps, in: Eremeev V.N., Gaevskaya A.V., eds., Present Time Conditions of Biological Diversity in the Nearshore Zone of Crimea Peninsula (the Black Sea sector). Ecosi-Gidrophizika, Sevastopol, pp. 258-267 (in Russian).

Sergeeva N.G. and Gulin, M.B., 2007. Meiobenthos from an active methane seepage area in the NW Black Sea. *Marine Ecology* 28, 152-159.

Trembanis, A., Skarke, A., Nebel, S., Coleman, D.F., Ballard, R.D., Fuller, S.A., Buynevich, I.V., and Voronov, S., 2011, Bedforms, hydrodynamics, and scour process observations from the continental shelf of the northern Black Sea, in: Buynevich, I., Yanko-Hombach, V., Gilbert, A., and Martin, R.E., eds., Geology and Geoarchaeology of the Black Sea Region: Beyond the Flood Hypothesis. Geological Society of America Special Paper 473, pp. 165-178, doi: 10.1130/2011.2473(10).

Trouwborst, R.E., Clement, B.G., Tebo, B.M., Glazer, B.T., Luther, G.W., 2006. Soluble Mn in suboxic zones. *Science* 313, 1955-1957.

Ünal, V., 2004. Viability of trawl fishing fleet Foca (the Aegean Sea), Turkey and some advices to central management authority. *Turkish Journal of Fisheries and Aquatic Sciences* 4, 93-97.

Vnukov, S.Y., 2003. Prichernomorskie amfory I v. do n.e.–II v. n.e. (morphologiya), Vol. I. Institut arkheologii RAN, Moscow (in Russian).

Ward, C. and Ballard, R., 2004. Black Sea shipwreck survey 2000. I*nternational Journal of Nautical Archaeology* 33, 2-13.

Ward, C. and Horlings, R., 2008. The remote exploration and archaeological survey of four Byzantine ships in the Black Sea, in: Ballard, R.D., ed., Archaeological Oceanography. Princeton University Press, Princeton, pp. 148-173.

Zeest, I.B., 1960. Keramicheskaya tara Bospora. Izd-vo Akademii nauk SSSR, Moscow (in Russian).

Table 2.1. Black Sea shipwrecks

Wreck	Depth (m)	Date	O2 (μM)	Trawled	Cargo
Sinop A	105*	mid 5th century AD	5.82	Yes	Amphorae
Sinop B	107*	mid 5th century AD	2.07	Yes	Amphorae
Sinop C	102*	mid 5th century AD	3.85	Yes	Amphorae
Sinop F	105	late 5th century AD	5.68	Yes	Amphorae
Sinop G	100	17th-19th century	5.59	No	Not apparent
Sinop H	103	17th-19th century	6.03	No	Not apparent
Sinop I	109	1st century A.D.	4.35	No	Amphorae
Ereğli A	103	17th-19th century	5.93	Yes	Not apparent
Ereğli B	112	17th-19th century	5.22	Yes	Not apparent
Ereğli C	112	6th century AD	3.90	Yes	Not apparent
Ereğli D	114	17th-19th century	1.95	No	Wood
Ereğli E	101	late 4th century B.C.	5.47	Yes	Amphorae

*Depths reported in Ballard et al. (2001) and subsequent publications do not correlate with depths logged in 2011.

Figures

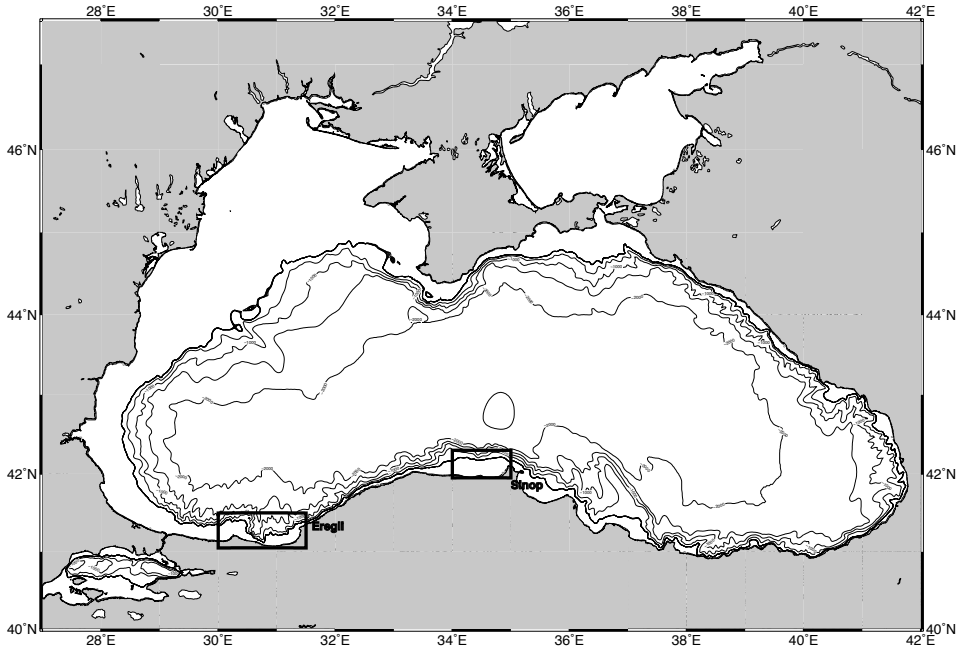

Figure 2.1. Map of Black Sea showing survey locations off Ereğli and Sinop, Turkey. Bathymetry data (in m) from the GEBCO_08 Grid, version 20091120, http://www.gebco.net.

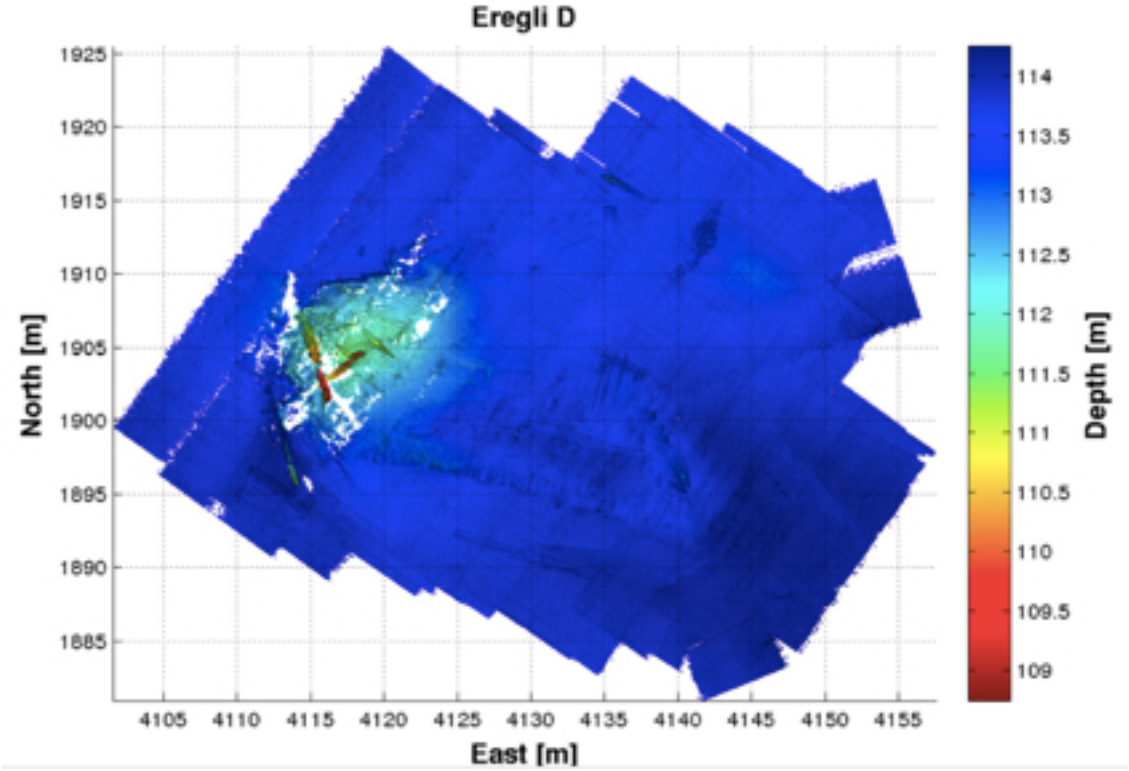

Figure 2.2. Complete bathymetric map of the Ereğli D wreck site made with the 2250 kHz multbeam data taken during the survey. All tracklines were run with the vehicle maintaining a constant heading and altitude of 3 m. A second pass at an altitude of 8.5 m was conducted over the higher-relief section of the wreck.

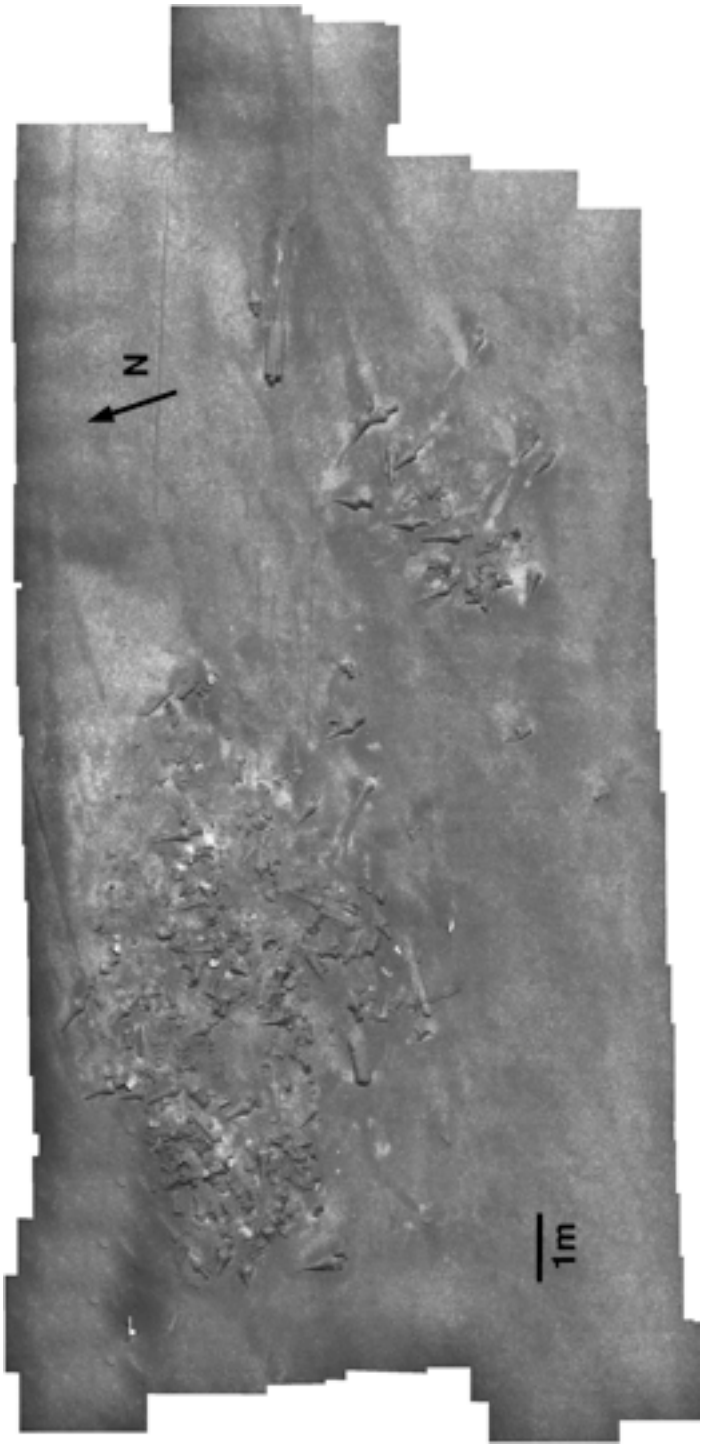

Figure 2.3. Composite 3D texture maps of the Sinop A wreck site made with the stereo cameras.

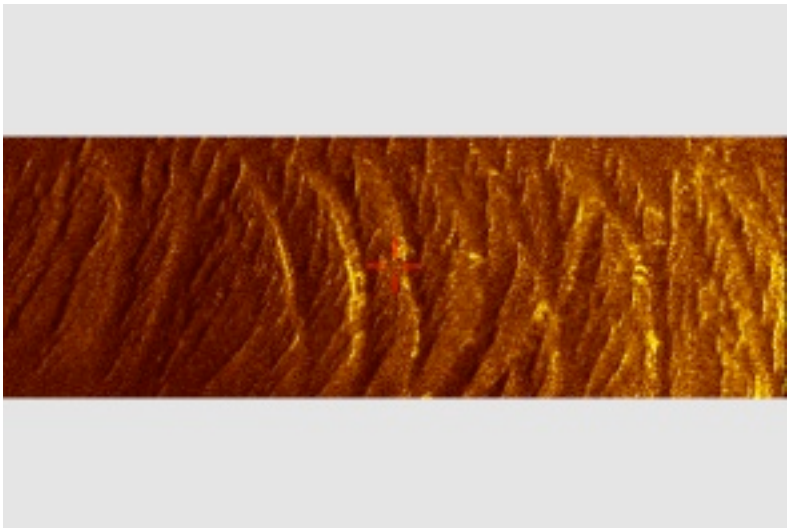

Figure 2.4. Side-scan sonar waterfall image of megaripple bedforms at 200 m depth off Sinop, Turkey.

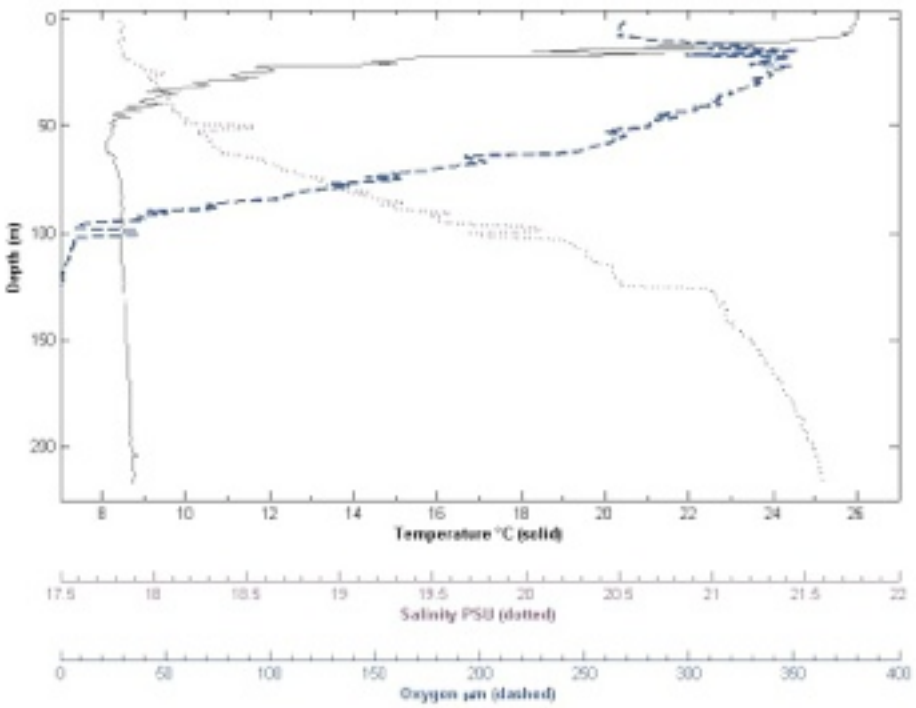

Figure 2.5. Salinity, temperature, and dissolved oxygen versus depth for ROV descents through the water column in the Black Sea.

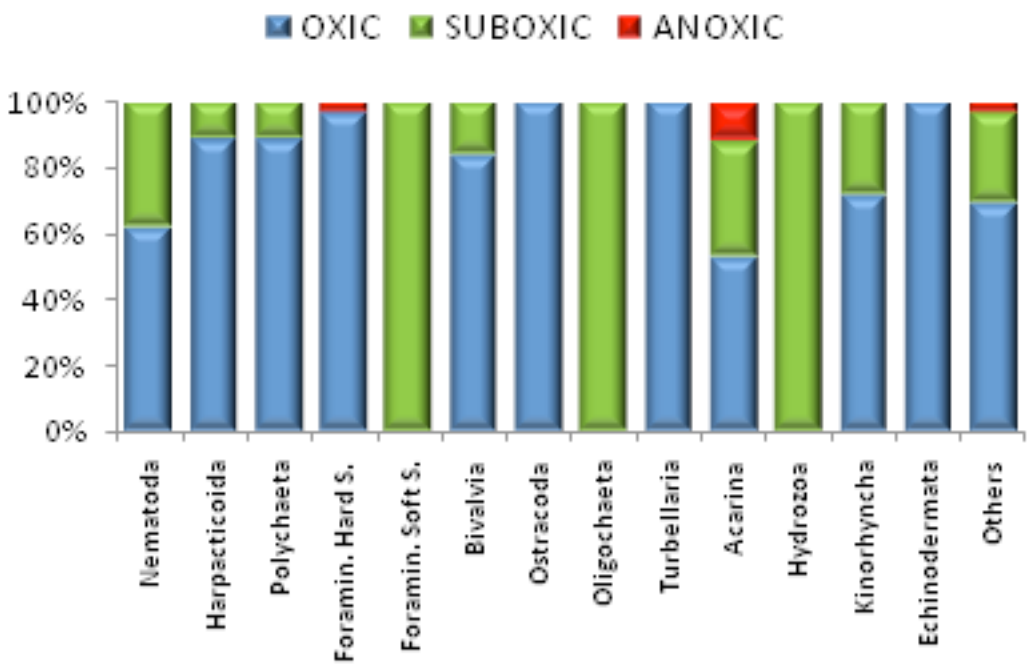

Figure 2.6. Contribution (%) of main taxa to total meiobenthos in cores from the three water layers.

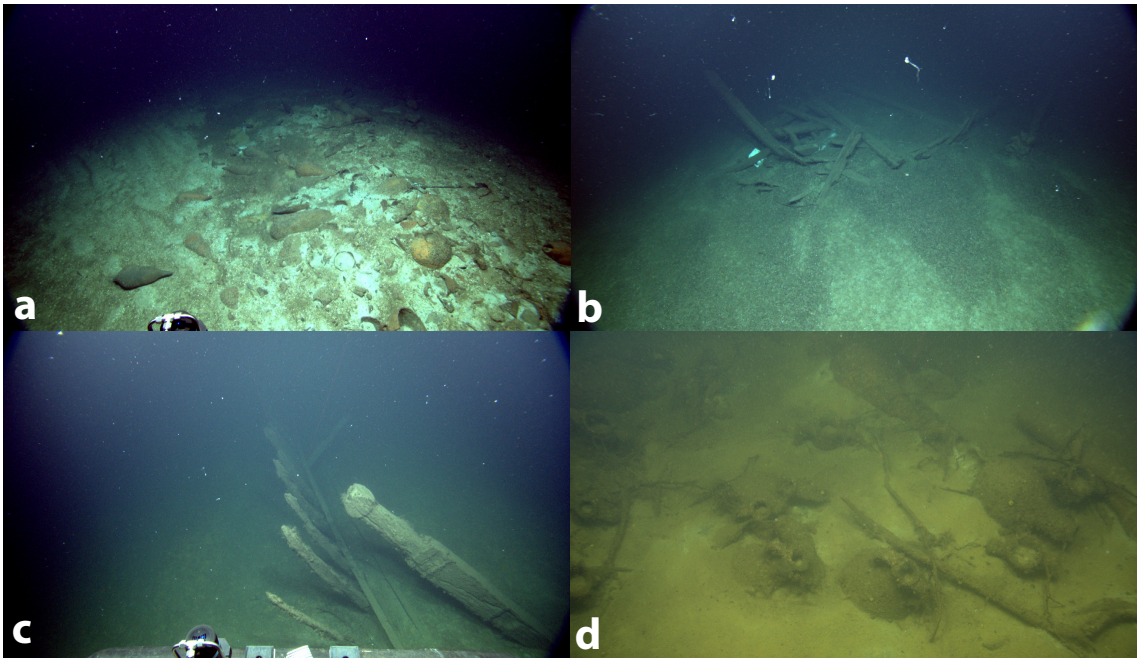

Figure 2.7. High definition video captures of wreck sites (a) Sinop F; (b) Sinop G; (c) Sinop H; (d) Sinop I. ©IFE/COE

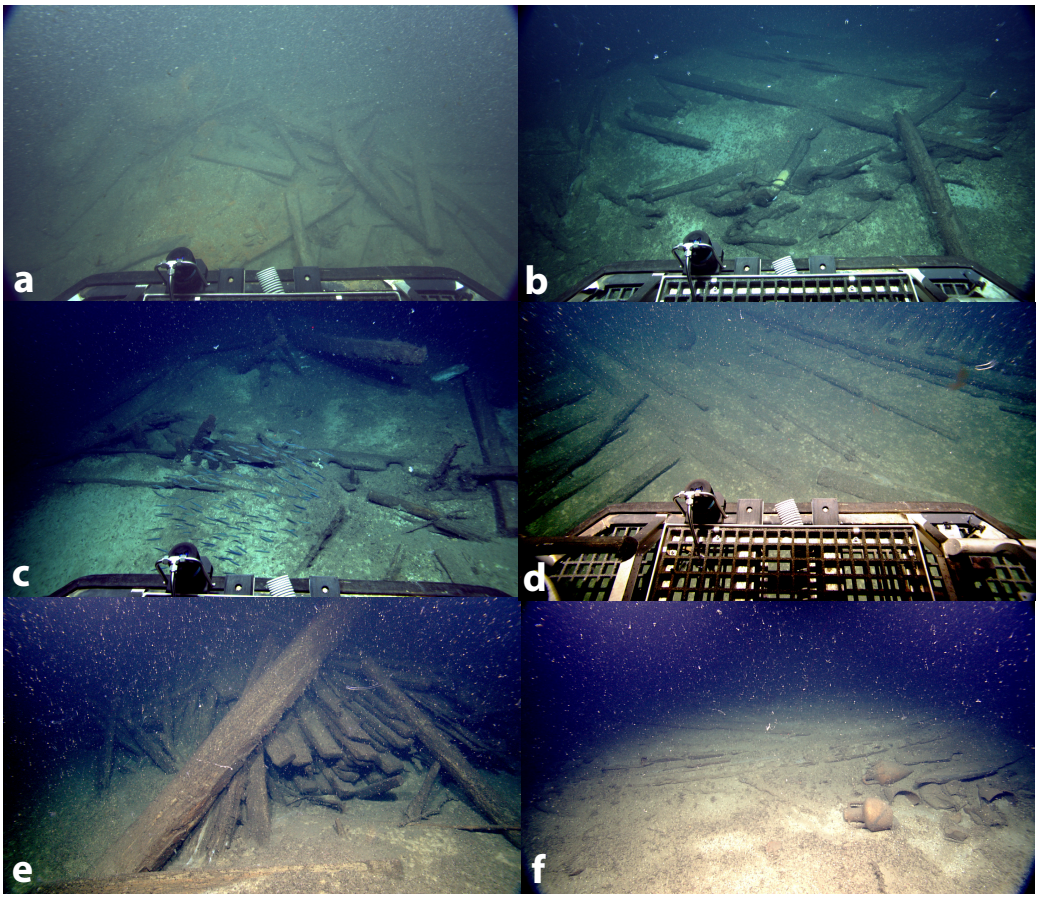

Figure 2.8. High definition video captures of wreck sites (a) Ereğli A; (b) Ereğli B; (c) Ereğli C; (d) Ereğli D; (e) wood pile on Ereğli D; (f) Ereğli E. ©IFE/COE

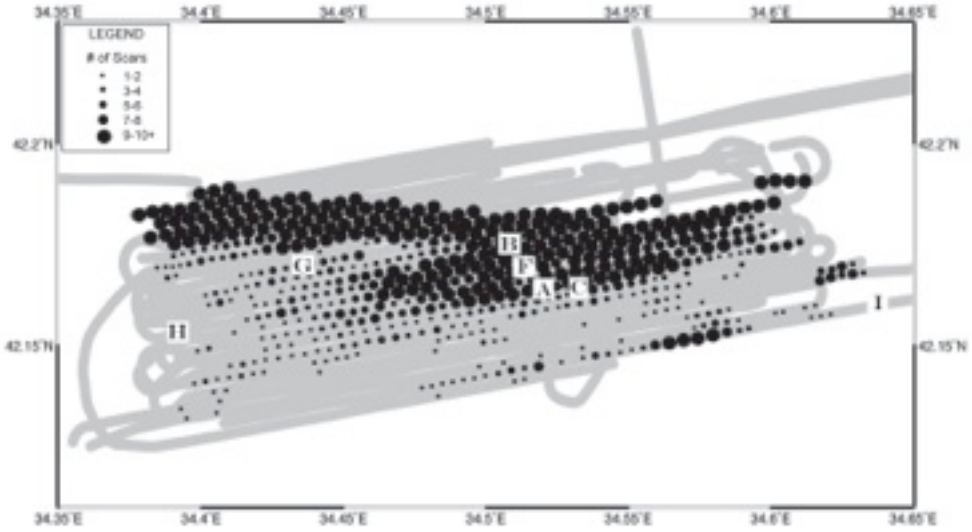

Figure 2.9. Map of survey area west of Sinop showing the extent and intensity of trawl scarring and the locations of shipwrecks.

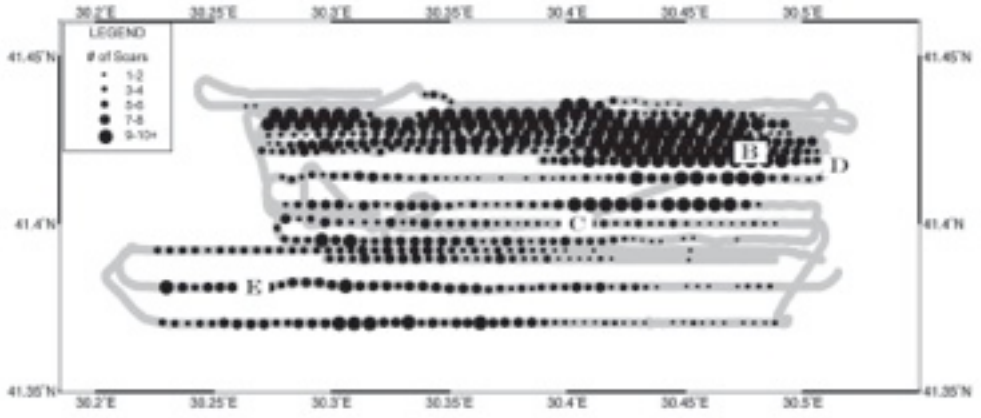

Figure 2.10. Map of survey area west of Ereğli showing the extent and intensity of trawl scarring and the locations of shipwrecks.

CHAPTER 3

Preliminary geochemical assessment of limestone resources and stone use at Maya sites in the Three Rivers Region, Belize

Prepared for submission to *Journal of Archaeological Science*, March 2012

Michael L. Brennan[a], Eleanor M. King[b], Leslie C. Shaw[c], Stanley L. Walling [d], Fred Valdez, Jr.[e]

[a]Graduate School of Oceanography, University of Rhode Island, Narragansett, RI, USA
[b]Department of Sociology and Anthropology, Howard University, Washington D.C., USA
[c]Department of Anthropology, Bowdoin College, Brunswick, ME, USA
[d]Department of Social Sciences, Community College of Philadelphia, USA
[e]Department of Anthropology, University of Texas at Austin, USA

Corresponding Author:
Michael L. Brennan
Graduate School of Oceanography
University of Rhode Island
South Ferry Road, Box 200
Narragansett, RI 02882
mlbrennan@gso.uri.edu
(401) 874-6186 office
(860) 777-6181 cell

3.1 Abstract

The carbonate bedrock of northwestern Belize is poorly understood both geochemically and from the standpoint of the use of stone as the building blocks of ancient Maya sites and monuments. This research analyzed 67 limestone samples collected from sites in the Three Rivers Region of Belize with ICP-MS and ICP-AES to characterize the major, minor, and trace element chemistry of the bedrock of the region. Bedrock, quarry, and possible monuments were sampled for this study for the purposes of tracing the movement of monument stone to either the local bedrock or quarries, or to determine if it was imported from outside of the sites' core. At Chawak But'o'ob along the flank of the Rio Bravo, changes downslope in Mg concentration suggest a leaching of the bedrock by meteoric waters based on differences in porosity. However, at Maax Na, a hilltop site, such leaching is not as apparent. Many monuments were found to be composed of stone with the same trace element chemistry as the bedrock, although this does not preclude them from being monuments. A few monuments were shown to be composed of material with a different chemical composition than the local bedrock, which included some of the stelae at Maax Na, and appear to have been made of stone imported from outside the site.

3.2 Introduction

Investigations of stone use patterns at archaeological sites rely on interpretations of a modern landscape that, in many cases, has been heavily modified by natural processes since the time of the sites' abandonment. Therefore, such research requires an understanding of the local geology on both intra-site and regional scales. This is especially important in rainforest-covered areas, such as the Yucatan Peninsula, where a lack of bedrock exposures and restricted access has inhibited formal geological studies. Geological research in this region benefits from the landscape modifications at archaeological sites, as the Maya extensively quarried areas on the periphery of site centers, which provide a large number of accessible bedrock exposures. This study looks at two Maya sites in different karst environments of the Three Rivers Region of northwestern Belize (Figure 3.1) to characterize the intra-site geochemical variability in the limestone bedrock, and also to begin to address differences on a regional scale. The bedrock of this area is soft and easily weathered, making it difficult to identify megaliths on the rainforest floor as fallen stelae or rock that has spalled off the bedrock by natural processes. The geochemical investigation of local variations in the bedrock chemistry help determine the ways in which the Maya modified the landscape and the movement of stone to create their constructed environment.

3.2.1 Geology of Northern Belize

Limestones are both a paleoenvironmental deposit and a modern landform, as the morphology and chemistry of these rocks reflect both formation conditions and the effects of post-diagenesis weathering processes. Carbonates dissolve in acidic waters, but

do not dissolve at equal rates, which is dependent on joints and fractures in the bedrock, as well as porosity (Trudgill, 1985). Geological investigation of the carbonate bedrock is therefore important for understanding both paleo- and modern landscapes. However, the stratigraphic sequence of rock formations in northern Belize have not been formalized and may require further study (King et al., 2004). The limestones of the northeastern Peten region of Guatemala and northwestern Belize appear to be the same formation, which was described separately by two authors as the El Cayo and Santa Amelia groups (Flores, 1952; Vinson, 1962). In a report summarizing the geological surveys conducted for the geological map of Belize, Flores (1952) provided only informal descriptions of the stratigraphy in northern Belize. Based on these descriptions, the Three Rivers Region is composed of the Lower Eocene limestone of the El Cayo Group. Similarly, in a report on the petroleum geology of the area, Vinson (1962) defined the Santa Amelia Formation as extending from the central Peten region of northern Guatemala towards the northeast into the northern half of Belize. Thus, both formations of interest seem to incorporate the area of northwestern Belize.

The Yucatan peninsula is a carbonate platform composed of shallow water sediments of the Jurassic through Tertiary periods (Hartshorn et al., 1984). These limestones are formed from shallow water, back-reef lagoonal environments (e.g., King et al., 2004; Vinson, 1962). A report on the physical properties of Yucatan limestones demonstrates a large amount of heterogeneity in their physical and mechanical properties, characteristic of those formed in shallow tropical seas (Espinosa et al., 1998). The stepped escarpment topography of this area on the northeastern edge of the Peten plateau is the result of compressional faulting, which has drastically altered the carbonate

landscape (Dunning et al., 2003). Weathering and karstification processes caused by the exposure of underlying carbonate strata add to the variability in composition, density, and porosity of the bedrock (Trudgill, 1985). Since its deposition, the limestone has been weathered into fractured formations of ridges and hills. Around the perimeter of these uplands are a series of swampy lowlands (*bajos*), which were used for resource procurement by the Maya (Dunning et al., 2003; Kunen, 2004; Kunen and Hughbanks, 2003).

3.2.2 Stone Use and the Maya

The relationship between people and their natural environment has drawn increasing interest over the past few decades as environmental archaeology has developed, encompassing many multidisciplinary fields, such as geoarchaeology, as an approach to investigating archaeological landscapes (e.g., David and Thomas, 2008; Denham, 2008; Dincauze, 2000; Knapp and Ashmore, 1999). Aston and Rowley (1974) described landscape as a palimpsest on which generations leave their mark as they build upon and overwrite those of previous generations. For both environmental and landscape studies, this can be extended for abandoned sites into the present day. Lowland Maya sites have seen multiple periods since their abandonment that have left their mark and overprinted much of the original sites, including rainforest reclamation following the Maya period, deforestation in the eighteenth century due to inland mahogany logging (Bolland, 1977), and a second period of subsequent regrowth. These factors, along with karst processes and weathering over time, have created what we see today as the modern landscape of these sites. The masking of the ancient landscape becomes compounded for

studies of Maya stone use at sites in northern Belize, where the limestone bedrock is soft and highly weathered, and as such, so too are monuments that were constructed with it.

For Maya studies, environmental and landscape archaeology are closely tied, as their architecture and engineering typically built upon and accentuated, but rarely overwrote, the natural landscape (Brady and Ashmore, 1999). Understanding how the Maya visualized their world requires a broad grasp of how their constructed environment reflected their worldview, including elements of their civic plans and ceremonial landscapes, which often overlapped (Ashmore, 1991, 2008; Knapp and Ashmore, 1999). In many cases, natural features of the landscape were strategically incorporated into a site's civic plan, such as when a site was built around a cave as an *axis mundi* (Ashmore, 2008; Brady and Ashmore, 1999). The Maya constructed environment was also heavily influenced by quarrying and water management engineering. Sites that utilized natural hills, such as La Milpa, required artificial reservoirs because they were built away from water sources (Scarborough, 1995). Quarries around the periphery of these hills were used as part of the construction plan and often incorporated into the water management system (Scarborough, 1998). Stone from the excavation of reservoirs was used to construct adjacent temples and structures, while other areas of natural topography were engineered into a flat surface by cutting away or filling in. The creation of such "water mountains" exhibits the Maya's ability to shape and engineer their natural landscape as physical representations of their worldview (Scarborough, 1995, 1998). Throughout Mesoamerica, water was associated with the underworld, accessible by caves in the bedrock, illustrating the important relationship between water sources and the geological landscape in the Maya worldview (e.g., Brady 1997).

The built environment of the Maya was composed predominantly of limestone, with exceptions in highland areas in the southern lowlands, as at Copan, where igneous tuff was also used (Abrams, 1994). In addition to architectural blocks, limestone was also burned to produce lime, a component of plaster, which was used as a surface finish on architecture and plazas where the landscape was filled in and smoothed over (Villaseñor, 2010). Studies of Maya stone use have focused on both the energetics of labor required for quarrying and construction (e.g., Abrams, 1994; Folan, 1982; Woods and Titmus, 1996) and the production of plaster (e.g., Mathews, 2002; Villaseñor, 2010). Quarries were commonly positioned near areas of construction, suggesting that stone would not have needed to be transported over large distances (Folan, 1982). For example, at the site of Kinal in Guatemala, extensive quarrying was observed along the margins of the central precinct (Scarborough et al., 1994). However, studies of the movement of stone per se across the Maya landscape is limited to artifacts. Granite and obsidian artifacts have been geochemically traced back to specific igneous sources in the highlands (e.g., Graham, 1987; Rice et al., 1985), but limestone is harder to source. Studies have successfully sourced the movement of limestone only on a small scale. Barba et al. (2009) used X-ray Fluorescence (XRF) to source lumps of limestone from plaster floors at Teotihuacan to local quarries. Nation et al. (n.d.) used Inductively Coupled Plasma Mass Spectrometry (ICP-MS) to establish the provenience of speleothem artifacts from excavations to specific caves in southern Belize after chemically characterizing the limestone of multiple cave sites. Similarly, this study aims to characterize the geochemistry of limestone bedrock formations from two Maya sites in the Three Rivers Region of northern Belize to assess the potential for mapping the movement of quarried stone on a site scale.

The sites in the Three Rivers Region of northwestern Belize have been defined as resource-specialized communities, a term that emphasizes the dependency relationships between sites of varying sizes and functions (Scarborough and Valdez, 2003). This region is also used as a prime example of a heterarchical social structure, which shows how the sites in this area developed in an unranked system as a result of its dispersed resources (Scarborough, Valdez, and Dunning, 2003). Kunen and Hughbanks (2003) show that sites located near important resources developed systems of specialized production through the procurement and use of those resources. The Three Rivers Region contains a large number of sites, including large centers, such as La Milpa and Dos Hombres, and mid-level sites, such as Las Abejas and Bolsa Verde, which may have acted as intermediaries between the larger sites (Tourtellot et al., 2003). An important feature of this region are the extensive *bajo* drainage areas that controlled both site locations as well as resources. Kunen (2004) defined three distinct zones for which the Maya had different uses: residential on hilltops, agricultural on terraced slopes, and resource-extractive in the interior. Space at hilltop centers, such as La Milpa and Maax Na, was limited to the plateaus upon which they were built, so the space had to be used effectively, planning both architectural construction and resource procurement around one another for both stone acquisition and shaping terrain. Terraced hillsides and low-lying *bajos* provided highly varied landscapes for modification to aid the Maya settlement in a seasonally dynamic environment and for access to resources such as clay and chert. This diversity of landscapes and resources makes this region an important area for studying the role of the Maya's natural and built environments (Scarborough and Valdez, 2003).

This research looks at the bedrock geochemistry of the sites of Maax Na, a large center on a hilltop near the Guatemalan border, and Chawak But'o'ob, a smaller residential site near the Rio Bravo (Figure 3.1). By examining the modern landscapes of the areas of these two sites through the geochemistry of Eocene limestone formations, we can begin to infer Classic Maya stone use patterns and movement of quarried material across the site. These sites provide good access to bedrock exposures that is not found in other areas of the rainforest-covered Peten plateau. This study is also important for this area because of the highly weathered condition of the soft limestone, making the discrimination between natural megaliths and man-made monuments difficult. The modern condition of the landscape - uplifted carbonate deposits, weathered rock, eroded quarry faces, and the rainforest cover - reflects some aspects of the ancient, overprinted landscape, but requires geochemistry to be to able to investigate it. Due to the soft nature of the limestone bedrock in this area, monuments were largely uncarved, with the exception of some at La Milpa. It is therefore difficult to interpret the ancient landscape and, most importantly, how the Maya modified it and moved quarried stone across the landscape. The objective of this research is to examine the geochemical data from bedrock samples at these two sites to determine the intra-site variability, then compare these to samples taken from possible monuments, some of which can be sourced to quarry locations at these sites or determined to be composed of rock that is foreign to these sites' underlying bedrock.

Maax Na

Maax Na was initially mapped in 1996 as part of a Programme for Belize Archaeology Project survey (Shaw and King, 1997). Long-term goals of the research include looking at the site through an integration of economic, political, and ideological spheres in order to examine multidimensional relationships in the region (King and Shaw, 2003). The site, an Early to Late Classic center (300-800 AD), follows a similar construction pattern to large site centers such as La Milpa and Dos Hombres (Figure 3.1), as well as others in the Peten region of Guatemala, but exhibits some unique features for the Three Rivers region. Most notable are the large reservoir located centrally and the expansive North Plaza (Figure 3.2). This plaza is broad and empty in relation to other sites, and is larger than those at all other centers in the region with the exception of La Milpa (Shaw et al., 1999). The site dates to the Early Classic (300-600 AD), with possible small-scale occupation in the Late Preclassic (250 BC-AD 300), and appears to have been abandoned early before construction was finished. Structures border the North Plaza, but with a less dense spacing than at La Milpa. Also unlike Dos Hombres and La Milpa, Maax Na's main temple is isolated and positioned to the south of the site core juxtaposed to the North Plaza in line with the ball court (King and Shaw, 2003). The North and West Plazas are linked by a causeway that extends past the main temple and upon which Stela 2, the only standing stela remaining at the site, was erected.

The Maya placement of architecture and their constructed landscapes was greatly influenced by cosmology (Ashmore, 1992). The layout of Maax Na follows common trends in site planning including a north-south axis linked by a ballcourt and the use of

causeways to link groups of structures. Additionally, the site has a number of caves and rock shelters, which are thought to have been linked to the underworld in Maya cosmology (Brady, 1997). Maax Na does not fit the Peten-style site plan identified by Houk (2003). While it has the north-south axis running through the ballcourt toward the large temple in the south, the site appears to have been intentionally positioned at this location on the plateau in alignment with cave features, helping to define the layout of the site based on this cosmological influence (King and Shaw, 2003; King et al., under review).

Surveys at Maax Na have further documented areas on the periphery of the site that include a large number of what are interpreted as quarry sites. In addition to the knolls near the reservoir, other quarries have been located to the west and north of the North Plaza and east of the main temple. Other parts of the site, especially on the periphery of the site core, appear to have been modified, likely in part due to quarrying activities. Small-scale water management features may have been associated with some quarries, as keeping limestone moist allows for easier cutting (Scarborough et al., 1995). These features are exposed at Maax Na to a greater extent than many other sites in the area; they may not have been as well masked by architecture due to the site's relatively rapid construction or early abandonment. For this reason, Maax Na is the ideal site within the Three Rivers Region at which to conduct this study, as its location on a hilltop and numerous quarries around the edge from the site's construction allow for broad sampling across the area of the site core.

Chawak But'o'ob

Chawak But'o'ob is a small residential, agricultural site located on the inclined slope of the Rio Bravo Escarpment about 7 km southeast of Maax Na, across the Rio Bravo from the large center of Dos Hombres (Figure 3.1). This mid-late Late Classic (600-800 AD) site consists of residential terraces, dense commoner housing, and series of complex water management features (Walling, 2005). Research here has uncovered primarily utilitarian artifacts and no formal ritual or elite structures. The number of houses constructed in the short period of time at this site suggest that there was a rapid population growth, driven by an influx of immigrants to the area (Walling, 2005). A ballcourt at the southern extent of the site is one of the few ceremonial structures, which was constructed as two mounds of small cobbles and appears to have had water running through it. The ballcourt is in line with one of the two caves present at the site.

The slope of the site on the escarpment places it in an active karst region where water flows through the bedrock toward the Rio Bravo. The Maya constructed a series of terraces, collection surfaces, interconnected water basins, and a central reservoir to direct the water to the occupation and agricultural areas further down the escarpment (Walling, 2005). This site serves as a good comparison to Maax Na on two fronts. First, the small nature of this site, in comparison to the large center of Maax Na, showcases a different aspect of Maya culture. Second, the carbonate environment of Chawak But'o'ob differs dramatically from the plateau upon which Maax Na sits, and is dominated by ridges and drainage gullies from the movement of water over the bedrock. However, both sites lie within the same drainage system of the Rio Hondo, so comparisons are between different

karst landscapes, but over a similar hydrological region and of the same limestone formation.

3.3. Methods

3.3.1 Sampling

Maax Na

Since few studies have attempted the geochemical sourcing of limestone from an archaeological context, the goal of this research was first to determine if discrimination between different bedrock samples is possible. A survey of the limestone resources and features at Maax Na was undertaken during the 2005 and 2006 field seasons. To begin this process, limestone samples were collected throughout the site core of Maax Na (Figure 3.2), including multiple locations where samples were taken both from megaliths identified as possible monuments and from the adjacent bedrock. The samples were chiseled off the stone with a hammer and collected in labeled bags with both a description of the stone and the zone code for the area of the site. In the case of known monuments, such as still-erect stela, we only took a sample of the stone if pieces had already spalled or broken off and could be collected without further damaging the monument. At least one sample was taken from as many of the accessible bedrock outcrops as possible within the 1 km^2 area of the site core. A few duplicate samples were discarded in the field due to weight limitations for their export.

Seven samples were taken from and around Megalith I (Figure 3.3), which is located southeast of the West Plaza adjacent to a linear series of chultuns (Shaw, 2002). Nine samples were taken from outcrops and possible monuments on the South Acropolis,

including a series of small, approximately 50 cm diameter stones, some of which may have had a plaster facing, and the underlying bedrock. Six samples came from megaliths and outcrops east of the main temple, including a large section of limestone that may have been uplifted by a tree-fall, and also from Stela 1, one of the few positively identified stelae at the site. In the North Plaza, a total of seven samples were collected, including one from a beveled stone removed from the face of the ballcourt during excavations in 2003. Other locations sampled here include a possible altar in the plaza north of the ballcourt, a possible monument east of the North Hill, and samples from inside and outside Spider Cave, the largest cave at the site, which is beneath the East Structure (King and Shaw, 2003; King et al., under review). Six samples were collected from a quarried area north of the North Plaza, including two possible monuments. The final area sampled during this survey is the West Plaza, where seven samples were collected. Features included Altar 2 in Plaza D, a quarried area behind the West Acropolis, two quarried knolls bordering the reservoir entrance, and a series of possible monument bases, similar to those found in the South Acropolis, behind the south buildings of the West Plaza.

Chawak But'o'ob

In June 2007, a similar survey of the limestone bedrock outcrops and possible stone monument features was undertaken at Chawak But'o'ob (Figure 3.4). Twenty-two samples were collected, primarily from bedrock outcrops along the sloped terrain of the site. Samples of cultural features included three cobbles from the ballcourt, a small spalled-off chip from a possible stela in Group A, and possible plaster from beneath this

megalith. Drainage features in the southern area of the site were included in the sampling, as was a knoll west of the ballcourt, and outcrops along the edge of the reservoir and other water management features at the site. As at Maax Na, samples were also taken from inside and outside a cave at Chawak But'o'ob, which is just west of the ballcourt.

Hun Tun

A megalith and a few bedrock outcrops were sampled at Hun Tun, a small site near La Milpa (Figure 3.1), in June 2009. Samples were collected from the megalith itself, the underlying possible plaster, and two areas of bedrock outcrops to the east. This small sample set is used as a test case for the methodology presented here.

3.3.2 Test analyses

The initial set of 37 samples collected at Maax Na in 2005 was thin sectioned and examined under a petrographic microscope. All of the samples are composed entirely of microcrystalline calcite (Figure 3.5), with one sample that had small veins of chert in the micrite. The lack of microfossils in the limestone for identification informed us that geochemical analysis would be necessary for this study. Six of these samples, a mix of possible monuments and bedrock, were selected for test analyses with a scanning electron microscope (SEM) and ICP-MS based on varied color and hardness of the rocks in hand sample. The SEM results provided bulk chemistry data, which showed that Mg was an important element in these samples, but that additional minor and trace elements would be necessary to differentiate between the samples. ICP-MS is a geochemical method used to quantify trace elements in dissolved rock material and is capable of very low detection

of trace elements. Ions from a dissolved sample are extracted from a plasma matrix into a pumped vacuum and focused with a lens into a mass spectrometer (Rollinson, 1993). The test of the ICP-MS showed that Sr and other minor elements (e.g., the rare earth elements; REE), may also be useful in discriminating between samples. This method was selected over laser ablation and electron microscopy analytical methods because the dissolution of the samples allows for analysis of the bulk trace element composition rather than a series of small points on the sample, thus enabling a better determination of a specimen's bulk chemistry. For the same reason, atomic emission spectroscopy (ICP-AES) was used for this study instead of the SEM for bulk major element chemistry.

3.3.3 Solution Preparation

ICP-MS and ICP-AES analyses require samples to be dissolved entirely into solution. In order to ensure that all components of each sample, including potential non-carbonate inclusions, were dissolved, the following procedures were followed. First, a rock hammer was used to break up the rock samples, and pieces were selected that did not contain any exterior, weathered surfaces. A mortar and pestle were then used to grind the stone into a fine powder, which was placed into a 2 ml centrifuge tube for storage. The mortar and pestle were cleaned with methanol between each sample. In a clean lab, 0.05 grams of each powdered sample was weighed into a 23 ml Teflon Savillex beaker, followed by 2 ml of nitric acid (HNO_3) and 2 ml of ultrapure water, then placed on a hot plate at <100° C overnight, following methods for sediment dissolution outlined in Kelley et al. (2003) and Plank et al. (2007). Seven standards (AGV-1, EN026-100-3, JCP-1, NBS-88a, RGM-1, W-2, and either IOFM or JB-3) and a procedural blank were

dissolved at the same time as the limestone samples following the same procedures. Once cooled, each solution was transferred to a 2 ml centrifuge tube and centrifuged at 11,000 rpm for 5 minutes. The supernatant liquid was transferred to 250 ml Nalgene dilution bottles. Each tube was rinsed 3x with ultrapure water, and the remaining solid material was then returned to the Teflon beaker.

Microcrystalline silica was observed in some of the samples in thin section, so 1.5 ml of hydrofluoric acid (HF) was added to the undissolved solid along with 3 ml of HNO_3 and placed on a hot plate overnight at <100° C. The beakers were then tapped down and the caps were removed to allow for the HF to evaporate off. Following this, 1.5 ml of hydrogen peroxide (H_2O_2) and 1.5 ml of HNO_3 were added to dissolve any organic matter present in the samples, which were again heated overnight. Calcium-rich spikes were calculated for the four non-carbonate standards in order to matrix-match the igneous rocks to calcite. We added the appropriate amount of 10,000 ppm Ca solution to each of these four samples to the equivalent of 56 wt. % CaO in the rock (equivalent to pure calcite). Half of the procedural blank was spiked, while the other was not. The remaining liquid in the beakers was added to the dilution bottles, then the beakers each rinsed three times with MilliQ H_2O. Ultrapure water was added to bring each solution to 150 g for a 3000x dilution. The bottles were sonicated for 5 minutes and 15 ml of the solution transferred to centrifuge tubes for analysis.

3.3.4 ICP-MS

The solutions were analyzed with a Thermo X-Series 2 quadrupole ICP-MS with an ESI SC-2 autosampler at the University of Rhode Island's Graduate School of

Oceanography. Each sample was analyzed twice to constrain analytical precision. The concentrations of 43 elements selected for potential importance in carbonate minerals were determined for each sample (Li, Be, K, Sc, Ti, V, Cr, Mn, Fe, Co, Ni, Cu, Zn, Ga, As, Rb, Sr, Y, Zr, Nb, Sb, Cs, Ba, La, Ce, Pr, Nd, Pm, Sm, Eu, Tb, Gd, Dy, Ho, Er, Tm, Yb, Lu, Hf, Ta, Pb, Th, U). Results for K, Ti, As, and Sb are not reported because they are below the instrument's detection limits. Either IOFM or EN026 standards were analyzed periodically throughout each 10-sample run to correct for the instrument's drift to improve accuracy.

3.3.5 ICP-AES

Finally, the solutions were analyzed with a JY2000 Ultrace ICP-AES with a JY AS 421 autosampler and 2400g/mm holographic grating at Brown University. The concentrations of seven elements that are major elements in carbonates were analyzed simultaneously (Na_2O, MgO, Al_2O_3, SiO_2, CaO, MnO, Fe_2O_3). Five synthetic solutions of varying concentrations of these elements were made for calibrating the instrument. Results for Na_2O and SiO_2 are not reported because they were below the instrument's detection limits for most of the samples and the dissolution method does not conserve Si in solution. The standards analyzed with the ICP-MS analysis were also analyzed and the results from these solutions were used to calibrate the results from the unknown samples. Calibration curves are linear ($r \geq 0.9993$) and replicate analyses are <3% RSD.

3.4. Results

3.4.1 Rock samples

The limestone of the Three Rivers Region of northwestern Belize is soft, and many of the samples collected exhibited the expected white, soft, micritic texture. A number of the bedrock samples from Maax Na, however, were composed of a denser, tan limestone. These less porous rocks comprise the few natural hills at the site, including the North Hill, two small knolls along the southeast edge of the reservoir, the bedrock of the west acropolis, and a small hill south of the West Plaza. A few samples from Chawak But'o'ob had small black inclusions in the micrite matrix, which were identified with the SEM as manganese oxides, and correspond to a harder white rock. This type of rock, as opposed to the more common, softer limestone at Chawak But'o'ob, occurs only along two of the three ridges that run across the site E-W. At both sites, these harder types of limestone are found on the naturally elevated features on the landscape, which is likely due to less chemical erosion as result of the lower porosity of these rocks.

3.4.2 Geochemical Data

The geochemical data provide a very fine-scaled look at the carbonate chemistry, in both major and trace elements. The nature of these data is such that even samples from the same location may not have completely identical results. Therefore, a statistical examination of some of the geochemical data is necessary to be able to draw appropriate comparisons between sample sets and sites. For each site, the results from the bedrock samples alone were examined to determine the variance in bedrock chemistry across the site. The coefficient of variation (CV), or percent relative standard deviation (%RSD) was

calculated for each element between the bedrock samples from each site. This value is the standard deviation of each element divided by the mean. This is an important calculation because the variance of a trace element, such as the REEs, could be high, but the standard deviation would be orders of magnitude lower than that of a minor element, such as strontium (Sr). The CV instead reflects the variation per ppm of each element, showing the relative variance and illustrating which elements vary the most in the bedrock of the sites. Figures 3.6 and 3.7 show graphs of the CV for Maax Na and Chawak But'o'ob, respectively. Low values reflect low variance. Elements such as Ca, Mg, Sr, Cr, and Ni that have low CV values are better elements to use for comparing possible monuments to bedrock samples, relative to those with a high CV, such as Rb, Ba, or Pb, because the low CV-elements reflect an average standard chemistry of the sites' bedrock. The objective of this work is determining the expected variance over the space of each site's bedrock, which is best done with the elements that vary the least for the purposes of comparing to possible external material.

3.4.3 Maax Na

It is expected that the chemistry of the limestone bedrock will vary across the space of a site due to the epigenetic processes at work since its deposition. Forty-two limestone samples from Maax Na were included in this study (bedrock samples $n = 18$, possible monument samples $n = 24$). As Figure 3.6 shows, elements vary differently among the bedrock samples analyzed. Highly variable elements, such as Ba and Pb, should not be used for comparison and their geochemistry will be discussed in section 4.1. Certain elements important in carbonate processes, such as Ca, Mg, Sr, Cr, and Ni,

are those that exhibit the least amount of variance. Specifically, ranges in magnesium concentrations in limestones indicate the degree of dolomitization in this formation. The Maax Na bedrock ranges between 3-22 wt% MgO with an average of 14.5%, corresponding to 28% dolomite ($MgCO_3$) on average, classifying the rock as a dolomitic limestone (Trudgill, 1985). One sample has a lower concentration due to large amounts of microcrystalline silica in the rock. These data show that while there is a range in Mg concentrations among the bedrock outcrops sampled across the site, the bedrock is dolomitic, with none of the Maax Na bedrock samples indicating a pure $CaCO_3$ limestone composition with <5% $MgCO_3$.

To assess the possibility of sourcing stone to where it was quarried, a similarity index was applied for the data set based on the analysis of similarity by Borchardt et al. (1972). The similarity coefficient ($d_{(A,B)}$) indicates the similarity of each sample compared to all others. A value of 1.0 indicates perfectly similar samples; the Maax Na samples range from d = 0.21-0.93 and the Chawak But'o'ob samples range from d = 0.30-0.90. This method was developed for comparing volcanic ash layers, which have specific chemical signatures that result in a similarity of d = 1.0 (Borchardt et al., 1972). Such a similarity is not expected for limestones, which are more chemically variable. All 38 elements analyzed in this study were compared, as well as the set of six elements with low CV values. These six low-CV elements differentiate between samples more clearly and were used for the full data set similarity analysis (Appendix B). This method is a measure of how similar the concentrations of these elements are in the samples in the study. Certain samples from Maax Na that contain high amounts of silica (e.g. 41, 44) have lower concentrations of CaO and MgO and have low similarity with other bedrock

samples ($d_{(9,44)} = 0.484$), but are still similar relative to one another, which is why ratios of CaO/MgO were used for comparative purposes.

Two samples of the bedrock from the South Acropolis at Maax Na (9, 16; Figure 3.1) are similar at $d_{(9,16)} = 0.706$, where samples 50, from south of the West Plaza, and 53, from north of the West Acropolis are similar at $d_{(50,53)} = 0.701$, showing little spatial variation. Two samples (29, 30) were taken as a control for weathering from the inside floor of Spider Cave as well as the outside face above the entrance of the cave. These two samples are similar at $d_{(29,30)} = 0.726$. However, the exterior sample is more similar at $d_{(29,52)} = 0.846$ with a sample (52) from a megalith above the cave. The sample from the interior of the cave came from what was identified as a travertine surface during the excavation of this cave in 2008 (King et al., under review). Travertine is formed from the movement of freshwater over carbonate (Flugel, 2004). The interior sample is depleted in all the elements relative to the exterior sample, with the exception of calcium, suggesting it is a more pure carbonate formed due to the leaching of trace elements from the rock by the movement of meteoric water, as illustrated by Figure 3.8.

3.4.4 Chawak But'o'ob

The samples collected at Chawak But'o'ob show more heterogeneity than those from Maax Na. Twenty-one limestone samples were analyzed (bedrock samples $n = 15$, possible monument samples $n = 6$). Figure 3.7 plots the CV for the Chawak But'o'ob bedrock samples, which shows a similar pattern to that from Maax Na, with Ca, Mg, Sr, and Ni among the least variable elements, and Rb one of the highest. The Mg concentrations at this site are somewhat higher than at Maax Na, ranging from 5-22 wt%

MgO with an average of 17.4 wt. %, or 33% dolomite, classifying the bedrock also as a dolomitic limestone (Trudgill, 1985). Chawak But'o'ob sits on a lower escarpment than Maax Na, near the banks of the Rio Bravo, and where Maax Na was constructed on a plateau, this smaller site is situated in a more active karst landscape, heavily affected by the movement of water downslope through the bedrock. As at Maax Na, the harder, denser rock type makes up the higher relief at Chawak But'o'ob. However, unlike the hilltop center, Mg concentrations decrease with elevation. The highest MgO was sample 1 at the 100 m contour at the site with 22.2 wt. %. Downslope to the west and in the drainage arroyo in the south ranged from 5.2-11.4 wt. %. The more porous, softer type of stone found off the ridges at the site are more easily eroded, which leaches Mg out.

A set of control samples were taken from the interior and exterior of the cave at Chawak But'o'ob, which are similar at $d_{(15,16)} = 0.811$. Contrasts between bedrock samples were stronger with elevation than distance. Sample 1, from Group E at the northwestern part of the site at the 100 m contour, and sample 17, collected from a hill at the southwest of the site, both of which have similarly high MgO concentrations, are similar at $d_{(1,17)} = 0.832$. These two samples were from opposite ends of the site (Figure 3.4), but at similar elevations. In contrast, sample 6 from the eastern end of the site and downslope correlates with sample 1 at $d_{(1,6)} = 0.646$. Elevation, and as such, porosity and subsequent element leaching, governs the geochemistry of the limestone at this site. Figure 3.9 shows the positive relationship of MgO concentration with elevation at Chawak But'o'ob. The differences between the two types of limestone observed in hand sample are in porosity and density, as well as MnO concentrations, due to the Mn-oxide inclusions. The three samples with the highest MnO concentrations - 4, 10, and 14 - are

those that had the most visible black oxide inclusions, which are useful in hand sample for identifying this type in the field.

3.5 Discussion

3.5.1 Limestone geochemistry

For this research, it is important to understand carbonate geochemistry in order to interpret the variations in data from samples collected across large areas of the two sites. The behavior of minor and trace elements, as either part of the calcite crystal lattice or as inclusions in the limestone itself, are important for distinguishing between different limestone samples as such elements reflect different formation and epigenetic conditions. Not only is characterizing the spatial geochemical variations at these sites important for understanding the evolution of the surface bedrock, but also for distinguishing between rock natural to the local bedrock, relative to rock moved into place by the Maya. As was discussed previously, the elevated ridges at Chawak But'o'ob are composed of a denser limestone that contains more MgO than the softer bedrock downslope. Magnesium and other divalent metals, such as Sr, are able to replace Ca in the calcite lattice. The concentrations of these elements in limestone depend on many factors, including the temperature, salinity, and chemistry of the seawater during formation (Flugel, 2004). Post-diagenesis processes, such as the movement of water over the carbonate landscape, also greatly affect the chemistry of the modern limestone formations. Meteoric water has a very low MgO/CaO ratio, and therefore leaches Mg from calcite, which occurs to a greater extent in more porous rock (Flugel, 2004). This explains the higher levels of Mg

in the denser rocks of the ridges at Chawak But'o'ob, and the depletion of Mg in the softer rocks in between.

The lattice structure of the calcite crystal is highly robust and can absorb a variety of divalent metal cations, in addition to Mg and Sr, without becoming disordered (Ford and Williams, 1989). Reeder et al. (1999) showed that divalent Co, Zn, Pb, and Ba commonly substitute in the Ca site of the calcite structure with varying degrees of local distortion, either dilation around Ba and Pb or contraction around the smaller ions, Co and Zn. This mode of sharing cations of varying sizes is favored by the calcite lattice because of its corner-sharing structure and can take in ions larger or smaller than calcium (Reeder, 1996; Reeder et al., 1999). Other metals commonly adsorb onto the calcite crystal surface rather than being incorporated into the crystal lattice; studies have investigated the behaviors of elements' interaction with calcite including Ba, Sr, Cd, Mn, Cr, Zn, Co, Ni (Garcia-Sanchez and Alvarez-Ayuso, 2002; Lakshtanov and Stipp, 2007; Zachara et al., 1991). A hydrating layer of water containing trace metals, adsorbed onto the calcite surface, initially interacts with partially unsatisfied charges of the Ca and CO_3 ions, which results in a hydrolyzed layer on the mineral surface that can become incorporated into the structure upon recrystallization (Lakshtanov and Stipp, 2007). However, the elements that substitute directly into the Ca site in the lattice are the most common minor components. The results from Maax Na and Chawak But'o'ob show low variance for Mg and Sr, but high CV values for Ba and Pb. These variable elements have much larger ionic radii than Ca, requiring the calcite lattice to dilate around the site of incorporation in order to allow for coprecipitation (Reeder et al., 1999), which explains the high variability between samples from across the area of the sites' bedrock, as the

conditions for accepting a Ba or Pb ion into the mineral are more demanding than those for Mg and Sr, or smaller radius elements that can fill that space, such as Co and Zn.

The rare earth elements are indicators of the chemical evolution of waters flowing through carbonates (Vaniman and Chipera, 1996). The Tertiary carbonate sediments on the Yucatan peninsula became emergent by the late Oligocene and have been exposed to subaerial processes since then (King et al., 2003). The identification of all the samples collected from these sites as microcrystalline calcite shows that the movement of meteoric water over and through the carbonate landscape since diagenesis has recrystallized the initial rock structure into micrite, leaving no microfossils preserved. While there are many epigenetic factors involved in such processes, recrystallization causes the leaching and migration of trace and minor elements (Wolf et al., 1967). Rare earth element concentrations are believed to be altered by dolomitization as well as other epigenetic weathering process, but the exact relationship is unclear and under study (e.g., Northdurft et al., 2004). Ji et al. (2004) show that weathering of dolomites causes uneven transport of REE, which is dependent on the climatic weathering conditions and the stability of the REE-carrying rock. Cerium (Ce) anomalies in REE profiles reflect the oxidation and its subsequent incorporation of Ce into manganese nodules, depleting Ce in seawater (Piper, 1974). However, the samples in this study do not depict a consistent depletion in Ce, as shown in the plot of the monument samples from Maax Na in Figure 3.10. In the case of Maax Na and Chawak But'o'ob, the porosity of the bedrock, which we have shown varies at both sites, greatly affects the dissolution and weathering rates.

Strontium is also a mobile element during carbonate weathering and dissolution (e.g., Vaniman and Chipera, 1996). A positive correlation between Sr and ∑REE, as

shown in Figure 3.11 for the Maax Na bedrock samples, reflects the epigenetic influence of meteoric waters moving over the bedrock (Tlig and M'Rabet, 1985). The differences shown in the trace and minor element composition of the bedrock at these sites is demonstrated in the Ba, Rb, and Pb concentrations and REE profiles illustrate the variable nature of components of the bedrock. This is why an understanding of the bedrock geochemistry is essential before developing a set of elements that are appropriate for the sites in question in order to identify rock brought in from outside the site area. For example, Nation et al. (n.d.) used Rb and Ni and some REE to source speleothems in the Sibun Valley, but these elements would not apply to Maax Na because Rb and the REE are more variable due to uneven weathering. The combination of elements to represent the sites' bedrock are a combination of those with low CVs (see Figures 3.6 and 3.7) and the geological framework discussed above. The ternary diagram in Figure 3.12 shows the bedrock samples plotted in blue. CaO/MgO indicates the percent dolomite as well as the leaching of Mg in the softer rocks. The Sr/La ratio links the mobility of Sr and the REEs during chemical weathering. Finally, Cr/Ni, the two transition metals with the lowest CV values, represent the elements adsorbed and incorporated into the calcite crystal. The ternary plot clearly illustrates a cluster of the Maax Na bedrock samples, which is used as a starting point for comparison to samples from megaliths and possible monuments.

3.5.2 Sourcing monuments

The research presented here is a pilot study aimed at assessing the possibility of geochemically sourcing limestone monuments and architecture components to their respective quarries. Numerous archaeological studies have used geochemistry as a

sourcing tool to track the movement of stone across the historical landscape by humans for obsidian artifacts, which have been shown to have clear chemical signatures. However, like a similar pilot study presented by Pitblado et al. (2008) on quartzite artifacts, the focus of this study, limestone, is not open to such absolute sourcing methods. A specific chemical signature for the limestone of Maax Na is not the end goal of this work, but rather a multifaceted approach incorporating both geochemistry and the archaeology of Maax Na to make inferences about stone use at the site. Like quartzite, certain amounts of variation have to be expected in limestone because of the wide range of formation conditions and post-diagenesis processes that affect limestone chemistry. The approach for this study was therefore to analyze the data from the bedrock samples collected at Maax Na and use a set of elements important in carbonate geology to compare these samples to those collected from megaliths and possible monuments from around the site. In addition to the geochemistry, the provenience of each sample at the site is equally important and helps place the geochemical data into context.

Maax Na

A series of monuments, megaliths, and other stone features at Maax Na were sampled to provide a comparative data set to that of the bedrock in order to determine if sourcing to local quarries is possible. In many cases, it was expected that the megaliths were spall from the bedrock and would have very similar chemistry, which in and of itself is a good test for this methodology. Samples 16 and 17 were taken from a megalith and the adjacent bedrock directly underneath, north of the South Acropolis. An excavation was conducted here in 2004 and little artifactual evidence supported this as a monument

feature. These two samples are less similar at $d_{(16,17)} = 0.913$, suggesting that the megalith is direct spall from the underlying bedrock and *in situ* in its original location. The excavation data together with the *in situ* appearance of the South Acropolis megalith suggests it is not a monument. Conversely, an erect stela at the eastern base of the North Hill and a bedrock sample from the hill are similar at $d_{(18,36)} = 0.389$, supporting its identification as a monument that was moved into place from elsewhere, either at the site or from outside Maax Na. A number of the possible monument samples (e.g. 37, 38, 52) are similar to bedrock samples at $d \geq 0.8$.

A set of histograms for Maax Na and Chawak But'o'ob show the results of the similarity indices in Figures 3.13 and 3.14, respectively. These histograms plot the frequency of the similarity results in each index. Maax Na shows a greatest values in the $d = 0.6$-0.7 range, and Chawak But'o'ob's is somewhat higher around d = 0.65-0.8. Maax Na also shows a large number of values at $d = 0.4$, where Chawak But'o'ob only shows a small number of values in this range. These results illustrate the primarily local nature of the Chawak But'o'ob monuments and that some of Maax Na's monuments were of stone imported to the site, resulting in lower similarity to the local monument and bedrock sample chemistry.

Figure 3.12 plots all the samples from Maax Na and Chawak But'o'ob on a ternary diagram with the ratios of CaO/MgO, Cr/Ni, and Sr/La to help look at stones that may have been imported to the site. Seven samples (1-8) were also collected from Megalith 1, a series of megaliths that have the appearance of a broken monument, south of the southeast corner of the West Plaza, as well as the surrounding bedrock. The samples from both of these features fall within the range of the Maax Na bedrock on the

diagram. The bedrock samples are plotted in blue, the possible monuments in red, and the set of six small, 50 cm diameter stones in the South Acropolis and West Plaza (10-15, 43), which will be discussed below, are plotted in green.

There is a general clustering of bedrock samples with low CaO/MgO and high Sr/La values. Most of the samples plot along the line between Sr/La and Cr/Ni due to the dolomitic limestone composition of the bedrock at Maax Na, and therefore have low CaO/MgO ratios. Most of the monuments plot within the range of the bedrock samples, showing that many of the megaliths sampled are either not monuments or were constructed from the local bedrock. There are, however, some samples that fall well outside the ranges established by the Maax Na bedrock. The three clear outliers among the monument samples (red dots) are three stela. Stela 1 to the east of the Main Temple, and the monument east of the North Hill and in sight of the entrance to Spider Cave, plot nearest the point of Cr/Ni, while a stela north of the North Plaza plots to the far right on the graph. The remaining monument samples plot within the general range of the bedrock, although the ballcourt and possible altar in the North Plaza (24, 25) plot somewhat above the Maax Na range.

The clear outliers in this data set in Figure 3.12 are plotted in green and fall toward the CaO/MgO corner. These small stones were found in two locations at Maax Na in groupings of three stones, a set in the South Acropolis (samples 10-15), and a set south of the West Plaza (sample 43; Figure 3.2). The function of these stones is unknown, but they were sampled because they are similarly shaped rocks in each location, and had a smoother weathered surface than most megaliths (Figure 3.15). The weathering pattern of these is because they are composed of a dense, tan, fine-grained limestone with a

conchoidal fracture rather than the common soft, white limestone at Maax Na. The chemistry of these stone features differs drastically from the Maax Na bedrock, primarily in the Sr and MgO concentrations. Magnesium is <0.5 wt. %, classifying these as pure limestone as opposed to the dolomitic limestone found elsewhere. Strontium concentrations are higher than most of the other samples, generally, because dolomites contain less Sr than calcite (Verheyden et al., 2000). The MgO/CaO and Sr/CaO ratios for all the Maax Na samples are plotted in Figure 3.16 (after Aharon et al., 2006). The dolomitic limestone of the bedrock and the other monuments at Maax Na shows a positive relationship, and the samples plot together along one line. The six limestone samples plot together on a nearly vertical line, indicating the purer limestone samples. The consistent dolomitic nature of the bedrock at both Maax Na and Chawak But'o'ob indicates that the source of these small monuments may have been quarried from some distance from these sites. The size of these stones is small, making it feasible that they were transported from outside this area.

Differences in the REE profiles for the monument samples from Maax Na also support some of them having been imported from quarries outside the site core. Figure 3.10 plots the REE profiles for the Maax Na possible monument and megalith samples, normalized to an average bedrock composition for Maax Na calculated from the bedrock samples analyzed. Four possible monument samples are plotted in light blue, which are megaliths whose identification as natural or cultural was unclear during the survey. Dark blue lines plot samples collected from Megalith 1, the identification of which as a monument was also in question. All of these samples plot within the general cluster of samples for the Maax Na bedrock in Figure 3.12 and have relatively flat REE profiles

when normalized to the Maax Na bedrock average. Alternately, the monuments that plot outside the cluster of the bedrock samples show more varying REE profiles. The three stela sampled during this survey are plotted in Figure 3.10 in red, the ballcourt sample and North Plaza altar in orange, and the six small monuments in green. These samples show much more pronounced negative Ce anomalies, and the small monuments in green also show a consistent negative Eu anomaly not present in the other samples, when normalized to the Maax Na bedrock, further confirming a difference between these rock samples and those from the site's bedrock.

Chawak But'o'ob

The sampling at Chawak But'o'ob was focused on the geochemical characterization of the site in an active karst environment as a comparison to Maax Na, which was constructed at the top of a plateau. Fewer monuments were included in the sampling at Chawak But'o'ob. Three cobbles from the ballcourt, a stela and the possible plaster surface beneath it, and a bridge base in a stream were the only cultural features sampled. The samples from this site are plotted in yellow against those from Maax Na on the ternary diagram in Figure 3.12, and they plot primarily in the same area as the Maax Na bedrock, with some variation in the same range. This shows that, despite a 7 km distance and a vertical change over three escarpments, the general bedrock chemistry is relatively consistent between these sites. Four samples plot near the Cr/Ni point of the diagram, away from the rest. These are two samples (3,4) from drainage channels, or arroyos, one at the southern end of the site and one near Group G (Figure 3.4), as well as two cobbles from the ballcourt. These cobbles likely came from the southern drainage,

which is near where the ballcourt was constructed. These samples may reflect a somewhat different chemistry at a lower stratum in the bedrock than the rest of the outcrops that were sampled.

Sample 12 plots to the right of the other samples. This was collected from a possible bridge base in a small stream at the eastern edge of the site. The sample has extremely high values of Sr, Ba, and REE, and very low MgO compared to the other samples. This feature is at the bottom of the slope on which Chawak But'o'ob was built, and the water flowing through the bedrock pools here and flows through this stream and over this stone feature. The high concentrations are likely due to the movement of leached elements from the bedrock above. The ratios of Sr/La and Cr/Ni are similar to the other bedrock, and this sample would plot in the cluster in Figure 3.12 with the exception of a higher CaO/MgO ratio due to the low Mg concentration. Meteoric waters have very low Ca/Mg, making Mg leaching more pronounced (Flugel, 2004). However, despite those discussed above, all the cultural features sampled appear to be made of stone local to the area of the site. Sample 7A from the stela at Group A matches the bedrock, but is composed of a hard, tan stone, similar in appearance, but not chemistry, to that from the small limestone monuments at Maax Na. It seems likely, therefore, that the stone for this stela was carefully selected, although from a nearby source.

3.5.3 Maya stone use

The results of this pilot study indicate that the Maya were very knowledgeable about the rock beneath their feet and, in some cases, may have gone to extreme effort to acquire stone from elsewhere for specific purposes. The three stelae sampled in this study

at Maax Na are clearly cut from stone that is not local to the area of Maax Na's site core. Given the results from the Chawak But'o'ob arroyo samples, the chemistry of the stelae may be local, but from an unknown quarry somewhere near the site. The six small, pure limestone monuments from two areas of Maax Na, however, are unlikely to have come from near the site, as no other low-Mg limestone was sampled in this study. However, these results show that the Maya at Maax Na carefully selected stone for the erection of certain monuments, but were able to use the local bedrock for other stone features, such as Megalith 1. The same careful selection of stone is also apparent at Chawak But'o'ob based on the physical appearance of the rock that comprises the stela in Group A. All of the sampled cultural features at Chawak But'o'ob, however, were of local bedrock. This site was constructed late in the Late Classic period without the monumental focus of site centers such as Maax Na, so less cost and effort may have been put into acquiring materials from outside the site.

Despite this, Chawak But'o'ob still underwent extensive landscape modifications that included terracing and water drainage and catchment features (Walling, 2005). These features are primarily small-scale and engineered to take advantage of the slope of the escarpment to channel water as and where needed. Maax Na, on the other hand, is a hilltop center that underwent significant quarrying to shape the landscape of the plateau, like La Milpa and Kinal. The reservoir was carved out, but certain topographical features were left in place at the site, although shaped, such as the two knolls forming the southeast edge of the reservoir and the North Hill. The small hill containing Spider Cave is also natural, and the layout of the site and the incorporation of the North Hill into the plan of the North Plaza are hypothesized to be linked to the presence of caves (King et

al., under review). The specific movement of stone from quarries at Maax Na to the final construction of architecture and monuments was not possible to determine given the small number of samples in this study. However, such a research question would be possible with more intensive sampling, as demonstrated by the differences between parts of the Megalith 1 feature discussed above. Now that a general understanding of the variability of the bedrock at Maax Na and Chawak But'o'ob has been acquired, further characterization may be warranted. This study provides a baseline for more intensive research to investigate the specific movement of stone. Both sites used local stone for monument construction, but this study did not find clear matches to the few quarry areas sampled. More intensive sampling, specifically along the perimeter of Maax Na, could help pintpoint the quarries from which certain stone was excavated. Additionally, more regional research may be able to elucidate the source of the pure limestone that the small monuments were quarried from, which may be some distance from Maax Na.

3.6 Application of Methods - Hun Tun

Four limestone samples were collected in 2009 at a small site located near the center of La Milpa, which was in the early stages of excavations. Hun Tun consists of six courtyard groups and is considered to be a support community settlement interacting with the greater La Milpa polity (Dodge, 2010). Ceramic dating shows this site to be primarily Late Classic, and other small finds including obsidian, greenstone, and eccentric flint artifacts, suggest the socioeconomic status was mid-level elite (Dodge, 2008). There are also an altar and two possible stela at the site, one of which was the focus of the samples collected in 2009. This fallen monument presents a good test case for the application of

the type of geochemical analysis developed above. A sample of the monument was collected in addition to the plaster-like material beneath it, and two samples of bedrock from outcrops to the east of the site core. These four samples were dissolved and analyzed along with those from Maax Na and Chawak But'o'ob.

The bedrock samples contain ~35% dolomite, classifying these rocks as dolomitic limestone, consistent with all other bedrock so far analyzed from the Three Rivers Region. The monument and plaster samples, however, contain <1 wt.% MgO, classifying the stone and parent rock to the plaster as nearly pure limestone, similar to the six small monuments at Maax Na. The hand sample collected from the monument is a crystalline calcite rather than fine-grained micrite, also illustrating the Maya's careful selection of stone for monuments. While the bedrock from Hun Tun plots similarly to the Maax Na and Chawak But'o'ob bedrock samples, the use of trace elements is unnecessary in this case, as major and minor elements are able to clearly differentiate between the bedrock and megalith samples. Magnesium and strontium are plotted in Figure 3.17, which shows the clear difference between monument and bedrock samples, suggesting the monument was not quarried from the local bedrock. This test suggests that, in theory, the application of geochemistry in such cases could initially be done in the field on fresh breaks with a handheld XRF, providing immediate bulk chemical compositions for elements such as Ca, Mg, and Sr. Such preliminary investigations could help characterize the dolomite contents of bedrock in the field and help broaden the scope of this research on a regional scale.

3.7 Conclusion

As has been shown for quartzite (Pitblado et al., 2008), variability was expected in the limestone samples from these sites. However, the data analysis discussed above shows a way to interpret such data so that geologically important comparisons can be made to determine the possible sources of stone at these sites. While there was a range in the geochemical results from samples across the areas of both sites, the majority of them do cluster. Further interpretation based on the context of sampled monuments help understand certain variations. While the sampling strategy was too sparse to source monuments to nearby quarries successfully, multiple stone features were identified as originating from quarries outside the sampled core of Maax Na: three stelae at the site and the six unknown small monuments were made from stone that was moved to the site from an external source. The source of the stelae, as well as the one from Chawak But'o'ob, might be a nearby quarry with better quality limestone, but the chemistry of the other six monuments suggests that that material may have come from quite some distance based on the low-Mg, nearly pure limestone composition that differs from the bedrock at these sites. The bedrock samples from all three sites investigated proved to be of similar compositions for the elements plotted in Figure 3.12, despite the fact that Chawak But'o'ob is below the escarpments and 7 km southeast of Maax Na, and Hun Tun is about 7 km north of Maax Na. Further regional investigations could help discern from how far away other types of limestone would have needed to be imported by identifying quarries.

This is the first study to look at the geochemical composition of the surface bedrock in this area of northern Belize, in part thanks to the areas the Maya cut away and quarried, leaving easily accessible bedrock outcrops for sampling. While the bedrock of

the Three Rivers Region is an extension of a large Eocene limestone formation spanning much of northern Guatemala and Belize, it is important to characterize it more locally to determine microvariations within the formation that can illustrate both post-diagenetic effects and the movement of stone by the ancient Maya. The bedrock of these two sites shows heavy epigenetic effects from the movement of water over the landscape that has changed both the chemistry and mineralogy of the limestone. The dolomitic limestone bedrock has been recrystallized into micrite, and ranges in porosity from a very soft, powdery white rock to a hard, dense tan type of rock. While the dolomite composition of the bedrock varies at both sites, the variation at Chawak But'o'ob indicates the removal of Mg from the bedrock by leaching of meteoric waters that weather the rocks unevenly due to differences in porosity. Due to Maax Na's location at the top of the plateau, this is not the case, as meteoric waters do not flow through the bedrock the way they do below the escarpments where Chawak But'o'ob is located. This sort of leaching of trace metals by the movement of meteoric water is also seen in the travertine surface on the floor of Spider Cave, which we geochemically confirmed had water flowing through it. More importantly, this study shows that the bedrock has been influenced unevenly based on the variability in porosity and density of the limestone.

This carbonate landscape was what the Maya used to construct their built environment and shape it according to their worldview. To this effect, we see the on the one hand North Hill and Spider Cave at Maax Na as natural topographic features that were worked into the site's plan, and likely defined the layout of the ceremonial center. On the other, the Maya's clear understanding of the local geology is evident in the types of stone used for certain stelae and monuments, and the transport of some of them to

Maax Na from outside the site core. Small scale variations may be able to pinpoint specific quarries from which stone was locally acquired, as shown by the small-scale changes in chemistry across the volume of Megalith 1. However, most important is the identification of stone not derived from the same carbonate material as the bedrock at Maax Na and Hun Tun, from which monuments were made, and the source of which may be some distance away. This speaks to the Maya's understanding of stone quality and the effort they went to to acquire certain stone. This determination indicates that basic geochemical data could be collected in the field that would help locate possible sources for this stone as well as find other monuments made from it. Handheld XRF and other such field devices can provide immediate bulk geochemical results, most important in this case is Mg concentration, or percent dolomite, and such implementation could accelerate and expand this form of research in the area.

References

Abrams, E.M., 1994. How the Maya Built Their World: Energetics and Ancient Architecture. University of Texas Press, Austin.

Aharon, P., Rasbury, M., Murgulet, V., 2006. Caves of Niue Island, South Pacific: Speleothems and water geochemistry, in: Harmon, R.S. and Wicks, C.M., eds., Perspectives on Karst Geomorphology, Hydrology, and Geochemistry: A tribute to Derek C. Ford and William B. White, pp. 283-295.

Ashmore, W., 1991. Site-planning principles and concepts of directionality among the ancient Maya. *Latin American Antiquity* 2(3), 199-226.

Ashmore, W., 1992. Deciphering Maya architectural plans, in: New Theories on the Ancient Maya, eds., Danien, E.C. and Sharer, R.J. University Museum Monograph 77. University Museum, University of Pennsylvania, Philidephia, pp. 173-184.

Ashmore, W., 2008. Visions of the cosmos: Ceremonial landscapes and civic plans, in: David, B. and Thomas, J., eds., Handbook of Landscape Archaeology. Left Coast Press, Inc., Walnut Creek, CA, pp. 167-175.

Aston, M. and Rowley, T, 1974. Landscape Archaeology. David and Charles, London.

Barba, L., Blancas, J., Manzanilla, L.R., Ortiz, A., Barca, D., Crisci, G.M., Miriello, D., Pecci, A., 2009. Provenance of the limestone used in Teotihuacan (Mexico): a methodological approach. *Archaeometry* 51, 525-545.

Bolland, O.N., 1977. The Formation of a Colonial Society: Belize, from Conquest to Crown Colony. The Johns Hopkins University Press, Baltimore.

Borchardt, G.A., Aruscavage, P.J., Millard, H.T., Jr., 1972. Correlation of the Bishop Ash, a Pleistocene marker bed, using instrument neuron activation analysis. *Journal of Sedimentary Petrology* 42, 301-306.

Brady, J.E., 1997. Settlement Configuration and Cosmology: The Role of Caves at Dos Pilas. *American Anthropologist* 99 (3), 602-618.

Brady, J. and Ashmore, W., 1999. Mountains, caves, water: Ideational landscapes of the Ancient Maya, in: Ashmore, W. and Knapp, A.B., eds., Archaeologies of Landscape: Contemporary Perspectives. Blackwell Publishers, Oxford, pp 124-145.

David, B. and Thomas, J., 2008. Landscape Archaeology: Introduction, in: David, B. and Thomas, J., eds., Handbook of Landscape Archaeology. Left Coast Press, Inc., Walnut Creek, CA, pp. 27-43.

Denham, T., 2008. Environmental Archaeology: Interpreting practices-in-the-landscape through geoarchaeology, in: David, B. and Thomas, J., eds., Handbook of Landscape Archaeology. Left Coast Press, Inc., Walnut Creek, CA, pp. 468-481.

Dincauze, D., 2000. Environmental Archaeology: Principles and Practice. Cambridge University Press, Cambridge.

Dodge, R.L., 2008. Research Report on Archaeological Excavations at Hun Tun. Report, The University of Texas at Austin.

Dodge, R.L., 2010. Research Report on Archaeological Excavations at Hun Tun. Report, The University of Texas at Austin. 123-131.

Dunning, N., Jones, J.G., Beach, T., Luzzadder-Beach, S., 2003. Physiography, habitats, and landscapes of the Three Rivers Region, in: Scarborough, V.L., Valdez Jr., F., Dunning, N.P., eds., Heterarchy, Political Economy, and the Ancient Maya. University of Arizona Press, Tucson, pp. 14-24.

Espinosa, L., Ceron, M., Sulub, Y.A., 1998. Limestone rocks of the Yucatan Peninsula. Description of the lithology and physical properties based on the results of exploration, investigation, and laboratory tests. *International Journal of Rock Mechanics and Mining Sciences* 35, 410-411.

Flores, G., 1952. Summary report of preliminary geological studies of the area N of 17o N latitude, British Honduras. Bahamas Exploration Company, Freeport, Bahamas.

Flugel, E., 2004. Microfacies of Carbonate Rocks: Analysis, Interpretation and Application. Springer, New York.

Folan, W.J., 1982. Mining and Quarrying Techniques of the Lowland Maya. *Anthropology* 6, 149-174.

Ford, D. and Williams, P., 1989. Karst Geomorphology and Hydrology. Unwin Hyman, London.

Garcia-Sanchez, A. and Alvarez-Ayuso, E., 2002. Sorption of Zn, Cd and Cr on calcite. Application to purification of industrial wastewater. *Minerals Engineering* 15, 539-547.

Graham, E., 1987. Resource Diversity in Belize and Its Implications for Models of Lowland Trade. *American Antiquity* 52(4), 753-767.

Hartshorn, G., Nicolait, L., Hartshorn, L., Bevier, G., Brightman, R., Cal, J., Cawich, A., Davidson, W., DuBois, R., Dyer, C., Gibson J., Hawley W., Leonard J., Nicolait,

R., Weyer, D., White, H., Wright, C. 1984. BELIZE Country Environmental Profile, A Field Study. USAID Contract. Trejos. Hnos. Sucs. S.A., San Jose.

Houk, Brett A., 2003. The ties that bind: Site planning in the Three Rivers Region, in: Scarborough, V.L., Valdez Jr., F., Dunning, N.P., eds., Heterarchy, Political Economy, and the Ancient Maya. University of Arizona Press, Tucson, pp. 52-63.

Ji, H., Wang S., Ouyang, Z., Zhang, S., Sun C., Liu, X., Zhou, D., 2004. Geochemistry of red residua underlying dolomites in karst terrains of Yunnan-Guizhou Plateau II. The mobility of rare earth elements during weathering. *Chemical Geology* 203, 29-50.

Kelley, K.A., Plank, T., Ludden, J., Staudigel, H., 2003. Composition of altered oceanic crust at ODP sites 801 and 1149. *Geochemistry Geophysics Geosystems* 4(6), 8910.

King, D.T., Jr., Petruny, L.W., Pope, K.O., 2003. Shallow-marine facies of the Orange Walk Group, Miocene-Pliocene, northern Belize (Central America). *GCAGS/ GCSSEPM Transactions* 53, 384-397.

King, D.T., Jr., Pope, K.O., Petruny, L.W., 2004. Stratigraphy of Belize, north of the 17th parallel. *Gulf Coast Association of Geological Societies Transactions* 54, 289-303.

King, E. and Shaw, L., 2003. A heterarchical approach to site variability: The Maax Na Archaeology Project, in: Scarborough, V.L., Valdez Jr., F., Dunning, N.P., eds., Heterarchy, Political Economy, and the Ancient Maya. University of Arizona Press, Tucson, pp. 64-76.

King, E.M., Brady, J.E., Shaw, L.C., Cobb, A.B., Kieffer, C.L., Brennan, M.L., Harris, C.L., in revision. Small caves and sacred geography: A case study from the Prehispanic Maya site of Maax Na, Belize. *Latin American Antiquity*.

Knapp, A.B. and Ashmore, W., 1999. Archaeological landscapes: Constructed, conceptualized, ideational, in: Ashmore, W. and Knapp, A.B., eds., Archaeologies of Landscape: Contemporary Perspectives. Blackwell Publishers, Oxford, pp 1-30.

Kunen, J.L., 2004. Ancient Maya Life in the Far West Bajo: Social and Environmental Change in the Wetlands of Belize. The University of Arizona Press, Tucson.

Kunen, J.L., Hughbanks, P.J., 2003. Bajo communities as resource specialists, in: Scarborough, V.L., Valdez Jr., F., Dunning, N.P., eds., Heterarchy, Political Economy, and the Ancient Maya. University of Arizona Press, Tucson, pp. 92-108.

Lakshtanov, L.Z. and Stipp, S.L.S., 2007. Experimental study of nickel(II) interaction with calcite: Adsorption and coprecipitation. *Geochimica et Cosmochimica Acta* 71, 3686-3697.

Mathews, R.. 2002. Geology, environment, and lime production variation in the Maya Lowlands. Unpublished Masters thesis. University of Texas, San Antonio.

Nation, H., Peterson, P.A., Brady, J.E., Neff, H., and McAnany, P.A. n.d. Speleothem Sourcing Using Inductively Coupled Plasma Mass Spectrometry. Paper submitted to *The Journal of Cave and Karst Studies*.

Northdurft, L.D., Webb, G.E., Kamber, B.S., 2004. Rare earth element geochemistry of Late Devonian reefal carbonates, Canning Basin, Western Australia: Confirmation of a seawtaer REE proxy in ancient limestones. *Geochimica et Cosmochimica Acta* 68(2), 263-283.

Piper, D.Z., 1974. Rare earth elements in ferromanganese nodules and other marine phases. *Geochimica et Cosmochimica Acta* 38, 1007-1022.

Pitblado, B.L., Dehler, C., Neff, H., Nelson, S.T., 2008. Pilot study experiments sourcing quartzite, Gunnison Basin, Colorado. *Geoarchaeology* 23(6), 742-778.

Plank, T., Kelley, K.A., Murray, R.W., Stern, L.Q., 2007. Chemical composition of sediments subducting at the Izu-Bonin trench. *Geochemistry Geophysics Geosystems 8*, Q04I16, doi:10.1029/2006GC001444.

Reeder, R.J., 1996. Interaction of divalent cobalt, zinc, cadmium, and barium with the calcite surface during layer growth. *Geochimica et Cosmochimica Acta* 60, 1543-1552.

Reeder, R.J., Lamble, G.M., Northrup, P.A., 1999. XAFS study of the coordination and local relaxation around Co^{2+}, Zn^{2+}, Pb^{2+}, and Ba^{2+} trace elements in calcite. *American Mineralogist* 84, 1049-1060.

Rice, P.M., Michel, H.V., Asaro, F., Stross, F., 1985. Provenience analysis of obsidians from the Central Peten Lakes Region, Guatemala. *Latin American Antiquity* 50(3), 591-604.

Rollinson, H., 1993. Using Geochemical Data: Evaluation, Presentation, Interpretation. Pearson Education Limited, Harlow, England.

Scarborough, V.L., Becher, M.E., Baker, J.L., Harris, G., and Valdez, F. Jr., 1995. Water and Land at the Ancient Maya Community of La Milpa. *Latin American Antiquity* 6, 98-119.

Scarborough, V.L., 1998. Ecology and ritual: Water management and the Maya. *Latin American Antiquity* 9: 135-159.

Scarborough, V.L. and Valdez, F. Jr., 2003. The engineered environment and political economy of the Three Rivers Region, in: Scarborough, V.L., Valdez Jr., F., Dunning, N.P., eds., Heterarchy, Political Economy, and the Ancient Maya. University of Arizona Press, Tucson, pp. 3-13.

Scarborough, V.L., Valdez, F. Jr., Dunning, N.P., 2003. Heterarchy, Political Economy, and the Ancient Maya. University of Arizona Press, Tucson.

Scarborough, V.L., Connolly, R.P., and Ross, S.P., 1994. The Pre-Hispanic Maya reservoir system at Kinal, Peten, Guatemala. *Ancient Mesoamerica* 5, 97-106.

Shaw, L.C., 1999. Constructed landscape as ideology: Archaeology and mapping at Maax Na in the Three Rivers Region of Belize. Paper presented at the 64th Annual Meeting of the Society for American Archaeology, Chicago.

Shaw, L.C., 2002. The Ma'ax Na Archaeology Project: Documentation of stelae, altars, and cave entrances in the west ceremonial group. FAMSI Report. <http:// www.famsi.org/reports/ 00100/>.

Shaw, L.C. and King, E.M., 1997. Research in high places: The hilltop center of Maax Na, Belize. Paper presented at the 62nd Annual Meeting of the Society for American Archaeology, Nashville, Tenn.

Tlig, S. and M'Rabet, A., 1985. A comparative study of the rare earth element (REE) distributions within the Lower Cretaceous dolomites and limestones of Central Tunisia. *Sedimentology* 32, 897-907.

Tourtellot, G., Belli, F.E., Rose, J.J., Hammond, N., 2003. Late Classic Maya heterarchy, hierarchy, and landscape at La Milpa, Belize, in: Scarborough, V.L., Valdez Jr., F., Dunning, N.P., eds., Heterarchy, Political Economy, and the Ancient Maya. University of Arizona Press, Tucson, pp. 37-51.

Trudgill, S., 1985. Limestone Geomorphology. Longman Inc., New York.

Vaniman, D.T. and Chipera, S.J., 1996. Paleotransport of lanthanides and strontium recorded in calcite compositions from tuffs at Yucca Mountain, Nevada, USA. *Geochimica et Cosmochimica Acta* 60, 4417-4433.

Verheyden, S., Keppens, E., Fairchild, I.J., McDermott, F., Weis, D., 2000. *Chemical Geology* 169, 131-144.

Villaseñor, I., 2010. Building Materials of the Ancient Maya: A Study of Archaeological Plasters. Lambert Academic Publishing, Saarbrucken, Germany.

Vinson, G.L., 1962. Upper Cretaceous and Tertiary stratigraphy of Guatemala. *Bulletin of the American Association of Petroleum Geologists* 46, 425-456.

Walling, S., 2005. Archaeological investigation of Prehispanic Maya residential terraces, commoner housing and hydrology at Chawak But'o'ob, Belize. *Antiquity* 79, Project Gallery. Available at <http://antiquity.ac.uk/Projgall/walling/>.

Wolf, K.H., Chilingar, G.V., Beales, F.W., 1967. Elemental composition of carbonate skeletons, minerals and sediments, in: Chilingar, G.V., Bissell, H.J., Fairbridge, R.W., eds, Carbonate Rocks: Physical and Chemical Aspects. Elsevier, Amsterdam, pp. 23-149.

Woods, J.C. and Titmus, G.L., 1996. Stone on stone: Perspectives on Maya civilization from lithic studies, in: Robinson, M.G., Macri, M.J., McHargue, J., eds., Eighth Palenque Round Table, 1993. The Pre-Columbian Art Research Institute, San Francisco.

Zachara, J.M., Cowan, C.E., Resch, C.T., 1991. Sorption of divalent metals on calcite. *Geochimica et Cosmochimica Acta* 55, 1549-1562.

Figures

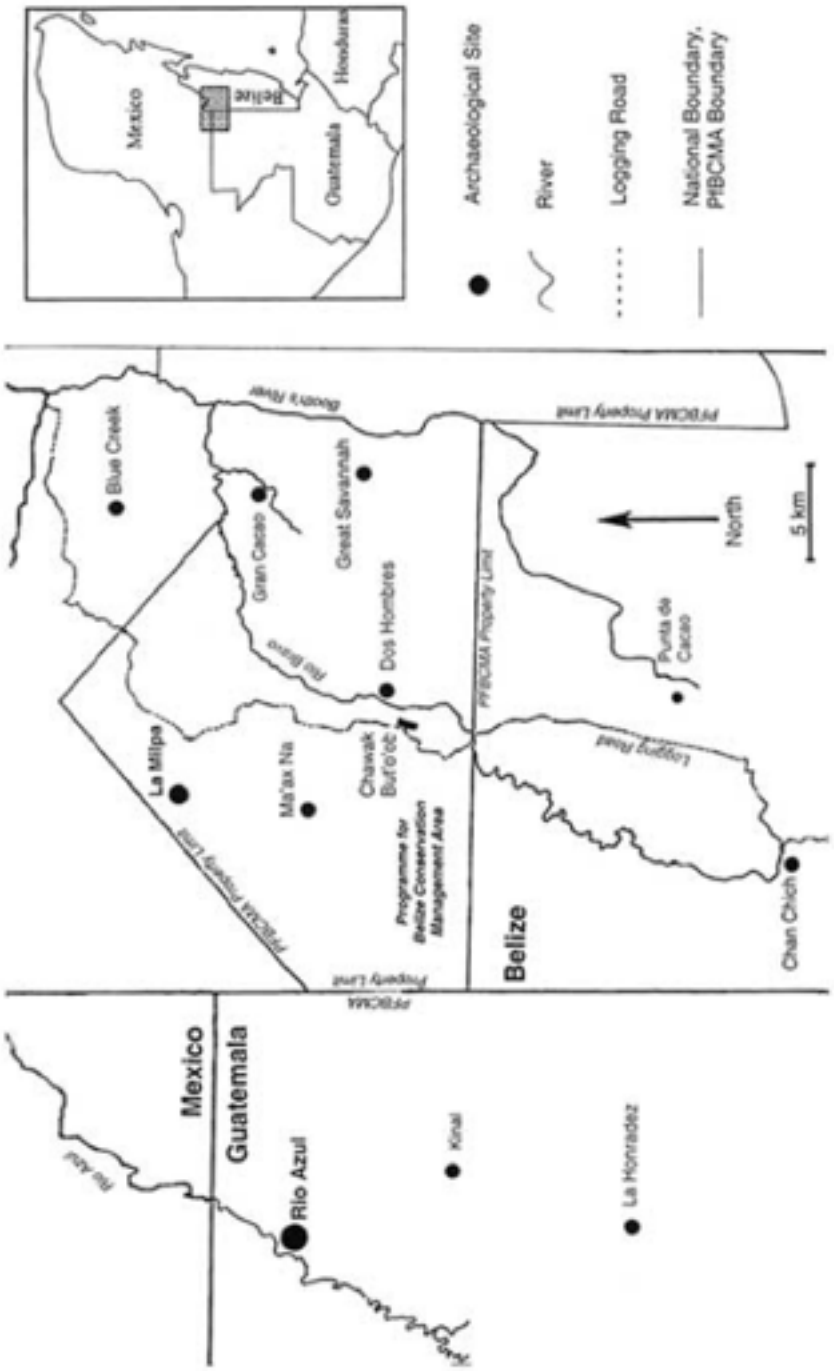

Figure 3.1. Map of the Three Rivers Region of northwestern Belize showing the boundary of the Programme for Belize Conservation and Management Area and major sites. From Walling, 2003.

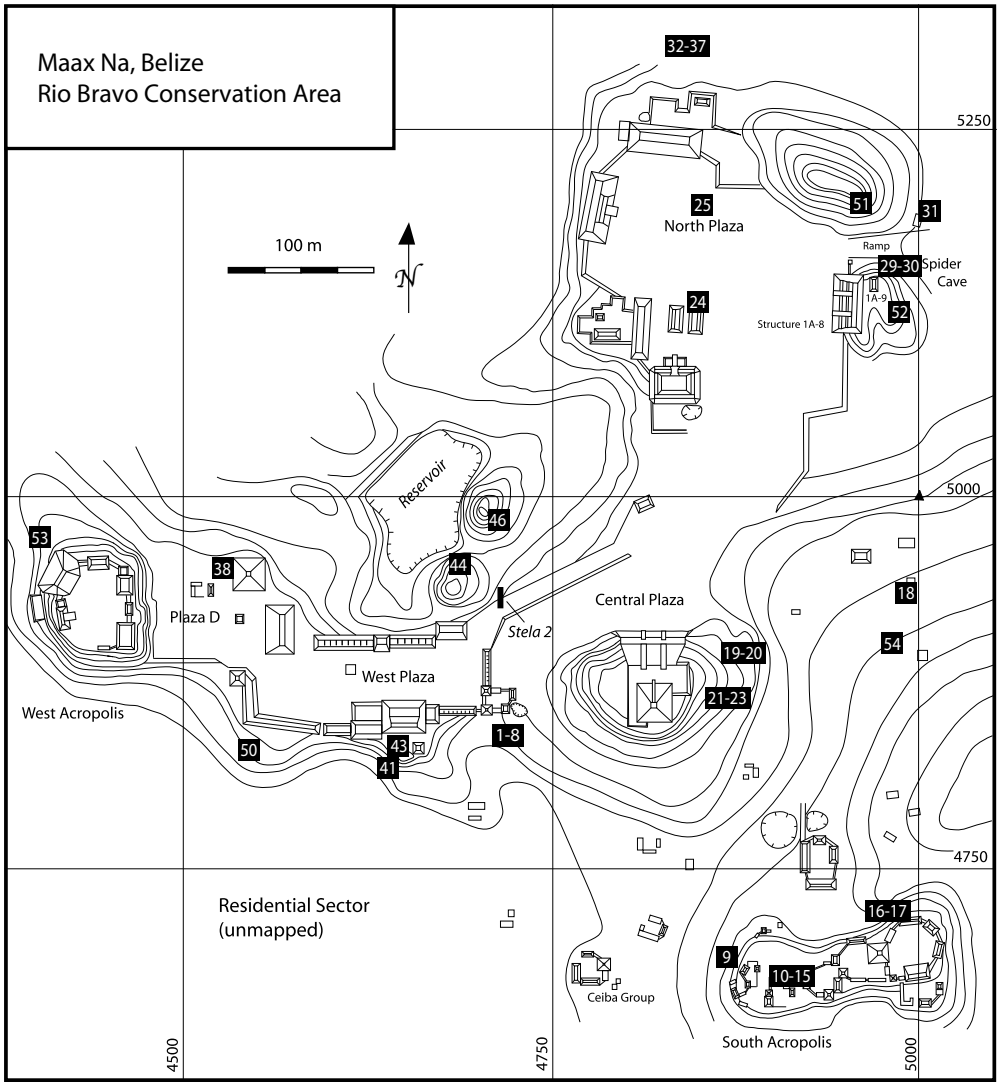

Figure 3.2. Map of Maax Na site core indicating location of samples. Adapted from King and Shaw, 2003.

Figure 3.3. Photo of heavily weathered and fallen Megalith 1 at Maax Na with North arrow for scale. Photo by Eleanor King.

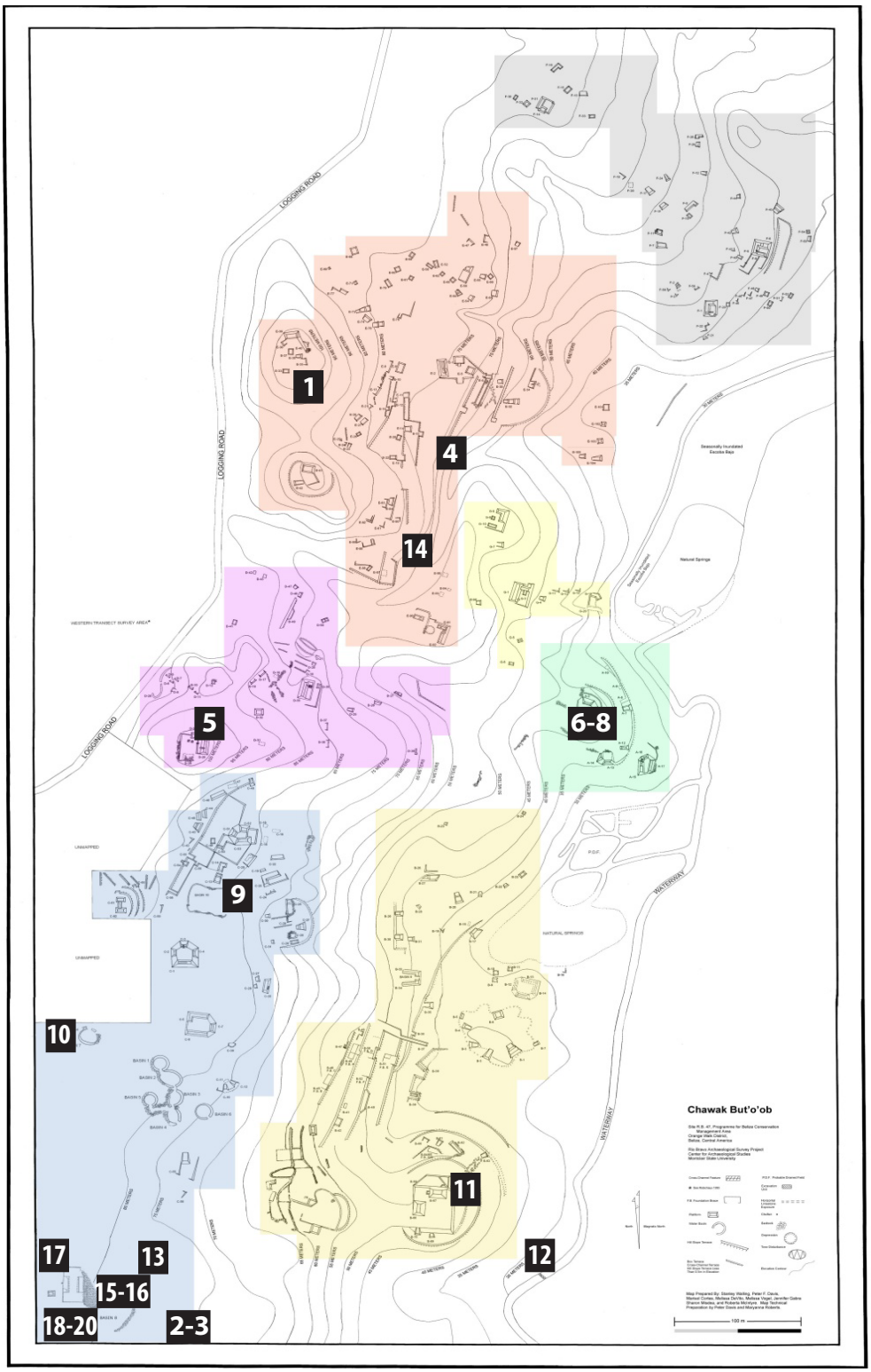

Figure 3.4. Draft map of Chawak But'o'ob site core indicating location of samples. Adapted from Walling, 2005.

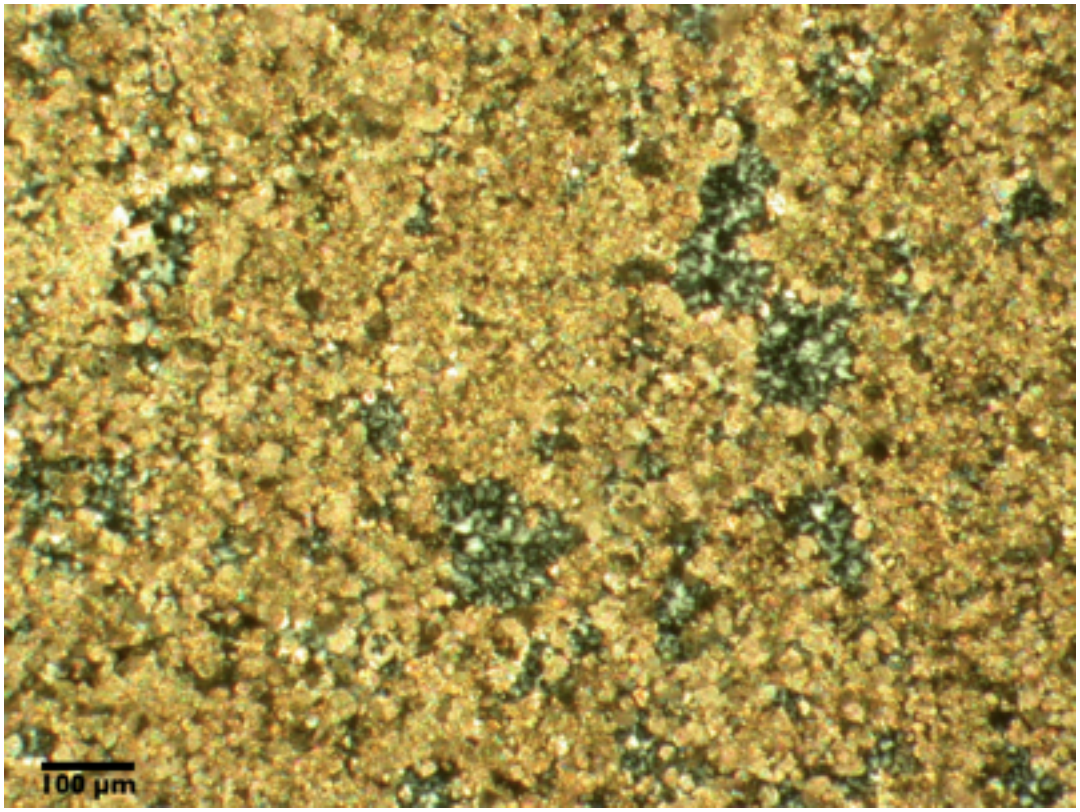

Figure 3.5. Photomicrograph of sample MN44 in thin section showing micrite texture in cross-polarized light (xpl), so calcite appears bright while silica appears as shades of gray.

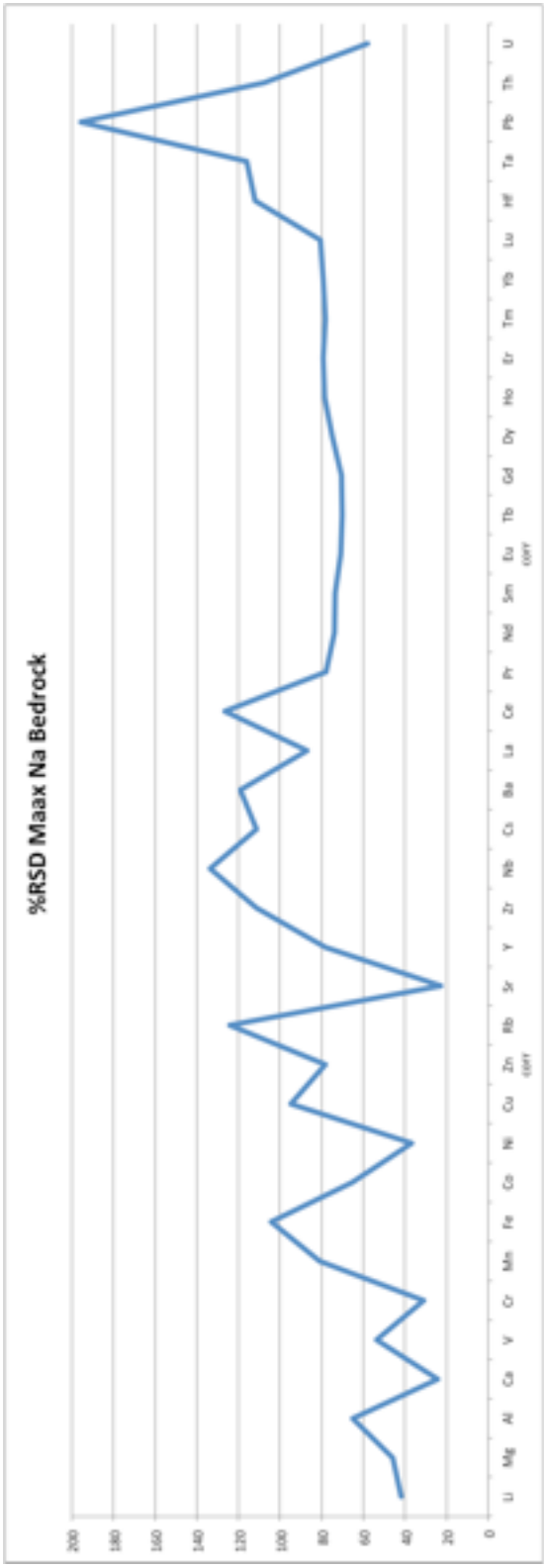

Figure 3.6. Plot of the coefficient of variation (CV) for elements from Maax Na bedrock samples.

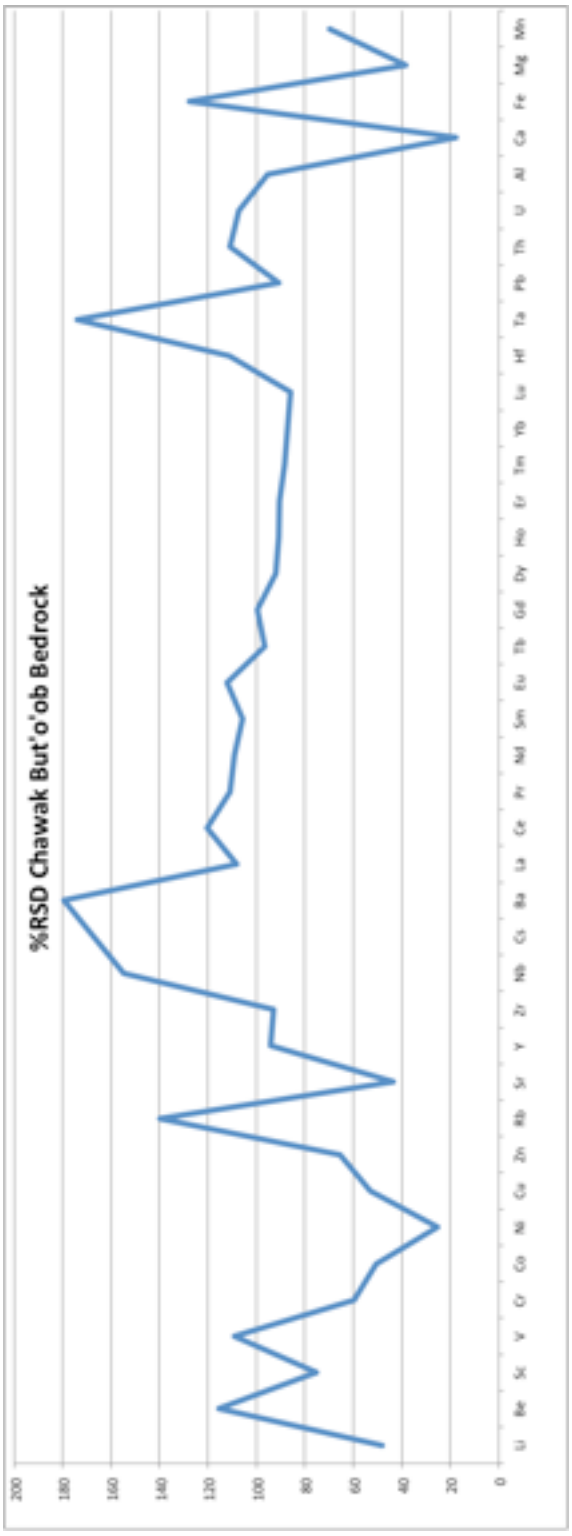

Figure 3.7. Plot of the coefficient of variation (CV) for elements from Chawak But'o'ob bedrock samples.

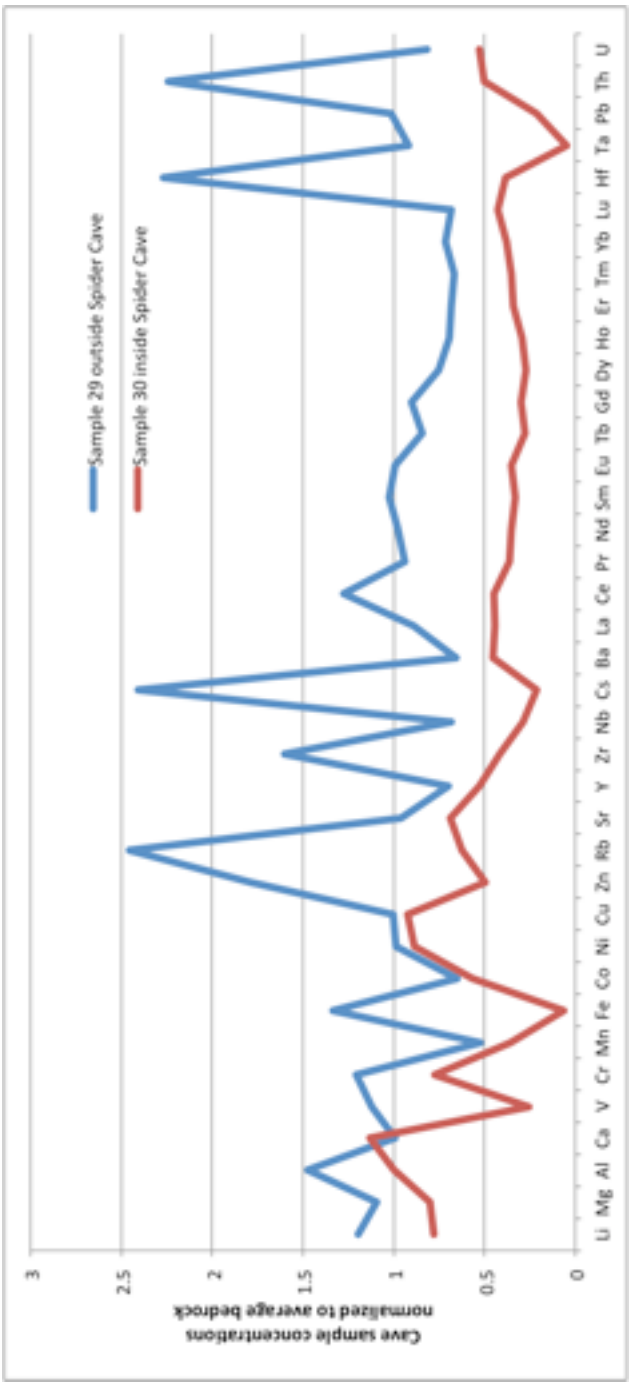

Figure 3.8. Plot of the trace and minor elements normalized to the average bedrock chemistry of Maax Na for samples 30 and 52 from inside and above Spider Cave.

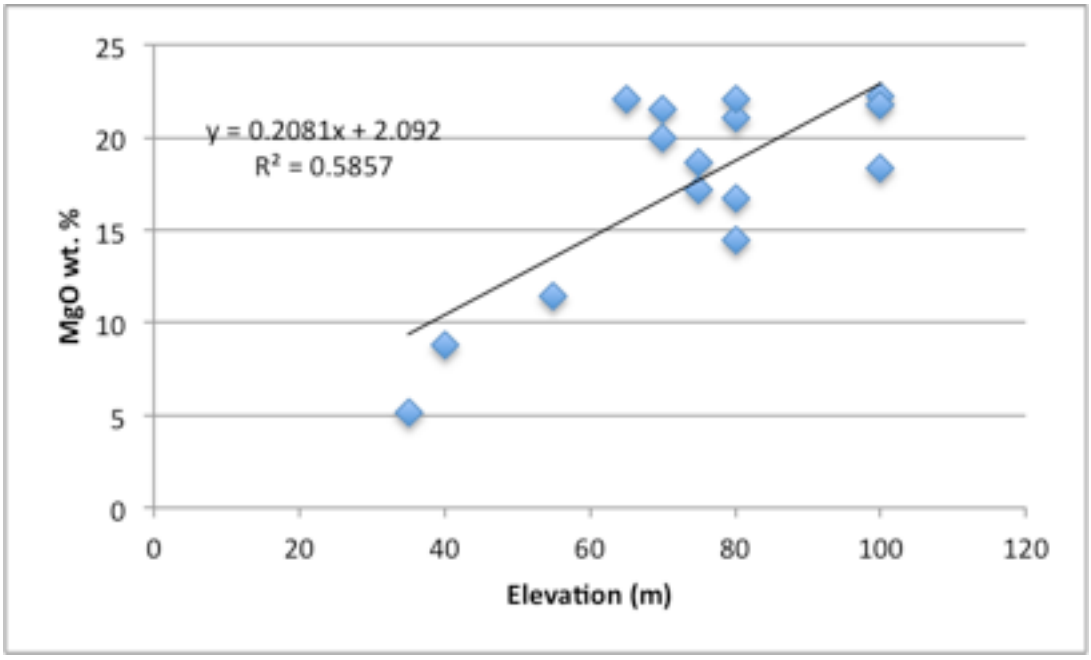

Figure 3.9. Plot of MgO wt. % versus elevation for bedrock samples at Chawak But'o'ob.

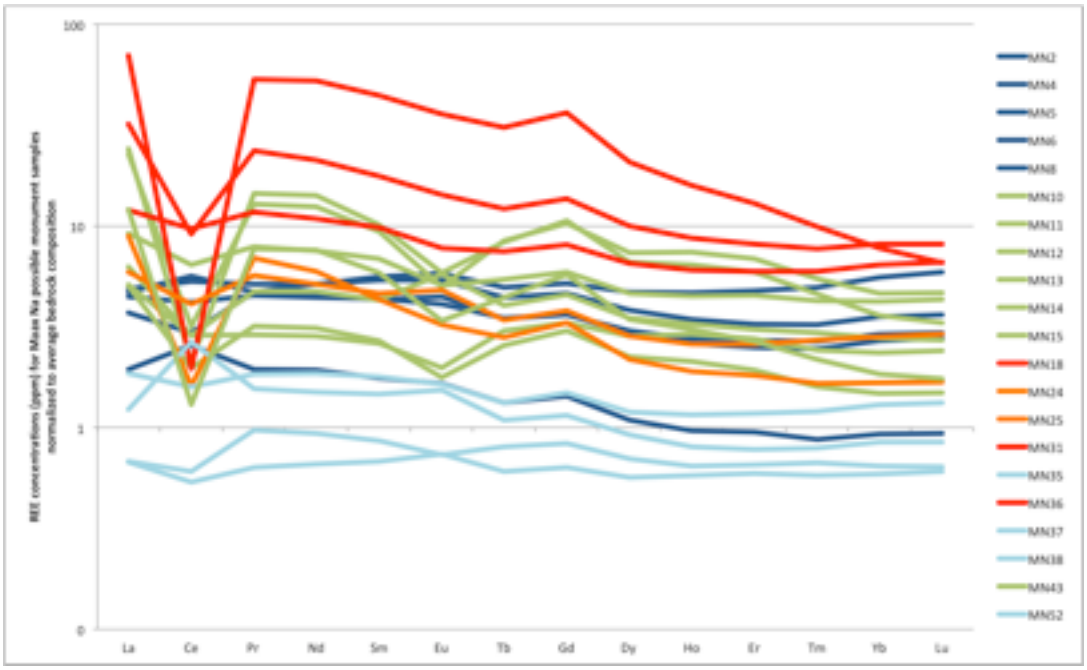

Figure 3.10. Plot of REE in possible monument samples from Maax Na, normalized to the average Maax Na bedrock chemistry. Red = stela samples, orange = ballcourt and altar, green = six small monuments, light blue = possible monuments, dark blue = Megalith 1.

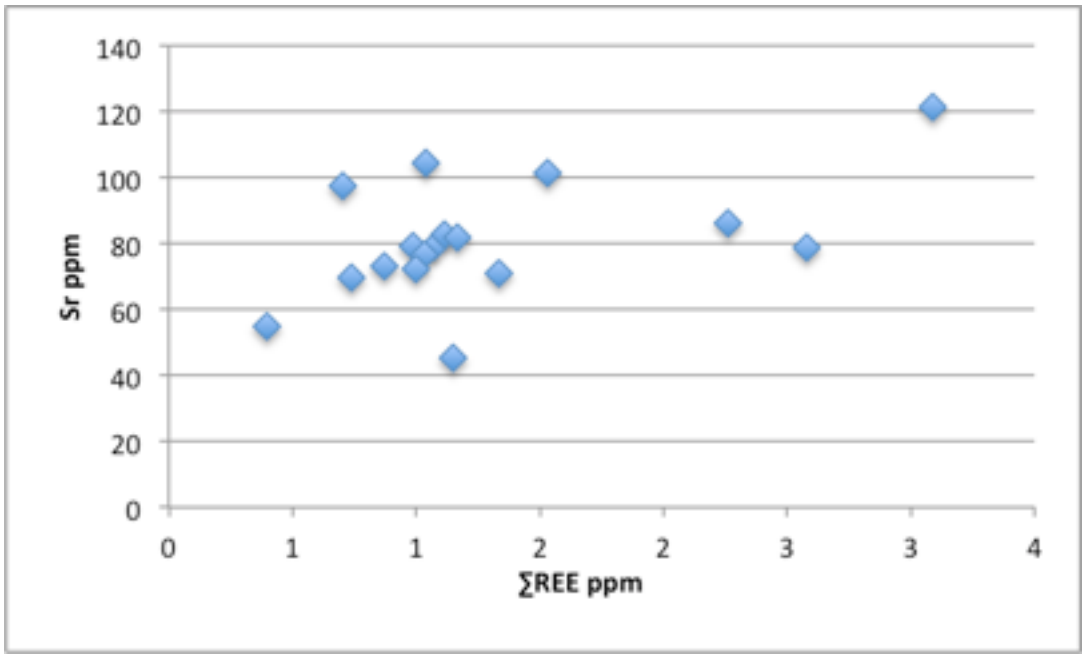

Figure 3.11. Plot of Sr vs ∑REE for Maax Na samples

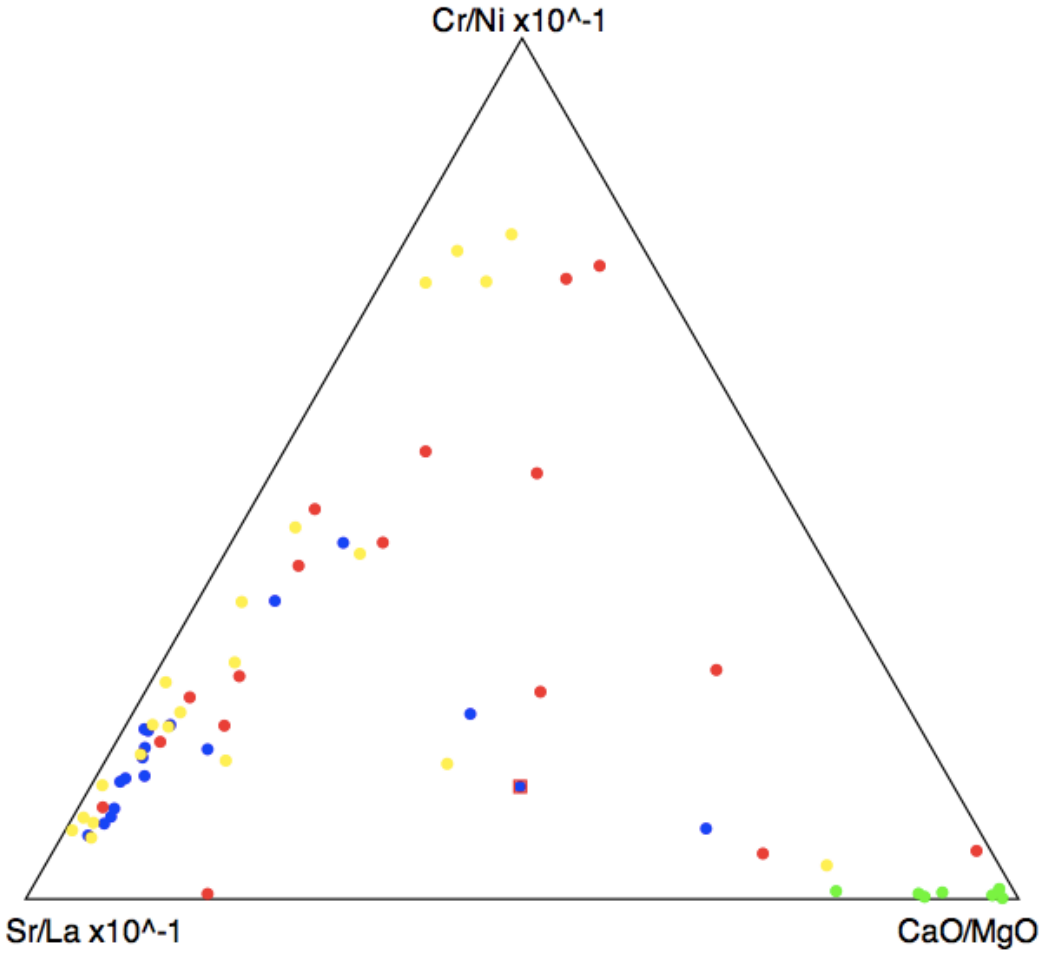

Figure 3.12. Ternary diagram plotting Cr/Ni, Sr/La, and CaO/MgO. Blue = Maax Na bedrock, red = Maax Na monuments, green = Maax Na small monuments, yellow = Chawak But'o'ob samples.

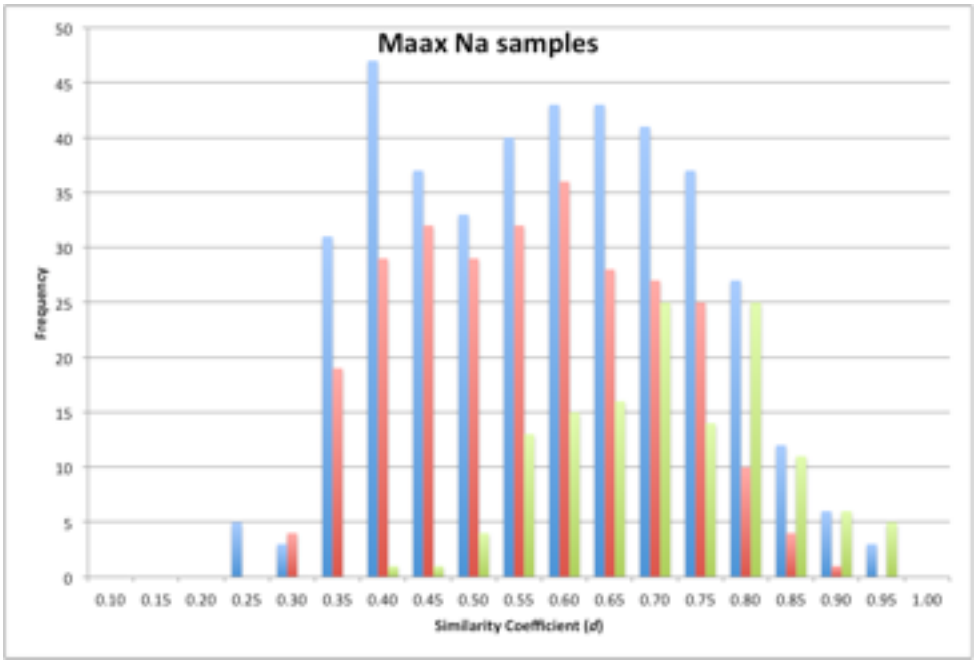

Figure 3.13. Histogram of the frequency of the similarity coefficients (*d*) for all the Maax Na samples. Green = *d* for bedrock vs. bedrock, red = *d* for monument vs. monument samples, blue = *d* for monument vs. bedrock samples.

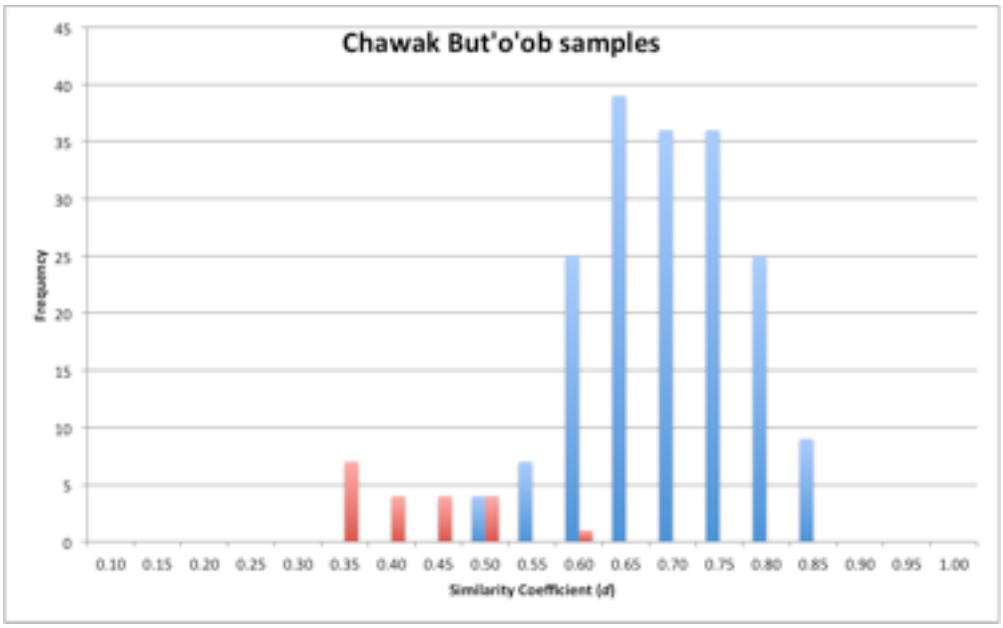

Figure 3.14. Histogram of the frequency of the similarity coefficients (*d*) for all the Chawak But'o'ob samples. Blue = *d* for bedrock vs. bedrock samples, red = *d* for sample 12 vs other samples.

Figure 3.15. Photograph of ~50 cm^3 small unknown monument at Maax Na. Photo by author.

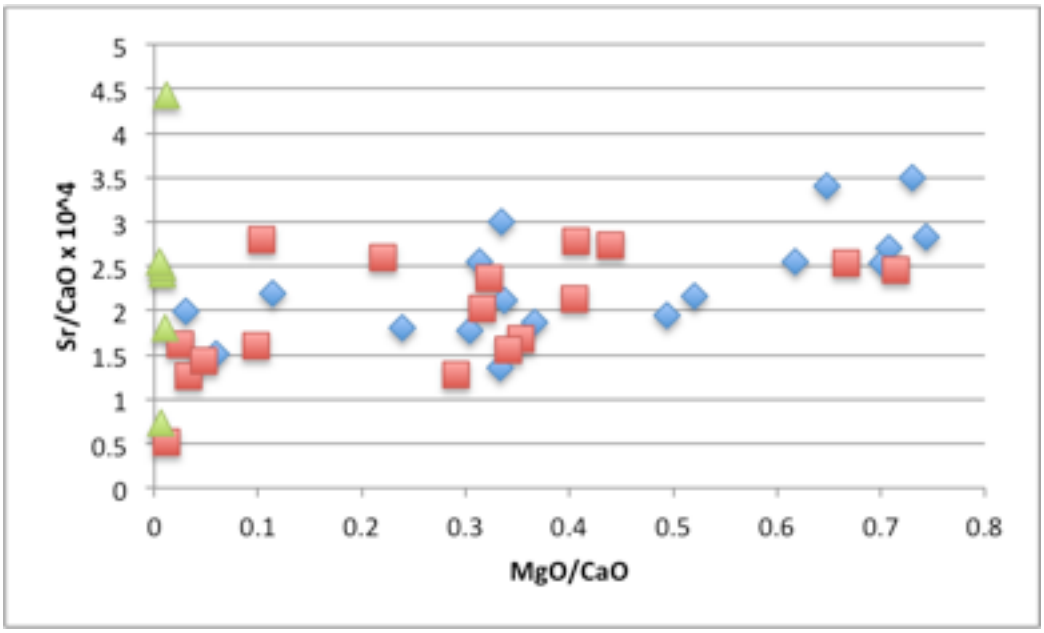

Figure 3.16. Bivariate plot of MgO/CaO vs Sr/CaO for Maax Na samples. Blue = bedrock, red = monuments, green = small monuments.

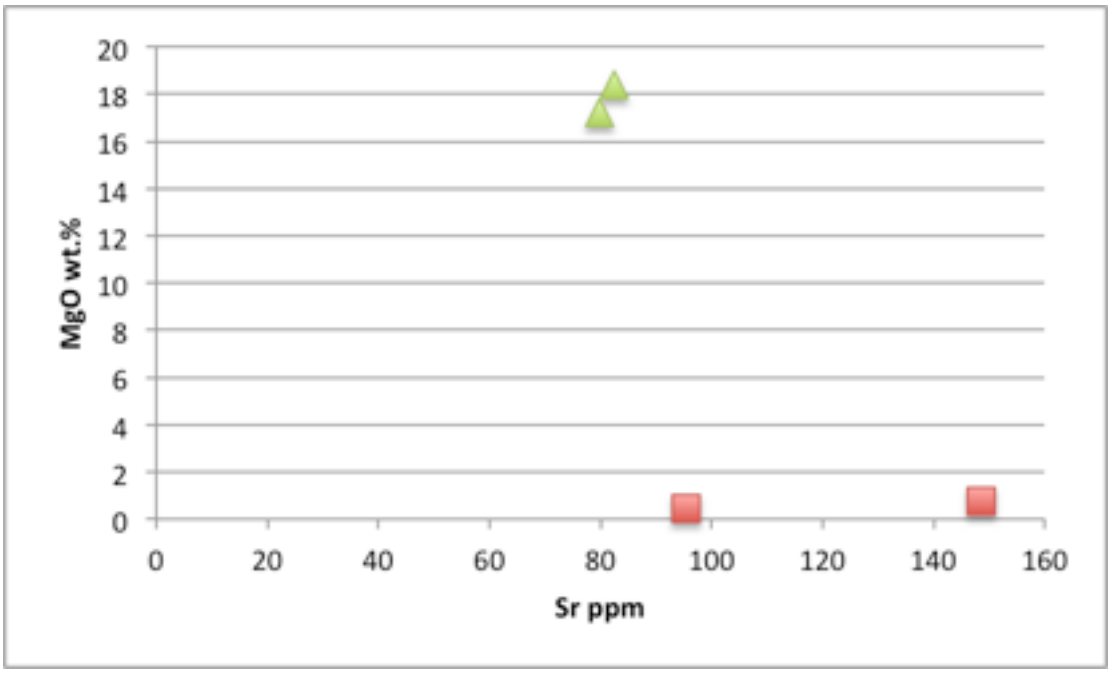

Figure 3.17. Bivariate plot of Mg vs Sr for Hun Tun samples. Green triangles = bedrock samples, red squares = monument samples.

APPENDIX A: Trace and minor element chemistry

	MN1	MN2	MN3	MN4	MN5	MN6	MN8	MN9	MN10	MN11	MN12	MN13
Li	1.453	1.239	1.117	1.381	2.395	1.977	2.844	0.842	0.719	0.963	0.961	2.591
V	2.254	8.628	4.693	0.702	11.892	7.181	13.527	3.966	6.422	6.818	9.336	8.337
Cr	4.769	6.906	5.385	2.762	14.670	10.246	19.087	10.298	0.758	0.392	0.275	0.490
Co	1.647	1.217	1.071	1.624	2.054	1.618	1.676	0.830	0.721	1.234	1.244	1.006
Ni	18.076	9.441	8.191	12.142	21.990	16.570	22.242	7.801	7.519	6.915	7.067	7.333
Cu	17.290	3.097	2.245	2.372	4.948	3.844	4.912	2.358	2.645	1.592	2.132	2.614
Zn	9.193	7.939	4.802	3.063	6.229	6.280	7.919	4.329	16.746	2.870	27.866	5.913
Rb	1.148	0.688	0.393	0.359	3.528	5.005	7.335	0.097	0.731	0.545	0.607	1.553
Sr	101.197	78.776	79.195	67.205	74.037	78.984	79.356	86.315	223.068	129.244	131.148	94.697
Y	0.611	0.546	0.449	2.345	1.253	1.407	1.667	1.694	2.174	5.999	2.162	1.606
Zr	2.338	1.184	0.754	1.762	2.901	3.731	4.715	0.369	4.689	1.317	1.436	3.291
Nb	0.078	0.059	0.026	0.002	0.130	0.203	0.159	*	0.337	0.096	0.113	0.275
Cs	0.092	0.027	0.036	0.015	0.157	0.246	0.336	0.007	0.077	0.037	0.035	0.075
Ba	90.101	7.973	7.745	82.388	10.929	70.412	43.736	12.631	221.906	6.431	6.233	7.360
La	0.242	0.352	0.204	0.676	0.809	0.851	0.884	0.393	1.135	4.130	0.930	0.914
Ce	0.507	0.802	0.386	0.925	1.318	1.772	1.662	0.397	0.897	0.992	0.898	0.619
Pr	0.062	0.085	0.044	0.206	0.198	0.206	0.225	0.095	0.208	0.561	0.127	0.140
Nd	0.278	0.364	0.186	0.974	0.836	0.846	0.972	0.449	0.896	2.356	0.537	0.586
Sm	0.066	0.075	0.039	0.239	0.186	0.185	0.230	0.106	0.183	0.403	0.112	0.115
Eu	0.030	0.020	0.012	0.070	0.050	0.054	0.066	0.025	0.070	0.060	0.024	0.022
Tb	0.012	0.012	0.008	0.046	0.032	0.032	0.041	0.029	0.037	0.078	0.028	0.024
Gd	0.076	0.078	0.047	0.284	0.200	0.198	0.253	0.166	0.248	0.561	0.181	0.165
Dy	0.083	0.072	0.050	0.309	0.192	0.199	0.251	0.228	0.230	0.486	0.187	0.148
Ho	0.020	0.015	0.012	0.073	0.041	0.043	0.054	0.056	0.051	0.116	0.046	0.033
Er	0.062	0.043	0.037	0.217	0.113	0.123	0.149	0.153	0.139	0.312	0.125	0.088
Tm	0.010	0.006	0.006	0.034	0.017	0.018	0.022	0.021	0.020	0.037	0.016	0.011
Yb	0.068	0.037	0.037	0.222	0.108	0.117	0.142	0.121	0.111	0.185	0.094	0.059
Lu	0.013	0.006	0.006	0.037	0.018	0.019	0.023	0.019	0.017	0.029	0.015	0.009
Hf	0.067	0.036	0.022	0.044	0.086	0.106	0.130	0.008	0.102	0.045	0.045	0.115
Ta	0.006	0.005	0.004	0.001	0.011	0.021	0.013	0.003	0.020	0.020	0.227	0.308
Pb	0.173	0.242	0.363	0.072	0.613	0.415	0.522	0.314	5.418	0.238	0.337	0.121
Th	0.105	0.050	0.039	0.263	0.118	0.224	0.186	0.018	0.150	0.164	0.082	0.237
U	0.182	1.072	1.523	0.036	0.993	0.223	0.429	0.662	0.514	0.688	1.285	0.788

Maax Na ICP-MS data in ppm, * = values below instrument detection limit

	MN14	MN15	MN16	MN17	MN18	MN19	MN20	MN21	MN22	MN23	MN24
Li	2.263	0.518	1.867	1.611	1.569	1.205	1.533	1.662	1.514	1.842	1.601
V	0.985	1.385	8.097	10.276	7.721	5.888	5.072	0.918	13.565	5.537	1.662
Cr	1.494	0.136	7.221	8.318	11.391	7.711	3.865	1.252	12.749	13.313	8.569
Co	1.577	0.633	0.575	0.563	1.553	0.971	0.909	1.185	1.340	0.973	1.601
Ni	7.665	6.442	10.163	8.062	13.184	7.481	7.690	9.286	8.005	17.574	8.514
Cu	5.463	1.362	4.239	2.785	3.089	2.467	2.926	2.310	2.051	4.733	3.480
Zn	71.517	1.627	4.729	1.668	1.502	14.435	3.498	4.472	4.515	14.080	42.213
Rb	2.947	0.117	1.513	0.270	0.456	0.098	0.150	0.030	0.160	3.534	0.569
Sr	37.459	139.595	79.409	82.716	80.675	66.481	69.456	85.866	100.840	71.127	69.189
Y	2.927	5.249	0.451	0.557	6.202	5.321	0.258	0.302	6.544	0.471	1.640
Zr	4.324	0.506	1.100	0.265	0.751	0.279	0.378	1.031	2.376	3.321	3.355
Nb	0.248	0.022	0.021	0.012	0.032	0.009	0.033	*	0.083	0.083	0.228
Cs	0.251	0.013	0.110	0.021	0.043	0.005	0.008	*	0.016	0.202	0.085
Ba	72.946	10.998	6.367	5.093	8.573	6.362	6.067	161.385	52.610	85.038	100.595
La	1.671	4.374	0.182	0.201	12.707	0.995	0.138	0.048	0.595	0.224	1.069
Ce	2.006	0.662	0.449	0.281	0.614	0.248	0.344	0.071	0.572	0.405	1.288
Pr	0.344	0.635	0.032	0.054	2.333	0.046	0.026	0.017	0.175	0.065	0.248
Nd	1.426	2.677	0.137	0.242	9.926	0.159	0.103	0.089	0.835	0.279	0.975
Sm	0.294	0.434	0.030	0.059	1.892	0.032	0.022	0.023	0.210	0.066	0.198
Eu	0.062	0.071	0.009	0.014	0.435	0.009	0.007	0.036	0.053	0.031	0.058
Tb	0.050	0.077	0.006	0.012	0.284	0.009	0.004	0.005	0.052	0.012	0.032
Gd	0.323	0.579	0.035	0.067	1.994	0.050	0.025	0.031	0.310	0.070	0.207
Dy	0.305	0.435	0.038	0.072	1.367	0.117	0.024	0.036	0.420	0.070	0.186
Ho	0.070	0.101	0.009	0.016	0.248	0.052	0.006	0.010	0.127	0.015	0.041
Er	0.205	0.268	0.027	0.047	0.586	0.236	0.018	0.032	0.468	0.042	0.118
Tm	0.029	0.031	0.004	0.007	0.067	0.044	0.003	0.005	0.083	0.007	0.019
Yb	0.169	0.144	0.025	0.037	0.312	0.263	0.015	0.040	0.601	0.042	0.113
Lu	0.027	0.021	0.004	0.006	0.042	0.043	0.002	0.008	0.123	0.007	0.018
Hf	0.117	0.012	0.031	0.006	0.021	0.007	0.010	0.014	0.048	0.049	0.099
Ta	0.022	0.004	0.003	0.002	0.003	0.000	0.005	0.005	0.022	0.006	0.016
Pb	1.043	0.154	0.287	0.191	0.497	0.448	0.363	*	0.245	5.120	13.188
Th	0.267	0.022	0.025	0.020	0.063	0.011	0.021	0.034	0.160	0.052	0.202
U	0.108	0.504	2.073	1.533	0.409	0.606	0.827	0.148	1.969	0.517	0.107

Maax Na ICP-MS data in ppm continued, * = values below instrument detection limit

	MN25	MN29	MN30	MN31	MN32	MN33	MN35	MN36	MN37	MN38	MN41
Li	0.892	1.484	0.965	2.788	0.684	0.728	1.056	2.099	0.919	1.258	1.654
V	4.070	7.440	1.704	15.507	3.304	1.875	3.858	1.815	4.122	18.162	3.425
Cr	13.032	9.565	6.144	13.363	7.569	8.686	10.239	4.662	7.541	9.113	5.952
Co	0.429	0.471	0.409	1.410	0.524	1.027	0.565	1.817	0.465	0.762	3.025
Ni	7.299	9.130	8.175	11.018	6.900	8.233	7.493	8.865	7.010	13.095	14.482
Cu	1.547	2.771	2.550	3.142	1.695	2.616	1.894	2.080	3.175	2.448	4.490
Zn	6.125	18.641	5.144	6.334	2.940	3.781	18.731	10.299	21.396	19.526	15.354
Rb	1.174	1.007	0.255	6.840	0.486	0.861	1.665	8.878	0.150	1.041	3.165
Sr	138.778	76.456	54.785	93.084	121.362	78.626	116.903	29.437	106.929	54.041	99.106
Y	1.187	0.374	0.284	4.777	1.618	1.741	0.963	3.404	0.450	0.379	1.481
Zr	1.355	0.787	0.204	5.775	0.387	2.322	1.047	5.355	0.160	2.198	3.889
Nb	0.079	0.013	0.005	0.248	0.014	0.100	0.095	0.512	0.006	0.102	0.247
Cs	0.087	0.075	0.007	0.465	0.017	0.098	0.103	0.917	0.030	0.072	0.166
Ba	2.334	8.379	5.759	79.882	5.221	31.929	3.243	41.970	8.106	27.600	138.129
La	1.618	0.162	0.081	5.803	0.968	0.360	0.338	2.177	0.122	0.224	0.721
Ce	0.504	0.401	0.141	2.853	0.410	0.767	0.500	3.030	0.168	0.831	2.997
Pr	0.302	0.041	0.016	1.034	0.183	0.103	0.081	0.514	0.028	0.068	0.207
Nd	1.118	0.184	0.067	4.000	0.731	0.461	0.352	2.042	0.125	0.284	0.849
Sm	0.184	0.044	0.014	0.754	0.142	0.113	0.076	0.419	0.029	0.062	0.200
Eu	0.039	0.012	0.004	0.174	0.032	0.033	0.020	0.094	0.009	0.019	0.063
Tb	0.026	0.008	0.003	0.112	0.025	0.025	0.012	0.069	0.006	0.010	0.034
Gd	0.181	0.049	0.016	0.747	0.160	0.147	0.081	0.441	0.035	0.063	0.207
Dy	0.143	0.050	0.018	0.658	0.160	0.185	0.078	0.427	0.037	0.061	0.206
Ho	0.030	0.011	0.005	0.137	0.037	0.046	0.018	0.095	0.009	0.013	0.045
Er	0.082	0.031	0.015	0.368	0.108	0.146	0.053	0.270	0.027	0.035	0.134
Tm	0.011	0.005	0.002	0.052	0.016	0.023	0.008	0.040	0.004	0.005	0.022
Yb	0.067	0.029	0.015	0.327	0.099	0.148	0.052	0.257	0.023	0.034	0.130
Lu	0.011	0.004	0.003	0.051	0.016	0.024	0.008	0.042	0.004	0.005	0.021
Hf	0.047	0.030	0.005	0.173	0.011	0.075	0.037	0.188	0.004	0.071	0.113
Ta	0.005	0.002	*	0.015	0.001	0.009	0.004	0.040	*	0.006	0.017
Pb	0.387	0.255	0.053	0.671	0.338	0.284	0.369	1.073	0.240	0.590	1.069
Th	0.072	0.058	0.013	0.402	0.077	0.191	0.055	0.503	0.014	0.054	0.200
U	0.329	0.992	0.640	1.071	1.127	0.184	0.382	0.096	0.966	0.974	0.188

Maax Na ICP-MS data in ppm continued, * = values below instrument detection limit

	MN43	MN44	MN46	MN50	MN51	MN52	MN53	MN54
Li	0.903	2.851	0.989	1.666	0.858	0.964	0.922	0.918
V	1.596	7.391	12.725	5.851	7.948	6.360	6.509	3.499
Cr	0.777	5.873	10.467	5.712	7.552	10.110	10.379	7.602
Co	0.610	0.791	0.944	0.808	0.723	0.555	0.622	1.107
Ni	7.744	4.538	10.739	13.039	8.249	8.373	8.383	10.138
Cu	2.670	3.362	3.620	2.729	1.608	1.725	1.610	3.220
Zn	24.906	18.552	7.047	27.705	8.228	18.204	7.077	26.631
Rb	0.603	0.500	0.186	0.192	0.022	0.038	0.172	0.643
Sr	206.155	45.357	72.292	104.299	97.444	62.868	72.926	81.766
Y	2.303	0.205	0.799	0.483	0.237	0.358	0.304	0.446
Zr	1.280	0.268	0.299	0.843	0.109	0.149	0.364	0.681
Nb	0.155	0.036	0.026	0.034	0.006	0.008	0.022	0.034
Cs	0.057	0.016	0.014	0.018	0.001	0.002	0.013	0.069
Ba	21.389	82.201	16.642	41.397	13.482	5.919	14.367	10.413
La	2.189	0.089	0.131	0.196	0.130	0.123	0.158	0.224
Ce	0.408	0.242	0.267	0.310	0.264	0.190	0.292	0.308
Pr	0.337	0.055	0.032	0.049	0.031	0.043	0.042	0.062
Nd	1.435	0.358	0.132	0.204	0.126	0.177	0.169	0.264
Sm	0.250	0.078	0.027	0.045	0.028	0.037	0.037	0.059
Eu	0.041	0.034	0.010	0.017	0.009	0.009	0.011	0.016
Tb	0.041	0.024	0.011	0.009	0.005	0.007	0.007	0.010
Gd	0.314	0.140	0.054	0.052	0.030	0.046	0.041	0.066
Dy	0.226	0.073	0.106	0.056	0.031	0.046	0.042	0.060
Ho	0.048	0.011	0.030	0.013	0.007	0.010	0.009	0.013
Er	0.121	0.023	0.088	0.038	0.019	0.030	0.027	0.037
Tm	0.015	0.003	0.014	0.006	0.003	0.005	0.004	0.006
Yb	0.074	0.017	0.082	0.038	0.018	0.026	0.027	0.034
Lu	0.011	0.002	0.013	0.006	0.003	0.004	0.004	0.005
Hf	0.038	0.008	0.011	0.016	0.003	0.004	0.009	0.017
Ta	0.011	0.001	0.002	0.002	0.001	0.001	0.002	0.003
Pb	12.767	6.676	0.213	0.263	0.358	0.093	0.148	0.319
Th	0.091	0.017	0.041	0.020	0.009	0.011	0.020	0.042
U	0.213	1.332	0.945	1.881	1.360	0.889	1.578	0.854

Maax Na ICP-MS data in ppm continued

	MN1	MN2	MN3	MN4	MN5	MN6	MN8	MN9	MN10	MN11	MN12
MgO	5.27	20.66	21.92	1.72	21.55	4.84	12.37	13.78	0.57	0.43	0.39
Al2O3	0.25	0.23	0.15	0.15	0.49	0.58	0.70	0.10	0.31	0.19	0.22
CaO	46.05	31.03	31.25	53.03	30.15	49.48	39.12	40.86	50.32	53.49	52.72
MnO	0.00	0.00	0.00	0.00	0.00	0.00	0.00	0.00	0.00	0.00	0.01
Fe2O3	0.03	0.04	0.01	0.01	0.21	0.26	0.35	*	0.10	0.01	0.03

	MN13	MN14	MN15	MN16	MN17	MN18	MN19	MN20	MN21	MN22	MN23
MgO	0.55	0.32	0.28	20.74	21.77	15.30	14.00	17.58	1.33	16.16	9.42
Al2O3	0.40	0.43	0.13	0.22	0.11	0.13	0.12	0.13	0.12	0.11	0.32
CaO	52.57	51.37	54.63	29.31	29.26	37.76	39.60	35.63	53.11	36.79	39.46
MnO	0.01	0.00	0.01	0.00	0.00	0.01	0.01	0.00	0.00	0.01	0.00
Fe2O3	0.08	0.06	0.00	0.02	0.00	0.03	*	0.03	*	0.01	0.09

	MN24	MN29	MN30	MN31	MN32	MN33	MN35	MN36	MN37	MN38	MN41
MgO	2.27	18.35	13.42	12.70	13.55	3.13	9.95	0.64	15.58	12.26	1.54
Al2O3	0.36	0.17	0.11	0.60	0.13	0.28	0.29	0.68	0.09	0.31	0.40
CaO	48.24	35.26	40.26	39.35	40.53	52.26	45.06	56.16	38.34	42.08	49.83
MnO	0.00	0.00	0.00	0.00	0.00	0.00	0.00	0.01	0.01	0.01	0.02
Fe2O3	0.08	0.02	*	0.11	0.00	0.04	0.03	0.16	0.00	0.07	0.10

	MN43	MN44	MN50	MN51	MN52	MN53	MN54
MgO	0.46	9.46	19.89	12.01	13.82	14.38	19.81
Al2O3	0.17	0.04	0.07	0.07	0.07	0.09	0.11
CaO	54.08	12.96	30.70	38.33	40.48	39.22	32.09
MnO	0.00	0.00	0.01	0.01	0.00	0.00	0.00
Fe2O3	0.05	0.07	0.02	0.01	0.01	0.03	0.03

Maax Na ICP-AES data in wt.%, * = values below instrument detection limit

	CB1	CB2	CB3	CB4	CB5	CB6	CB7A	CB8	CB9A	CB9B	CB10
Li	0.809	1.048	2.381	0.827	0.695	1.638	1.729	1.048	0.604	0.623	0.521
V	14.213	22.415	3.013	7.033	10.601	1.228	22.045	2.003	4.664	2.452	2.787
Cr	9.309	10.078	18.904	11.800	8.295	3.215	6.890	7.416	4.849	7.786	8.702
Co	0.596	1.107	1.463	0.499	0.616	0.909	0.573	1.798	0.466	0.814	0.639
Ni	5.891	7.014	7.264	6.734	6.038	7.700	10.313	7.074	7.853	6.915	10.543
Cu	2.367	2.746	2.211	2.297	4.909	3.010	5.194	3.132	7.982	2.723	6.568
Zn	5.980	6.360	12.920	7.640	24.690	10.960	7.669	8.595	4.094	7.102	4.221
Rb	0.157	0.199	1.783	0.083	0.336	3.805	1.594	1.337	0.141	0.046	0.026
Sr	88.943	108.327	69.871	73.212	74.660	97.316	112.411	117.996	69.300	71.340	66.468
Y	0.143	0.480	2.843	4.420	0.518	1.068	2.517	2.585	0.631	1.179	0.268
Zr	0.277	0.910	6.919	0.969	1.222	5.878	1.380	3.726	2.335	0.566	1.010
Nb	0.011	0.030	0.697	0.094	0.114	0.363	0.035	0.209	*	0.011	*
Cs	0.008	0.027	0.244	0.022	0.057	0.805	0.249	0.203	0.009	0.004	0.002
Ba	5.915	14.587	22.007	13.705	16.150	124.665	28.305	68.857	5.690	16.656	14.416
La	0.049	0.080	1.666	1.668	0.308	0.737	0.446	0.976	0.089	0.534	0.080
Ce	0.070	0.135	2.229	0.986	0.616	1.502	0.339	1.408	0.078	0.254	0.073
Pr	0.014	0.020	0.445	0.358	0.084	0.199	0.051	0.158	0.018	0.115	0.017
Nd	0.058	0.090	1.731	1.357	0.301	0.771	0.203	0.639	0.070	0.508	0.075
Sm	0.013	0.021	0.356	0.244	0.060	0.158	0.044	0.142	0.013	0.113	0.016
Eu	0.004	0.007	0.074	0.051	0.012	0.050	0.015	0.042	0.004	0.025	0.006
Tb	0.002	0.005	0.059	0.051	0.010	0.026	0.013	0.035	0.002	0.023	0.004
Gd	0.014	0.028	0.362	0.306	0.060	0.155	0.070	0.191	0.015	0.143	0.025
Dy	0.015	0.035	0.359	0.360	0.067	0.151	0.139	0.285	0.015	0.143	0.029
Ho	0.003	0.009	0.077	0.092	0.016	0.033	0.044	0.077	0.003	0.032	0.008
Er	0.009	0.031	0.227	0.297	0.051	0.096	0.147	0.236	0.017	0.091	0.025
Tm	0.001	0.005	0.037	0.049	0.009	0.016	0.023	0.037	0.004	0.014	0.004
Yb	0.008	0.033	0.227	0.295	0.060	0.098	0.129	0.216	0.030	0.082	0.022
Lu	0.001	0.006	0.037	0.049	0.011	0.016	0.021	0.033	0.006	0.013	0.003
Hf	0.007	0.032	0.241	0.037	0.058	0.183	0.036	0.115	0.022	0.014	0.006
Ta	0.001	0.002	0.051	0.013	0.017	0.025	0.000	0.010	*	*	*
Pb	0.076	0.053	0.823	0.478	0.107	0.504	0.322	0.324	0.043	0.215	0.062
Th	0.008	0.032	0.556	0.402	0.311	0.309	0.041	0.221	0.012	0.049	0.015
U	2.569	4.897	0.347	1.969	0.318	0.172	1.957	0.525	0.372	0.583	0.433

Chawak But'o'ob ICP-MS data in ppm, * = values below instrument detection limit

	CB11	CB12	CB13	CB14	CB15	CB16	CB17	CB18	CB19	CB20
Li	1.163	0.802	0.801	0.667	0.626	1.034	0.843	0.696	0.627	1.904
V	1.456	3.803	27.354	30.515	49.623	20.235	4.433	18.528	2.034	11.129
Cr	4.722	1.726	8.649	3.032	11.425	8.541	10.945	24.196	8.719	15.576
Co	1.192	1.703	0.428	0.488	0.818	1.116	0.455	0.524	0.380	1.419
Ni	7.074	7.912	5.261	5.936	10.503	10.567	4.672	5.193	5.240	6.821
Cu	2.087	1.574	2.183	2.362	5.227	3.896	2.027	1.593	4.238	2.320
Zn	5.873	14.579	5.069	24.339	6.854	3.448	2.171	2.267	4.832	3.549
Rb	1.055	0.445	0.289	0.121	0.134	1.036	0.155	0.353	0.031	1.988
Sr	86.564	246.471	127.509	97.549	89.559	106.772	88.652	129.191	52.530	84.368
Y	0.738	4.304	0.248	3.125	0.617	0.572	0.230	1.605	0.298	3.661
Zr	3.134	2.714	0.520	0.477	3.105	1.618	0.535	0.878	1.326	5.065
Nb	0.081	0.201	0.015	0.012	0.049	0.111	0.013	0.053	0.009	0.424
Cs	0.104	0.153	0.033	0.008	0.023	0.097	0.028	0.046	0.003	0.482
Ba	71.365	361.494	6.112	10.662	15.255	12.839	6.052	2.945	2.565	31.157
La	0.291	2.545	0.120	0.805	0.173	0.390	0.130	0.831	0.083	1.494
Ce	0.658	3.491	0.157	0.129	0.251	0.724	0.199	0.759	0.108	1.911
Pr	0.070	0.560	0.023	0.228	0.042	0.087	0.030	0.175	0.040	0.405
Nd	0.292	2.232	0.100	1.014	0.168	0.354	0.119	0.691	0.208	1.706
Sm	0.063	0.441	0.023	0.191	0.037	0.074	0.026	0.149	0.051	0.374
Eu	0.024	0.142	0.006	0.043	0.011	0.018	0.006	0.028	0.012	0.085
Tb	0.012	0.075	0.005	0.043	0.009	0.012	0.004	0.030	0.010	0.067
Gd	0.074	0.473	0.026	0.272	0.046	0.079	0.026	0.179	0.066	0.422
Dy	0.080	0.450	0.030	0.284	0.069	0.080	0.025	0.191	0.051	0.431
Ho	0.019	0.100	0.007	0.067	0.017	0.018	0.006	0.041	0.010	0.100
Er	0.059	0.285	0.020	0.194	0.054	0.050	0.016	0.117	0.026	0.300
Tm	0.010	0.043	0.003	0.029	0.010	0.008	0.002	0.017	0.004	0.050
Yb	0.067	0.249	0.019	0.161	0.063	0.049	0.015	0.095	0.021	0.323
Lu	0.012	0.038	0.003	0.025	0.010	0.008	0.002	0.015	0.003	0.056
Hf	0.060	0.080	0.013	0.013	0.086	0.047	0.010	0.019	0.006	0.197
Ta	0.004	0.013	0.001	*	0.001	0.007	0.001	0.002	*	0.030
Pb	0.173	0.556	0.098	0.055	0.064	0.235	0.049	0.410	0.098	0.529
Th	0.129	0.297	0.017	0.022	0.104	0.108	0.037	0.063	0.012	0.431
U	0.398	0.356	3.253	7.101	2.016	1.736	1.188	1.786	0.597	2.534

Chawak But'o'ob ICP-MS data in ppm continued, * = values below instrument detection limit

	CB1	CB2	CB3	CB4	CB5	CB6	CB7A	CB8	CB9A	CB9B	CB10
MgO	22.22	19.96	11.43	22.08	18.37	5.16	21.61	11.34	14.46	21.02	16.73
Al2O3	0.07	0.09	0.85	0.13	0.15	0.48	0.21	0.26	0.10	0.08	0.08
CaO	30.55	33.13	39.75	29.86	32.88	47.43	31.47	40.34	38.06	30.54	37.12
MnO	0.00	0.00	0.00	0.01	0.00	0.00	0.00	0.00	0.00	0.00	0.01
Fe2O3	0.01	0.01	0.18	0.06	0.02	0.09	0.02	0.06	0.01	0.03	0.01

	CB11	CB12	CB13	CB14	CB15	CB16	CB17	CB18	CB19	CB20
MgO	8.79	1.17	22.04	21.51	17.13	18.64	21.76	13.50	16.58	12.35
Al2O3	0.19	0.38	0.10	0.09	0.11	0.23	0.08	0.12	0.08	0.52
CaO	44.16	51.33	30.58	29.23	35.50	32.86	30.67	39.33	36.26	41.34
MnO	0.00	0.10	0.00	0.01	0.00	0.00	0.00	0.00	0.00	0.00
Fe2O3	0.03	0.22	0.01	0.03	0.02	0.04	0.01	0.02	0.02	0.12

Chawak But'o'ob ICP-AES data in wt.%, * = values below instrument detection limit

	HT1	HT2	HT3	HT4
Li	0.105	1.870	1.056	1.489
V	1.571	1.879	16.211	9.294
Cr	15.640	6.562	11.605	8.021
Co	0.510	0.827	1.436	0.693
Ni	8.963	10.170	12.344	9.505
Cu	1.457	2.447	4.132	28.575
Zn	10.221	6.044	4.196	18.382
Rb	0.094	0.486	0.774	0.414
Sr	148.523	95.449	79.930	82.588
Y	5.476	9.619	6.832	2.275
Zr	0.339	4.165	3.860	1.396
Nb	0.013	0.078	0.039	0.037
Cs	0.010	0.050	0.101	0.039
Ba	2.244	30.730	21.308	17.177
La	2.597	8.580	1.258	0.257
Ce	2.225	11.102	0.740	0.458
Pr	0.553	2.056	0.275	0.064
Nd	2.274	7.775	1.343	0.277
Sm	0.510	1.495	0.304	0.063
Eu	0.098	0.289	0.073	0.018
Tb	0.102	0.246	0.074	0.013
Gd	0.588	1.476	0.470	0.082
Dy	0.694	1.540	0.536	0.098
Ho	0.159	0.337	0.137	0.029
Er	0.487	1.004	0.423	0.118
Tm	0.078	0.168	0.065	0.023
Yb	0.507	1.202	0.400	0.165
Lu	0.081	0.202	0.068	0.036
Hf	0.009	0.094	0.102	0.037
Ta	0.001	0.007	0.003	0.003
Pb	0.866	0.901	0.567	0.409
Th	0.025	0.468	0.170	0.052
U	0.122	0.922	1.261	3.902

Hun Tun ICP-MS data in ppm

	HT1	HT2	HT3	HT4
MgO	0.75	0.44	17.22	18.36
Al2O3	0.14	0.31	0.18	0.14
CaO	54.70	53.89	36.51	34.06
MnO	0.03	0.01	0.01	0.00
Fe2O3	0.05	0.13	0.06	0.02

Hun Tun ICP-AES data in wt.%

APPENDIX B: Similarity Indices

	2	4	5	6	8	10	11	12	13	14	15
2	1.000										
4	0.406	1.000									
5	0.507	0.505	1.000								
6	0.430	0.527	0.768	1.000							
8	0.401	0.532	0.742	0.776	1.000						
10	0.413	0.534	0.588	0.632	0.600	1.000					
11	0.451	0.557	0.438	0.456	0.452	0.540	1.000				
12	0.575	0.500	0.568	0.534	0.476	0.619	0.604	1.000			
13	0.539	0.444	0.614	0.586	0.512	0.625	0.468	0.679	1.000		
14	0.311	0.608	0.746	0.638	0.622	0.586	0.522	0.443	0.488	1.000	
15	0.687	0.470	0.806	0.330	0.359	0.435	0.636	0.441	0.378	0.424	1.000

Similarity index test on a small number of samples from Maax Na for all 38 elements

	2	4	5	6	8	10	11	12	13	14	15	18	19	21
2	1.000													
4	0.537	1.000												
5	0.701	0.522	1.000											
6	0.593	0.656	0.695	1.000										
8	0.595	0.530	0.825	0.737	1.000									
10	0.369	0.511	0.344	0.455	0.389	1.000								
11	0.347	0.439	0.282	0.381	0.321	0.665	1.000							
12	0.396	0.523	0.394	0.498	0.444	0.725	0.797	1.000						
13	0.447	0.591	0.439	0.552	0.492	0.798	0.742	0.821	1.000					
14	0.389	0.548	0.340	0.437	0.369	0.647	0.594	0.625	0.630	1.000				
15	0.321	0.391	0.264	0.354	0.301	0.555	0.796	0.706	0.584	0.565	1.000			
18	0.648	0.479	0.644	0.637	0.669	0.313	0.374	0.332	0.380	0.344	0.355	1.000		
19	0.724	0.585	0.665	0.675	0.723	0.516	0.417	0.533	0.576	0.520	0.388	0.669	1.000	
21	0.478	0.640	0.343	0.477	0.384	0.536	0.508	0.495	0.591	0.556	0.435	0.426	0.438	1.000
22	0.731	0.537	0.712	0.635	0.699	0.457	0.422	0.506	0.546	0.423	0.394	0.711	0.765	0.444
24	0.611	0.716	0.565	0.744	0.588	0.572	0.457	0.558	0.611	0.556	0.419	0.545	0.776	0.568
25	0.494	0.498	0.517	0.710	0.556	0.575	0.552	0.588	0.555	0.556	0.537	0.539	0.638	0.454
31	0.614	0.472	0.617	0.601	0.695	0.363	0.476	0.385	0.439	0.381	0.460	0.800	0.674	0.452
35	0.712	0.497	0.537	0.654	0.601	0.474	0.472	0.520	0.520	0.426	0.440	0.612	0.708	0.464
36	0.456	0.565	0.343	0.461	0.361	0.573	0.539	0.508	0.576	0.691	0.478	0.389	0.517	0.503
37	0.717	0.431	0.531	0.521	0.561	0.403	0.440	0.455	0.467	0.384	0.408	0.654	0.754	0.487
38	0.689	0.550	0.585	0.645	0.653	0.330	0.311	0.342	0.379	0.404	0.290	0.697	0.712	0.431
43	0.345	0.467	0.285	0.387	0.323	0.854	0.747	0.692	0.708	0.684	0.630	0.325	0.435	0.536
52	0.692	0.495	0.576	0.600	0.617	0.368	0.361	0.380	0.422	0.424	0.337	0.691	0.782	0.500
1	0.601	0.578	0.513	0.717	0.566	0.378	0.375	0.405	0.449	0.368	0.343	0.521	0.528	0.490
9	0.788	0.528	0.629	0.670	0.700	0.437	0.414	0.470	0.525	0.436	0.386	0.713	0.803	0.491
16	0.889	0.495	0.673	0.559	0.565	0.329	0.327	0.352	0.402	0.355	0.302	0.654	0.685	0.482
17	0.851	0.456	0.674	0.551	0.552	0.363	0.360	0.388	0.441	0.381	0.334	0.636	0.708	0.472
20	0.727	0.548	0.563	0.480	0.533	0.391	0.377	0.394	0.446	0.453	0.345	0.602	0.712	0.509
23	0.639	0.517	0.690	0.698	0.731	0.308	0.302	0.333	0.377	0.335	0.282	0.679	0.638	0.425
29	0.814	0.486	0.656	0.604	0.606	0.353	0.352	0.375	0.423	0.381	0.328	0.711	0.719	0.506
30	0.683	0.491	0.500	0.510	0.562	0.367	0.356	0.368	0.408	0.453	0.330	0.609	0.759	0.528
32	0.679	0.513	0.607	0.644	0.693	0.544	0.502	0.616	0.590	0.466	0.467	0.623	0.894	0.421
33	0.731	0.654	0.513	0.725	0.537	0.469	0.449	0.499	0.557	0.480	0.415	0.553	0.664	0.582
41	0.582	0.791	0.563	0.735	0.581	0.514	0.449	0.544	0.607	0.461	0.406	0.527	0.598	0.598
44	0.505	0.346	0.366	0.384	0.379	0.222	0.231	0.236	0.264	0.335	0.223	0.398	0.523	0.359
46	0.698	0.530	0.608	0.652	0.674	0.345	0.345	0.364	0.410	0.379	0.322	0.728	0.722	0.511
50	0.801	0.502	0.639	0.533	0.546	0.331	0.341	0.366	0.397	0.323	0.314	0.644	0.605	0.440
51	0.726	0.466	0.525	0.563	0.681	0.395	0.405	0.423	0.474	0.394	0.375	0.649	0.760	0.522
53	0.735	0.495	0.617	0.622	0.647	0.376	0.371	0.394	0.442	0.409	0.346	0.727	0.779	0.501
54	0.893	0.507	0.669	0.580	0.588	0.345	0.340	0.371	0.423	0.364	0.315	0.678	0.714	0.486

Similarity index of Maax Na samples for elements Mg, Ca, Cr, Ni, Sr, La

	22	24	25	31	35	36	37	38	43	52	1	9	16	17
2														
4														
5														
6														
8														
10														
11														
12														
13														
14														
15														
18														
19														
21														
22	1.000													
24	0.626	1.000												
25	0.674	0.681	1.000											
31	0.738	0.556	0.631	1.000										
35	0.767	0.631	0.706	0.660	1.000									
36	0.421	0.594	0.524	0.433	0.429	1.000								
37	0.756	0.568	0.581	0.647	0.740	0.411	1.000							
38	0.645	0.606	0.509	0.674	0.722	0.655	0.685	1.000						
43	0.416	0.486	0.570	0.392	0.441	0.641	0.387	0.309	1.000					
52	0.724	0.643	0.561	0.684	0.734	0.450	0.833	0.800	0.357	1.000				
1	0.557	0.554	0.593	0.532	0.661	0.469	0.606	0.674	0.355	0.554	1.000			
9	0.841	0.655	0.632	0.728	0.864	0.438	0.761	0.757	0.409	0.823	0.606	1.000		
16	0.671	0.573	0.466	0.618	0.632	0.421	0.764	0.726	0.317	0.733	0.608	0.706	1.000	
17	0.725	0.609	0.515	0.601	0.692	0.412	0.773	0.724	0.352	0.753	0.591	0.766	0.913	1.000
20	0.680	0.558	0.474	0.565	0.619	0.476	0.796	0.659	0.380	0.823	0.594	0.695	0.766	0.762
23	0.668	0.562	0.565	0.693	0.714	0.357	0.625	0.815	0.287	0.720	0.729	0.710	0.671	0.670
29	0.750	0.623	0.529	0.665	0.703	0.430	0.800	0.765	0.342	0.846	0.580	0.835	0.870	0.859
30	0.646	0.592	0.501	0.622	0.644	0.503	0.775	0.753	0.359	0.845	0.561	0.725	0.694	0.688
32	0.774	0.696	0.564	0.674	0.769	0.475	0.800	0.651	0.468	0.698	0.561	0.785	0.642	0.667
33	0.656	0.804	0.650	0.550	0.757	0.524	0.621	0.658	0.448	0.664	0.655	0.771	0.641	0.692
41	0.675	0.716	0.569	0.530	0.579	0.555	0.540	0.564	0.449	0.482	0.689	0.577	0.540	0.693
44	0.427	0.411	0.377	0.340	0.510	0.382	0.586	0.550	0.211	0.594	0.453	0.484	0.536	0.522
46	0.694	0.620	0.554	0.748	0.733	0.420	0.785	0.832	0.333	0.906	0.603	0.797	0.764	0.839
50	0.668	0.486	0.458	0.604	0.631	0.408	0.747	0.727	0.319	0.650	0.711	0.654	0.863	0.823
51	0.741	0.611	0.575	0.701	0.758	0.441	0.910	0.747	0.387	0.855	0.643	0.784	0.774	0.783
53	0.763	0.646	0.573	0.706	0.757	0.436	0.818	0.793	0.364	0.925	0.586	0.848	0.791	0.806
54	0.711	0.594	0.490	0.645	0.677	0.426	0.770	0.776	0.330	0.732	0.647	0.751	0.933	0.903

Similarity index of Maax Na samples for elements Mg, Ca, Cr, Ni, Sr, La, continued

	20	23	29	30	32	33	41	44	46	50	51	53	54
2													
4													
5													
6													
8													
10													
11													
12													
13													
14													
15													
18													
19													
21													
22													
24													
25													
31													
35													
36													
37													
38													
43													
52													
1													
9													
16													
17													
20	1.000												
23	0.627	1.000											
29	0.826	0.716	1.000										
30	0.765	0.623	0.726	1.000									
32	0.629	0.575	0.659	0.696	1.000								
33	0.584	0.622	0.680	0.604	0.623	1.000							
41	0.479	0.542	0.507	0.520	0.625	0.665	1.000						
44	0.574	0.510	0.522	0.712	0.486	0.438	0.384	1.000					
46	0.762	0.782	0.843	0.772	0.667	0.652	0.528	0.561	1.000				
50	0.731	0.663	0.775	0.655	0.631	0.555	0.629	0.518	0.685	1.000			
51	0.786	0.684	0.810	0.805	0.767	0.747	0.570	0.600	0.856	0.733	1.000		
53	0.807	0.765	0.909	0.789	0.704	0.692	0.500	0.546	0.903	0.701	0.850	1.000	
54	0.753	0.718	0.865	0.686	0.676	0.674	0.557	0.509	0.759	0.856	0.779	0.784	1.000

Similarity index of Maax Na samples for elements Mg, Ca, Cr, Ni, Sr, La, continued

	1	2	3	4	5	6	9A	9B	10	11	13	14	15	16
1	1.000													
2	0.837	1.000												
3	0.567	0.600	1.000											
4	0.748	0.724	0.796	1.000										
5	0.770	0.758	0.640	0.751	1.000									
6	0.646	0.532	0.594	0.534	0.637	1.000								
9A	0.676	0.751	0.662	0.618	0.704	0.606	1.000							
9B	0.755	0.740	0.663	0.810	0.858	0.610	0.689	1.000						
10	0.738	0.811	0.628	0.649	0.746	0.497	0.834	0.709	1.000					
11	0.595	0.621	0.646	0.574	0.742	0.734	0.742	0.677	0.604	1.000				
13	0.820	0.826	0.515	0.689	0.761	0.477	0.663	0.733	0.711	0.579	1.000			
14	0.703	0.660	0.574	0.721	0.707	0.747	0.607	0.763	0.543	0.633	0.680	1.000		
15	0.714	0.772	0.623	0.691	0.759	0.536	0.706	0.689	0.816	0.661	0.715	0.597	1.000	
16	0.700	0.771	0.578	0.672	0.836	0.586	0.638	0.797	0.765	0.666	0.734	0.678	0.811	1.000
17	0.832	0.810	0.564	0.747	0.762	0.479	0.663	0.733	0.700	0.602	0.880	0.679	0.799	0.696
7A	0.693	0.730	0.546	0.680	0.763	0.598	0.630	0.828	0.694	0.652	0.735	0.727	0.742	0.905
8	0.617	0.686	0.754	0.673	0.688	0.706	0.660	0.730	0.628	0.726	0.654	0.692	0.633	0.711
12	0.326	0.372	0.471	0.431	0.350	0.558	0.415	0.374	0.341	0.453	0.346	0.443	0.349	0.373
18	0.566	0.602	0.729	0.616	0.620	0.610	0.568	0.614	0.536	0.582	0.644	0.683	0.593	0.617
19	0.767	0.801	0.598	0.643	0.767	0.463	0.789	0.695	0.871	0.588	0.781	0.575	0.712	0.663
20	0.623	0.645	0.896	0.798	0.663	0.624	0.639	0.669	0.614	0.681	0.561	0.625	0.670	0.617

Similarity index of Chawak But'o'ob samples for elements Mg, Ca, Cr, Ni, Sr, La

	17	7A	8	12	18	19	20
1							
2							
3							
4							
5							
6							
9A							
9B							
10							
11							
13							
14							
15							
16							
17	1.000						
7A	0.688	1.000					
8	0.584	0.722	1.000				
12	0.302	0.386	0.480	1.000			
18	0.599	0.603	0.770	0.405	1.000		
19	0.754	0.598	0.617	0.314	0.599	1.000	
20	0.623	0.581	0.784	0.467	0.747	0.605	1.000

Similarity index of Chawak But'o'ob samples for elements Mg, Ca, Cr, Ni, Sr, La, continued

BIBLIOGRAPHY

Abrams, E.M., 1994. How the Maya Built Their World: Energetics and Ancient Architecture. University of Texas Press, Austin.

Aharon, P., Rasbury, M., Murgulet, V., 2006. Caves of Niue Island, South Pacific: Speleothems and water geochemistry, in: Harmon, R.S. and Wicks, C.M., eds., Perspectives on Karst Geomorphology, Hydrology, and Geochemistry: A tribute to Derek C. Ford and William B. White, pp. 283-295.

Aksu, A.E., Yaşar, D., Mudie, P.J., 1995. Origin of late glacial-Holocene hemipelagic sediments in the Aegean Sea: clay mineralogy and carbonate cementation. *Marine Geology* 123, 33–59.

Aksu, A.E., Yaşar, D., Uslu, O., 1998. Assessment of marine pollution in Gulf of İzmir: heavy metal and organic compound concentrations in surficial sediments. *TUBITAK Translations and Journal of Engineering and Environmental Science* 22, 387-415.

Aksu, A.E., Piper, D.J.W., Konuk, T., 1987. Quaternary growth patterns of Büyük Menderes and Kucuk Menderes deltas, western Turkey. *Sedimentary Geology* 52, 227-250.

Aleem, A.A., 1972. Effect of river outflow management on marine life. *Marine Biology* 15, 200-208.

Almaç, Ö., 2005. Problems caused by coastal law and decision making mechanism in small coastal settlements: case study Mugla-Bozburun. Unpublished Masters thesis. Middle East Technical University.

Anderson, R.F., Lyons, T.W., Cowie, G.L., 1994. Sedimentary record of a shoaling of the oxic/ anoxic interface in the Black Sea, in: M.I. Scranton (Ed), Variability in Anoxic Systems. *Marine Geology* 116, 373-384.

Ashmore, W., 1991. Site-planning principles and concepts of directionality among the ancient Maya. *Latin American Antiquity* 2(3), 199-226.

Ashmore, W., 1992. Deciphering Maya architectural plans, in: New Theories on the Ancient Maya, eds., Danien, E.C. and Sharer, R.J. University Museum Monograph 77. University Museum, University of Pennsylvania, Philidephia, pp. 173-184.

Ashmore, W., 2008. Visions of the cosmos: Ceremonial landscapes and civic plans, in: David, B. and Thomas, J., eds., Handbook of Landscape Archaeology. Left Coast Press, Inc., Walnut Creek, CA, pp. 167-175.

Aston, M. and Rowley, T, 1974. Landscape Archaeology. David and Charles, London.

Atkinson, C., 2010. From the bottom up: further discussion of bottom trawling. *INA Quarterly* 37(1), 10-11.

Avram, A., Hind, J., Tsetskhladze, G, 2004. The Black Sea Area, in Hansen, M.H. and Nielsen, T.H. (eds.), An Inventory of Archaic and Classical Poleis. Oxford: Oxford University Press, pp. 924-973.

Ballard, R.D., 2008. Searching for ancient shipwrecks in the deep sea, in: Ballard, R.D., (ed.), Archaeological Oceanography. Princeton University Press, Princeton, pp. 131-147.

Ballard, R., Buxton, B., Brennan, M., Coleman, D., Croff, K., Davis, D., Piechota, D., Voronov, S., 2008. Byzantium beneath the Black Sea. Poster presented at the 2008 Meeting of the Archaeological Institute of America, Chicago.

Ballard, R.D., Stager, L.E., Master, D., Yoerger, D., Mindell, D., Whitcomb, L.L., Singh, H., Piechota, D., 2002. Iron Age shipwrecks in deep water off Ashkelon, Israel. *American Journal of Archaeology* 106, 151-168.

Ballard, R.D., Hiebert, F.T., Coleman, D.F., Ward, C., Smith, J.S., Willis, K., Foley, B., Croff, K., Major, C., Torre, F., 2001. Deepwater archaeology of the Black Sea: The 2000 season at Sinop, Turkey. *American Journal of Archaeology* 105, 607-623.

Ballard, R.D., McCann, A.M., Yoerger, D., Whitcomb, L., Mindell, D., Oleson, J., Singh, H., Foley, B., Adams, J., Piechota, D., Giangrande, C., 2000. The discovery of ancient history in the deep sea using advanced deep submergence technology. *Deep-Sea Research I* 47, 1591-1620.

Ballard, R.D., Stager, L.E., Master, D., Yoerger, D., Mindell, D., Whitcomb, L., Singh, H., Piechota, D., 2002. Iron Age shipwrecks in deep water off Ashkelon, Israel. *Journal of American Archaeology* 106, 151-168.

Barba, L., Blancas, J., Manzanilla, L.R., Ortiz, A., Barca, D., Crisci, G.M., Miriello, D., Pecci, A., 2009. Provenance of the limestone used in Teotihuacan (Mexico): a methodological approach. *Archaeometry* 51, 525-545.

Bascom, W., 1976. Deep Water, Ancient Ships. New York: Doubleday & Company, Inc.

Bass, G. and van Doorninck Jr., F.H., 1971. A fourth-century shipwreck at Yassı Ada. *Journal of American Archaeology* 75, 27-37.

Bass, G.F. and van Doorninck Jr., F.H., 1982. Yassı Ada Volume I: A seventh-century Byzantine shipwreck. Texas A&M University Press, College Station.

Bean, G.E. and Cook, J.M., 1955. The Halicarnassus Peninsula. *The Annual of the British School at Athens* 50, 85-171.

Beltrame, C. and Gaddi, D., 2002. Report on the first research campaign on the Napoleonic brick, Mercure, wrecked off Lignano, Udine, Italy in 1812. *International Journal of Nautical Archaeology* 31, 60-73.

Bergstrand, T., 2010. The Danish 7th-century Man-of-War *Stora Sofia*: Documentation and *in situ* preservation. *International Journal of Archaeology* 39, 56-65.

Berkes, F., 1986. Local-level management and the commons problem: A comparative study of Turkish fisheries. *Marine Policy* 10, 215-229.

Bolland, O.N., 1977. The Formation of a Colonial Society: Belize, from Conquest to Crown Colony. The Johns Hopkins University Press, Baltimore.

Borchardt, G.A., Aruscavage, P.J., Millard, H.T., Jr., 1972. Correlation of the Bishop Ash, a Pleistocene marker bed, using instrument neuron activation analysis. *Journal of Sedimentary Petrology* 42, 301-306.

Brady, J.E., 1997. Settlement Configuration and Cosmology: The Role of Caves at Dos Pilas. *American Anthropologist* 99 (3), 602-618.

Brady, J. and Ashmore, W., 1999. Mountains, caves, water: Ideational landscapes of the Ancient Maya, in: Ashmore, W. and Knapp, A.B., eds., Archaeologies of Landscape: Contemporary Perspectives. Blackwell Publishers, Oxford, pp 124-145.

Brennan, M.L., 2009. Ancient shipwreck survey and the modern submarine landscape off Yalıkavak, Turkey. *Marine Technology Society Journal* 43, 47-49.

Brennan, M.L., 2010. The disarticulation of ancient shipwreck sites by mobile fishing gear: A case study from the southeast Aegean Sea. *INA Quarterly* 36(4), 6-7.

Brennan, M.L. and Ballard, R.D., in press. Archaeological Oceanography. Encyclopedia of Natural Resources.

Brennan, M.L., Ballard, R.D., Croff Bell, K.L., and Piechota, D., 2011a. Archaeological oceanography and environmental characterization of shipwrecks in the Black Sea, in Buynevich, I., Yanko-Hombach, V., Gilbert, A., and Martin, R.E., eds., Geology and Geoarchaeology of the Black Sea Region: Beyond the Flood Hypothesis. Geological Society of America Special Paper 473, pp. 179-188, doi: 10.1130/2011.2473(11).

Brennan, M.L., Ballard, R.D., Roman, C., Bell, K.L.C., Buxton, B., Coleman, D.F., Inglis, G., Koyagasioglu, O., Turanli, T., in press. Evaluation of the modern submarine landscape off southwestern Turkey through the documentation of ancient shipwreck sites. *Continental Shelf Research*.

Brennan, M.L., Turanli, T., Buxton, B., Bell, K.L.C., Roman, C.N., Kofahl, M., Koyagasioglu, O., Whitesell, D., Chamberlain, T., Sullivan, R., Ballard, R., 2011b. Landscape imaging of the southeast Aegean Sea, in: Bell, K.L.C. and Fuller, S.A., eds. New Frontiers in Ocean Exploration: The *E/V Nautilus* 2010 Field Season. *Oceanography* 24(1), supplement, p. 18-19.

Brylinsky, M., Gibson, J., Gordon, D.C., 1994. Impacts of flounder trawls on the intertidal habitat and community of the Minas Basin, Bay of Fundy. *Canadian Journal of Fisheries and Aquatic Sciences* 51, 650-661.

Burstein, S.M., 1976. Outpost of Hellenism: The Emergence of Heraclea on the Black Sea. University of California Press, Berkley.

Buynevich, I.V., Damusyte, A., Bitinas, A., Olenin, S., Mazeika, J., Petrosius, R., 2011. Pontic-Baltic pathways for invasive aquatic species: Geoarchaeological implications, in Buynevich, I., Yanko-Hombach, V., Gilbert, A., and Martin, R.E., eds., Geology and Geoarchaeology of the Black Sea Region: Beyond the Flood Hypothesis. Geological Society of America Special Paper 473, p. 189-196, doi: 10.1130/2011.2473(12).

Caddy, J.F., 1973. Underwater observations on tracks of dredges and trawls and some effects of dredging on scallop ground. *Journal of the Fisheries Research Board of Canada* 30(2), 173-180.

Casson, L., 1995. Ships and Seamanship in the Ancient World. Johns Hopkins University Press, London.

Coleman, D.F. and Ballard, R.D., 2001. A highly concentrated region of cold hydrocarbon seeps in the southeastern Mediterranean Sea. *Geo-Marine Letters* 21, 162-167.

Coleman, D.F. and Ballard, R.D., 2004. Archaeological Oceanography of the Black Sea, in: Akal, T., Ballard, R.D., and Bass, G.F., eds., The Application of Recent Advances in Underwater Detection and Survey Techniques to Underwater Archaeology. Uluburun Publishing, Istanbul.

Coleman, D.F., Ballard, R.D., Gregory, T., 2003. Marine archaeological exploration of the Black Sea. *OCEANS 2003 MTS/IEEE Conference Proceedings* 2, 1287-1295.

Collie, J.S., Escanerol G.A., Valentine, P.C., 2000. Photographic evaluation of the impacts of bottom fishing on benthic epifauna. *ICES Journal of Marine Science* 57: 987-1001.

Culha, M., 2010. The presence of *Teredo navalis* Linnaeus, 1758 (Mollusca, Bivalvia, Teredinidae) in the southern Black Sea, Turkey. *Journal of Animal and Veterinary Advances* 9, 1515-1518.

David, B. and Thomas, J., 2008. Landscape Archaeology: Introduction, in: David, B. and Thomas, J., eds., Handbook of Landscape Archaeology. Left Coast Press, Inc., Walnut Creek, CA, pp. 27-43.

Davidde, B., 2002. Underwater archaeological parks: a new perspective and a challenge for conservation - the Italian panorama. *International Journal of Underwater Archaeology* 31, 83-88.

Davis, D.L., 2009. Commercial Navigation in the Greek and Roman World. Unpublished Ph.D. diss. University of Texas at Austin.

DeAlteris, J., Skrobe, L., Lipsky, C., 1999. The significance of seabed disturbance by mobile fishing gear relative to natural processes: A case study in Narragansett Bay, Rhode Island. *American Fisheries Society Symposium* 22, 224-237.

Denham, T., 2008. Environmental Archaeology: Interpreting practices-in-the-landscape through geoarchaeology, in: David, B. and Thomas, J., eds., Handbook of Landscape Archaeology. Left Coast Press, Inc., Walnut Creek, CA, pp. 468-481.

Dincauze, D., 2000. Environmental Archaeology: Principles and Practice. Cambridge University Press, Cambridge.

Dodge, R.L., 2008. Research Report on Archaeological Excavations at Hun Tun. Report, The University of Texas at Austin.

Dodge, R.L., 2010. Research Report on Archaeological Excavations at Hun Tun. Report, The University of Texas at Austin. 123-131.

Doonan, O.P., 2004. Sinop Landscapes: Exploring Connections in a Black Sea Hinterland. University of Pennsylvania Museum of Archaeology and Anthropology, Philadelphia.

Duman, M., Avcı, M., Duman, Ş., Demirkurt, E., Düzbastılar, M.K., 2004. Surficial sediment distribution and net sediment transport pattern in İzmir Bay, western Turkey. *Continental Shelf Research* 24, 965-981.

Duman, M., Duman, S., Lyons, T.W., Avci, M., Izdar, E., Demirkurt, E., 2006. Geochemistry and sedimentology of shelf and upper slope sediments of the south central Black Sea. *Marine Geology* 227: 51-65.

Dunning, N., Jones, J.G., Beach, T., Luzzadder-Beach, S., 2003. Physiography, habitats, and landscapes of the Three Rivers Region, in: Scarborough, V.L., Valdez Jr., F., Dunning, N.P., eds., Heterarchy, Political Economy, and the Ancient Maya. University of Arizona Press, Tucson, pp. 14-24.

Durrieu de Madron, X., Ferre, B., Le Corre, G., Grenz, C., Conan, P., Pujo-Pay, M., Buscail, R., Bodoit, O., 2005. Trawling-induced resuspension and dispersal of muddy sediments and dissolved elements in the Gulf of Lion (NW Mediterranean). *Continental Shelf Research* 25, 2387-2409.

Empereur, J.-Y. and Picon, M., 1986. A la recherché des four d'amphores, in: Empereur, J.-Y., and Y. Garlan, eds., Recherches sur les amphores grecques. Actes du Colloque International organisé par le Centre National de la Recherche Scientifique, L'Université de Rennes II et L'École Française d'Athènes, 10–12 Septembre 1984. BCH Supplement 13. École Française d'Athènes, Athènes.

Empereur, J.-Y. and Tuma, N., 1988. Zénon de Caunos et l'épave de Serçe Limani. *BCH* 112, 341-357.

Ergin, M. and Yemenicioglu, S., 1997. Geologic assessment of environmental impact in bottom sediments of the eastern Aegean Sea. *International Journal of Environmental Studies* 51, 323-334.

Ergin, M., Kadir, S., Keskin, Ş., Turhan-Akyüz, N., Yaşar, D., 2007. Late Quaternary climate and sea-level changes recorded in sediment composition off the Büyük Menderes River delta (eastern Aegean Sea, Turkey). *Quaternary International* 167-168, 162-176.

Espinosa, L., Ceron, M., Sulub, Y.A., 1998. Limestone rocks of the Yucatan Peninsula. Description of the lithology and physical properties based on the results of exploration, investigation, and laboratory tests. *International Journal of Rock Mechanics and Mining Sciences* 35, 410-411.

FAO General Fisheries Commission for the Mediterranean, 2006. Report of the thirtieth session. Istanbul, Turkey, 24–27 January 2006. GFCM Report 30.

Filonov, A.E., 2000. Thermic structure and intense internal waves on the narrow continental shelf of the Black Sea. *Journal of Marine Systems* 24, 27–40.

Flores, G., 1952. Summary report of preliminary geological studies of the area N of 17o N latitude, British Honduras. Bahamas Exploration Company, Freeport, Bahamas.

Flugel, E., 2004. Microfacies of Carbonate Rocks: Analysis, Interpretation and Application. Springer, New York.

Folan, W.J., 1982. Mining and Quarrying Techniques of the Lowland Maya. *Anthropology* 6, 149-174.

Foley, B., 2008. Archaeology in deep water: Impact of fishing on shipwrecks. Woods Hole Oceanographic Institution. <http://www.whoi.edu/sbl/liteSite.do?litesiteid=2740&articleId=4965>. Accessed December 2009.

Ford, D. and Williams, P., 1989. Karst Geomorphology and Hydrology. Unwin Hyman, London.

Friedlander, A.M., Boehlert, G.W., Field, M.E., Mason, J.E., Gardner, J.V., Dartnell, P., 1999. Sidescan-sonar mapping of benthic trawl marks on the shelf and slope off Eureka, *California*. *Fishery Bulletin* 97, 786-801.

Gajdukevich, V.F., 1969. On How Ancient Greek Ships Sailed Across the Pontus Euxine. *KSIA* 116, 11–19 (in Russian).

Garcia-Sanchez, A. and Alvarez-Ayuso, E., 2002. Sorption of Zn, Cd and Cr on calcite. Application to purification of industrial wastewater. *Minerals Engineering* 15, 539-547.

Gifford, J.A., 1974. A survey of shipwreck sites off the southwestern coast of Turkey. *Journal of Field Archaeology* 1, 23-25.

Glazer, B.T., Luther, G.W. III, Konovalov, S.K., Friederich, G.E., Nuzzio, D.B., Trouwborst, R.E., Tebo, B.M., Clement, B., Murray, K., Romanov, A.S., 2006a. Documenting the suboxic zone of the Black Sea via high-resolution real-time redox profiling. *Deep-Sea Research II* 53, 1740-1755.

Glazer, B.T., Luther, G.W. III, Konovalov, S.K., Friederich, G.E., Trouwborst, R.E., Romanov, A.S., 2006b, Spatial and temporal variability of the Black Sea suboxic zone. *Deep-Sea Research II* 53, 1756-1768.

Goitein, S.D., 1999. A Mediterranean Society: The Jewish Communities of the World as Portrayed in the Documents of the Cairo Geniza. Vol. 1, Economic Foundations. University of California Press, Berkley.

Graham, E., 1987. Resource Diversity in Belize and Its Implications for Models of Lowland Trade. *American Antiquity* 52(4), 753-767.

Greene, E.S., Leidwanger, J., Leventhal, R.M., Daniels, B.I., 2011. Mare nostrum? Ethics and archaeology in Mediterranean waters. *American Journal of Archaeology* 115, 311-319.

Halim, Y., Morcos, S.A., Rizkalla, S., El-Sayed, M.K., 1995. The impact of the Nile and the Suez Canal on the living marine resources of the Egyptian Mediterranean waters (1958-1986), in: FAO Marine Resource Services (ed.) Effects of riverine inputs on coastal ecosystems and fisheries resources. FAO Fisheries Technical Paper no. 349, FAO, Rome.

Hartshorn, G., Nicolait, L., Hartshorn, L., Bevier, G., Brightman, R., Cal, J., Cawich, A., Davidson, W., DuBois, R., Dyer, C., Gibson J., Hawley W., Leonard J., Nicolait, R., Weyer, D., White, H., Wright, C. 1984. BELIZE Country Environmental Profile, A Field Study. USAID Contract. Trejos. Hnos. Sucs. S.A., San Jose.

Hind, J.G.F., 1988. The Colonisation of Sinope and the S.E. Black Sea Area, in: Mestnye etnopoliticheskie obedineniya Prichernomor'ya VII-IV vekakh do n.e., Materialy IV Vsesoyuznogo Sympozyuma po drevnej istorii (Tblisi) 207-23.

Hopkins, T. S., 1978. Physical processes in the Mediterranean basins, in: B. Kjerfve (ed.) Estuarine Transport Processes. University of South Carolina Press, pp. 269–310.

Houk, Brett A., 2003. The ties that bind: Site planning in the Three Rivers Region, in: Scarborough, V.L., Valdez Jr., F., Dunning, N.P., eds., Heterarchy, Political Economy, and the Ancient Maya. University of Arizona Press, Tucson, pp. 52-63.

Humborstad, O.-B., Nottestad, L., Lokkeborg, S., Rapp, H.T., 2004. RoxAnn bottom classification system, sidescan sonar and video-sledge: spatial resolution and their use in assessing trawling impacts. *ICES Journal of Marine Science* 61, 53-63.

Inglis, G. and Roman, C., 2009. Terrain constrained stereo correspondence. Paper presented at the 2009 OCEANS conference, Biloxi, Mississippi.

Isager, S. and Hansen, M.H., 1975. Aspects of Athenian Society in the Fourth Century B.C. Odense University Press, Odense.

Ji, H., Wang S., Ouyang, Z., Zhang, S., Sun C., Liu, X., Zhou, D., 2004. Geochemistry of red residua underlying dolomites in karst terrains of Yunnan-Guizhou Plateau II. The mobility of rare earth elements during weathering. *Chemical Geology* 203, 29-50.

Johnson-Roberson, M., Pizarro, O., Williams, S.B., Mahon, I.J., 2010. Generation and Visualization of Large-Scale Three-Dimensional Reconstructions from Underwater Robotic Surveys. *Journal of Field Robotics*, 27, p. 21-51.

Jones, J.B. 1992. Environmental impact of trawling on the seabed: a review. *New Zealand Journal of Marine and Freshwater Research* 26, 59-67.

Kac, V.I., Monachov, S.Y., Stolba, V.F., Shcheglov, A.N., 2002. Tiles and ceramic containers, in: Hannestad, L., V.F. Stolba, and A.N. Shcheglov, eds., Panskoye I. Vol.1. The Monumental Building U6. Aarhus University Press, Aarhus, pp. 101-126.

King, D.T., Jr., Petruny, L.W., Pope, K.O., 2003. Shallow-marine facies of the Orange Walk Group, Miocene-Pliocene, northern Belize (Central America). *GCAGS/ GCSSEPM Transactions* 53, 384-397.

King, D.T., Jr., Pope, K.O., Petruny, L.W., 2004. Stratigraphy of Belize, north of the 17th parallel. *Gulf Coast Association of Geological Societies Transactions* 54, 289-303.

King, E. and Shaw, L., 2003. A heterarchical approach to site variability: The Maax Na Archaeology Project, in: Scarborough, V.L., Valdez Jr., F., Dunning, N.P., eds., Heterarchy, Political Economy, and the Ancient Maya. University of Arizona Press, Tucson, pp. 64-76.

King, E.M., Brady, J.E., Shaw, L.C., Cobb, A.B., Kieffer, C.L., Brennan, M.L., Harris, C.L., in revision. Small caves and sacred geography: A case study from the Prehispanic Maya site of Maax Na, Belize. *Latin American Antiquity*.

Kelley, K.A., Plank, T., Ludden, J., Staudigel, H., 2003. Composition of altered oceanic crust at ODP sites 801 and 1149. *Geochemistry Geophysics Geosystems* 4(6), 8910.

Knapp, A.B. and Ashmore, W., 1999. Archaeological landscapes: Constructed, conceptualized, ideational, in: Ashmore, W. and Knapp, A.B., eds., Archaeologies of Landscape: Contemporary Perspectives. Blackwell Publishers, Oxford, pp 1-30.

Koruma ve Kontrol Genel Müdürlüğü (KKGM), 2006. Circular No. 37/1 of 2006-2008 Fishing Year Regulating Commercial Fishing in Seas and Inland Waters. Koruma ve Kontrol Genel Müdürlüğü, Ankara, Turkey. <http://www.kkgm.gov.tr/ regulation/circular/37-1.html>. Accessed December 2009.

Kunen, J.L., 2004. Ancient Maya Life in the Far West Bajo: Social and Environmental Change in the Wetlands of Belize. The University of Arizona Press, Tucson.

Kunen, J.L., Hughbanks, P.J., 2003. Bajo communities as resource specialists, in: Scarborough, V.L., Valdez Jr., F., Dunning, N.P., eds., Heterarchy, Political Economy, and the Ancient Maya. University of Arizona Press, Tucson, pp. 92-108.

Kurt, H., Demirbag, E., Kuscu, I., 1999. Investigation of the submarine active tectonism in the Gulf of Gökova, southwest Anatolia - southeast Aegean Sea, by multi-channel seismic reflection data. *Tectonophysics* 305, 477-496.

Kuscu, I., Parke, J.R., White, R.S., McKenzie, D., Anderson, G.A., Minshull, T.A., Gorur, N., Sengor, A.M.C., 2004. Active slumping offshore Amasra (southwest Black Sea) and its relation with regional tectonics. *Bulletin of the Mineral Research and Exploration* 128, 27-47.

Lampadariou, N., Hatziyanni, E., Tselepides, A., 2005. Meiofaunal community structure in Thermaikos Gulf: Response to intense trawling pressure. *Continental Shelf Research* 25, 2554-2569.

Lakshtanov, L.Z. and Stipp, S.L.S., 2007. Experimental study of nickel(II) interaction with calcite: Adsorption and coprecipitation. *Geochimica et Cosmochimica Acta* 71, 3686-3697.

Lok, A., Metin, C., Ulas, A., Duzbastilar, F.O., Tokac, A., 2002. Artificial reefs in Turkey. *ICES Journal of Marine Science* 59, S192-S195.

Luth U. and Luth, C., 1998. Benthic meiofauna and macrofauna of a methane seep area South- west of the Crimean Peninsula, Black Sea. In: Luth U., Luth C., Thiel H., eds., MEGA- SEEPS- Methane Gas Seeps Exploration in the Black Sea. Berichte aus dem Zentrum fuer Meeres-und Klimatoforsch, Hamburg: 14, 59-77.

Malanotte-Rizzoli, P., Manca, B.B., d'Alcala, M.R., Theocharis, A., Brenner, S., Budillon, G., Ozsoy, E., 1999. The Eastern Mediterranean in the 80s and in the 90s: the big transition in the intermediate and deep circulations. *Dynamics of Atmospheres and Oceans* 29, 365-395.

Mathews, R.. 2002. Geology, environment, and lime production variation in the Maya Lowlands. Unpublished Masters thesis. University of Texas, San Antonio.

Maximova, M.I., 1959. Der Kurze Seeweg über das Schwarze Meer im Altertum. *Klio* 37, 101-118.

McNinch, J.E., Wells, J.T., Trembanis, A.C., 2006. Predicting the fate of artefacts in energetic, shallow marine environments: An approach to site management. *International Journal of Nautical Archaeology* 35, 290-309.

Metaxas, D.A., 1973. Air-sea interaction in the Greek seas and resulted Etesian wind characteristics. Univ. Ioannina Tech. Rep. 5.

Michaels, W.L., 2007. Review of acoustic seabed classification systems, in: Anderson, J.T., Holliday, D.V., Kloser, R., Reid, D., Simard, Y., (eds.) Acoustic seabed

classification of marine physical and biological landscapes. ICES Cooperative Research Report, no. 286, 94-115.

Micu, D., 2007. Recent records of *Pholas dactylus* (Bivalvia: Myoida: Pholadidae) from the Romanian Black Sea, with considerations on its habitat and proposed IUCN regional status. *Acta Zoologica Bulgarica* 59, 267-273.

Monachov, S.Y., 1989. Amfory Chersonesa Tavricheskogo IV-II vv. Do n.e. Opyt sistemnogo analiza. Saratov (in Russian).

Monachov, S.Y., 1992. Dinamika form i standartov sinopskih amfor, in: Grecheskie amfor'. Saratov, (Capatob) pp. 163-204 (in Russian).

Monachov, S.Y., 1999. Grecheskis amfory v Prichernomor'e: kompleksy keramicheskoiy tary VII-II vv. do n.e. Saratov (Capatob) (in Russian).

Morton, J., 2001. The Role of the Physical Environment in Ancient Greek Seafaring. Brill Academic Publishers, Boston.

Murray, J.W., Jannasch, H.W., Honjo, S., Anderson, R.F., Reeburgh, W.S., Top, Z., Friedrich, G.E., Codispoti, L.A., and Izdar, E., 1989, Unexpected changes in the oxic/anoxic interface in the Black Sea *Nature* 338, 411-413.

Murray, J.W., Stewart, K., Kassakian, S., Krynytzky, M., and DiJulio, D., 2007, Oxic, suboxic, and anoxic conditions in the Black Sea, in: Yanko-Hombach, V., Gilbert, A.S., Panin, N., and Dolukhanov, P.M., eds., The Black Sea flood question: Changes in coastline, climate and human settlement: Dordrecht, Springer, p. 1-22.

Murray, William M., 1987. Do modern winds equal ancient winds? *Mediterranean Historical Review* 2, 139-167.

Nation, H., Peterson, P.A., Brady, J.E., Neff, H., and McAnany, P.A. n.d. Speleothem Sourcing Using Inductively Coupled Plasma Mass Spectrometry. Paper submitted to *The Journal of Cave and Karst Studies*.

National Research Council (NRC), 2002. Effects of Trawling & Dredging on Seafloor Habitat. National Academy Press, Washington, D.C.

Negueruela, I., 2000. Managing the maritime heritage: the National Maritime Archaeological Museum and National Centre for Underwater Research, Cartagena, Spain. *International Journal of Nautical Archaeology* 29, 179-198.

Newman, J.B., Gregory, T.S., Howland, J., 2008. The development of towed optical and acoustical vehicle systems and remotely operated vehicles in support of archaeological oceanography, in: Ballard, R.D., (ed.), Archaeological Oceanography. Princeton University Press, Princeton, pp. 15-29.

Newton, C.T. and Pullan, R.P., 1863. A history of discoveries at Halicarnassus, Cnidus, and Branchidae. Day and Son, London.

Northdurft, L.D., Webb, G.E., Kamber, B.S., 2004. Rare earth element geochemistry of Late Devonian reefal carbonates, Canning Basin, Western Australia: Confirmation of a seawtaer REE proxy in ancient limestones. *Geochimica et Cosmochimica Acta* 68(2), 263-283.

Oguz, T., La Violette, P.E., Unluata, U., 1992. The upper layer circulation of the Black Sea: Its variability as inferred from hydrographic and satellite observations. *Journal of Geophysical Research* 97, 12569-12584.

Okuş, E., Yüksek, A., Yılmaz, İ.N., Yılmaz, A.A., Karhan, S.Ü., Öz, M.İ., Demirel, N., Taş, S., Demir, V., Zeki, S., Koç, E.M., Tural, U., Yokeş, B., Kalkan, E., Deniz, N., Çaylarbaşı, Z., Savut, E., Murat, E., 2007. Marine biodiversity of Datça- Bozburun specially protected area (Southeastern Aegean Sea, Turkey). *Journal of the Black Sea / Mediterranean Environment* 13, 39-49.

Olenin, S. and Leppakoski, E., 1999. Non-native animals in the Baltic Sea: alteration of benthic habitats in coastal inlets and lagoons. *Hydrobiologia* 393, 233-243.

Oleson, J.P. and Adams, J., 1997. Formation, survey, and sampling of the wreck sites, in: McCann, A.M. and Oleson, J.P. (eds.) Deep-Water Shipwrecks off Skerki Bank: The 1997 Survey. *Journal of Roman Archaeology* (Suppl.) Ser. 58.

Opaiţ, A., 1997-1998. New pottery from the circular harbour at Carthage. *CEDAC Carthage* 18, 21–35.

Opaiţ, A., 2010. On the origin of Carthage LR Amphora 1, in: Menchelli, S., Santoro, S., Pasquinuci, M., Guiducci, G., eds., LRCW3. Late Roman Coarse Wares, Cooking Wares and Amphorae in the Mediterranean (BAR-IS 2185), 1015-1022.

Opaiţ, A., 2010. Sinopean, Heraklean and Chersonesan "Carrot" Amphorae" *Ancient Civilizations from Scythia to Siberia* 16, 371-401, 552-556.

Parker, A.J., 1992. Ancient shipwrecks of the Mediterranean and the Roman provinces. British Archaeological Reports International Series 580.

Pickard, G.L., and Emery, W.J., 1990. Descriptive Physical Oceanography. Pergamon, Oxford.

Piper, D.J.W. and Perissoratis, C., 2003. Quaternary neotectonics of the South Aegean arc. *Marine Geology* 198, 259-288.

Piper, D.Z., 1974. Rare earth elements in ferromanganese nodules and other marine

phases. *Geochimica et Cosmochimica Acta* 38, 1007-1022.

Pitblado, B.L., Dehler, C., Neff, H., Nelson, S.T., 2008. Pilot study experiments sourcing quartzite, Gunnison Basin, Colorado. *Geoarchaeology* 23(6), 742-778.

Pitcher, T.J., 2006. An estimation of compliance of the fisheries of Turkey with Article 7 (Fisheries Management) of the UN Code of Conduct for responsible fishing. <ftp://aerl03.aerl.ubc.ca/CodeConduct/CountriesCodePDF/Turkey-CCRF.pdf>. Accessed Januray 2011.

Pizarro, O. and Singh, H., 2003. Toward large-area mosaicing for underwater scientific applications. *Journal of Oceanic Exploration* 28(4), 651-672.

Plank, T., Kelley, K.A., Murray, R.W., Stern, L.Q., 2007. Chemical composition of sediments subducting at the Izu-Bonin trench. *Geochemistry Geophysics Geosystems 8*, Q04I16, doi:10.1029/2006GC001444.

Poulos, S.E., 2009. Origin and distribution of the terrigenous component of the unconsolidated surface sediment of the Aegean floor: A synthesis. *Continental Shelf Research* 29, 2045-2060.

Poulos, S.E., Drakopoulos, P.G., Collins, M.B., 1997. Seasonal variability in sea surface oceanographic conditions in the Aegean Sea (Eastern Mediterranean): an overview. *Journal of Marine Systems* 13, 225-244.

Preston, J., 2008. Automated acoustic seabed classification of multibeam images of Stanton Banks. *Applied Acoustics* 70, 1277-1287.

Preston, J.M., Christney, A.C., Collins, W.T., Bloomer, S., 2004. Automated acoustic classification of sidescan images. OCEANS 2004 MTS/IEEE Conference Proceedings 4, 2060-2065.

Pusceddu, A., Fiordelmondo, C., Polymenakou, P., Polychronaki, T., Tselepides, A., Danovaro, R., 2005. Effects of bottom trawling on the quantity and biochemical composition of organic matter in coastal marine sediments (Thermaikos Gulf, northwestern Aegean Sea). *Continental Shelf Research* 25, 2491-2505.

Quester Tangent Corp. (QTC), 2010. QTC CLAMS visualization and mapping tools user manual and reference. Sidney, B.C.

Reeder, R.J., 1996. Interaction of divalent cobalt, zinc, cadmium, and barium with the calcite surface during layer growth. *Geochimica et Cosmochimica Acta* 60, 1543-1552.

Reeder, R.J., Lamble, G.M., Northrup, P.A., 1999. XAFS study of the coordination and local relaxation around Co^{2+}, Zn^{2+}, Pb^{2+}, and Ba^{2+} trace elements in calcite. *American Mineralogist* 84, 1049-1060.

Rice, P.M., Michel, H.V., Asaro, F., Stross, F., 1985. Provenience analysis of obsidians from the Central Peten Lakes Region, Guatemala. *Latin American Antiquity* 50(3), 591-604.

Richards B.R., Hillman, R.E., and Maciolek, N.J.. 1984. Shipworms, in: Kennish M.J., Lutz, R.A., eds., Lecture Notes on Coastal and Estuarine Studies - Ecology of Barnegat Bay, New Jersey. Springer-Verlag, New York, pp. 201-225.

Robinson, A.R., Leslie, W.G., Theocharis, A., Lascaratos, A., 2001. Mediterranean Sea circulation. *Encyclopedia of Ocean Sciences*, Academic Press, pp. 1689-1706.

Robinson, D., 1906. Ancient Sinope. *American Journal of Philology* 27, 125-53, 245-79.

Rollinson, H., 1993. Using Geochemical Data: Evaluation, Presentation, Interpretation. Pearson Education Limited, Harlow, England.

Roman, C., Inglis, G., Rutter, J., 2010. Application of structured light imaging for high resolution mapping of underwater archaeological sites. IEEE OCEANS, Sydney.

Roman, C. and Singh, H., 2007. A Self Consistent Bathymetric Mapping Algorithm. *Journal of Field Robotics* 24(1-2), 23-50.

Royal, J.G., 2008. Description and analysis of finds from the 2006 Turkish coastal survey: Marmaris and Bodrum. *International Journal of Nautical Archaeology* 37, 88-97.

Royal, J., 2009. Albanian coastal survey project: 2008 field season. *The INA Annual 2008*, 21-25.

Ryan, W.B.F., Pitman, W.C. III, Major, C.O., Shimkus, K., Moskalenko, V., Jones, G.A., Dimitrov, P., Görür, N., Sakınç, M., Yüce, H., 1997. An abrupt drowning of the Black Sea shelf. *Marine Geology* 138, 119–126.

Sakellariou, D., Georgiou, P., Mallios, A., Kapsimalis, V., Kourkoumelis, D., Micha, P., Theodoulou, T., Dellaporta, K., 2007. Searching for ancient shipwrecks in the Aegean Sea: The discovery of Chios and Kythnos Hellenistic wrecks with the use of marine geological-geophysical methods. *International Journal of Nautical Archaeology* 36, 365-381.

Saprykin, S.J., 1997. Heracleia Pontica and Tauric Chersonesus before Roman Domination: VI-I Centuries B.C. A.M. Hakkert, Amsterdam.

Scarborough, V.L., Becher, M.E., Baker, J.L., Harris, G., and Valdez, F. Jr., 1995. Water and Land at the Ancient Maya Community of La Milpa. *Latin American Antiquity* 6, 98-119.

Scarborough, V.L., 1998. Ecology and ritual: Water management and the Maya. *Latin American Antiquity* 9: 135-159.

Scarborough, V.L. and Valdez, F. Jr., 2003. The engineered environment and political economy of the Three Rivers Region, in: Scarborough, V.L., Valdez Jr., F., Dunning, N.P., eds., Heterarchy, Political Economy, and the Ancient Maya. University of Arizona Press, Tucson, pp. 3-13.

Scarborough, V.L., Valdez, F. Jr., Dunning, N.P., 2003. Heterarchy, Political Economy, and the Ancient Maya. University of Arizona Press, Tucson.

Scarborough, V.L., Connolly, R.P., and Ross, S.P., 1994. The Pre-Hispanic Maya reservoir system at Kinal, Peten, Guatemala. *Ancient Mesoamerica* 5, 97-106.

Sergeeva N.G., 2003. Meiobenthos in the region with the methane gas seeps, in: Eremeev V.N., Gaevskaya A.V., eds., Present Time Conditions of Biological Diversity in the Nearshore Zone of Crimea Peninsula (the Black Sea sector). Ecosi-Gidrophizika, Sevastopol, pp. 258-267 (in Russian).

Sergeeva N.G. and Gulin, M.B., 2007. Meiobenthos from an active methane seepage area in the NW Black Sea. *Marine Ecology* 28, 152-159.

Shaw, L.C., 1999. Constructed landscape as ideology: Archaeology and mapping at Maax Na in the Three Rivers Region of Belize. Paper presented at the 64th Annual Meeting of the Society for American Archaeology, Chicago.

Shaw, L.C., 2002. The Ma'ax Na Archaeology Project: Documentation of stelae, altars, and cave entrances in the west ceremonial group. FAMSI Report. <http://www.famsi.org/reports/00100/>.

Shaw, L.C. and King, E.M., 1997. Research in high places: The hilltop center of Maax Na, Belize. Paper presented at the 62nd Annual Meeting of the Society for American Archaeology, Nashville, Tenn.

Shumchenia, E.J. and King, J.W., 2010. Comparison of methods for integrating biological and physical data for marine habitat mapping and classification. *Continental Shelf Research* 30, 1717-1729.

Smith, C. J., Banks, A. C., Papadopoulou, K.-N., 2007. Improving the quantitative estimation of trawling impacts from sidescan-sonar and underwater-video imagery. *ICES Journal of Marine Science* 64, 1692–1701.

Smith, C.J., Rumohr, H., Karakassis, I., Papadopoulou, K.-N., 2003. Analysing the impact of bottom trawls on sedimentary seabeds with sediment profile imagery. *Journal of Experimental Marine Biology and Ecology* 285-286, 479-496.

Stanley, D.J., and Perissoratis, C., 1977. Aegean ridge barrier-and-basin sedimentation patterns. *Marine Geology* 24, 97-107.

Theocharis, A., Georgopoulos, D., Lascaratos, A., Nittis, K., 1993. Water masses and circulation in the central region of the Eastern Mediterranean: Eastern Ionian, South Aegean and Northwest Levantine, 1986-1987. *Deep-Sea Research II* 40(6), 1121-1142.

Theocharis, A., Balopoulos, E., Kioroglou, S., Kontoyiannis, H., Iona, A., 1999. A synthesis of the circulation and hydrography of the South Aegean Sea and the Straits of the Cretan Arc (March 1994-January 1995). *Progress in Oceanography* 44, 469-509.

Tlig, S. and M'Rabet, A., 1985. A comparative study of the rare earth element (REE) distributions within the Lower Cretaceous dolomites and limestones of Central Tunisia. *Sedimentology* 32, 897-907.

Tourtellot, G., Belli, F.E., Rose, J.J., Hammond, N., 2003. Late Classic Maya heterarchy, hierarchy, and landscape at La Milpa, Belize, in: Scarborough, V.L., Valdez Jr., F., Dunning, N.P., eds., Heterarchy, Political Economy, and the Ancient Maya. University of Arizona Press, Tucson, pp. 37-51.

Trembanis, A., Skarke, A., Nebel, S., Coleman, D.F., Ballard, R.D., Fuller, S.A., Buynevich, I.V., and Voronov, S., 2011, Bedforms, hydrodynamics, and scour process observations from the continental shelf of the northern Black Sea, in: Buynevich, I., Yanko-Hombach, V., Gilbert, A., and Martin, R.E., eds., Geology and Geoarchaeology of the Black Sea Region: Beyond the Flood Hypothesis. Geological Society of America Special Paper 473, pp. 165-178, doi: 10.1130/2011.2473(10).

Trouwborst, R.E., Clement, B.G., Tebo, B.M., Glazer, B.T., Luther, G.W., 2006. Soluble Mn in suboxic zones. *Science* 313, 1955-1957.

Trudgill, S., 1985. Limestone Geomorphology. Longman Inc., New York.

Ünal, V., 2004. Viability of trawl fishing fleet Foca (the Aegean Sea), Turkey and some advices to central management authority. *Turkish Journal of Fisheries and Aquatic Sciences* 4, 93-97.

Vaniman, D.T. and Chipera, S.J., 1996. Paleotransport of lanthanides and strontium recorded in calcite compositions from tuffs at Yucca Mountain, Nevada, USA. *Geochimica et Cosmochimica Acta* 60, 4417-4433.

Verheyden, S., Keppens, E., Fairchild, I.J., McDermott, F., Weis, D., 2000. *Chemical Geology* 169, 131-144.

Villaseñor, I., 2010. Building Materials of the Ancient Maya: A Study of Archaeological Plasters. Lambert Academic Publishing, Saarbrucken, Germany.

Vinson, G.L., 1962. Upper Cretaceous and Tertiary stratigraphy of Guatemala. *Bulletin of the American Association of Petroleum Geologists* 46, 425-456.

Vnukov, S.Y., 2003. Prichernomorskie amfory I v. do n.e.–II v. n.e. (morphologiya), Vol. I. Institut arkheologii RAN, Moscow (in Russian).

Walling, S., 2005. Archaeological investigation of Prehispanic Maya residential terraces, commoner housing and hydrology at Chawak But'o'ob, Belize. *Antiquity* 79, Project Gallery. Available at <http://antiquity.ac.uk/Projgall/walling/>.

Ward, C. and Ballard, R., 2004. Black Sea shipwreck survey 2000. I*nternational Journal of Nautical Archaeology* 33, 2-13.

Ward, C. and Horlings, R., 2008. The remote exploration and archaeological survey of four Byzantine ships in the Black Sea, in: Ballard, R.D., ed., Archaeological Oceanography. Princeton University Press, Princeton, pp. 148-173.

Wolf, K.H., Chilingar, G.V., Beales, F.W., 1967. Elemental composition of carbonate skeletons, minerals and sediments, in: Chilingar, G.V., Bissell, H.J., Fairbridge, R.W., eds, Carbonate Rocks: Physical and Chemical Aspects. Elsevier, Amsterdam, pp. 23-149.

Woods, J.C. and Titmus, G.L., 1996. Stone on stone: Perspectives on Maya civilization from lithic studies, in: Robinson, M.G., Macri, M.J., McHargue, J., eds., Eighth Palenque Round Table, 1993. The Pre-Columbian Art Research Institute, San Francisco.

Wust, G., 1961. On the vertical circulation of the Mediterranean Sea. *Journal of Geophysical Research* 66, 3261–3271.

Zachara, J.M., Cowan, C.E., Resch, C.T., 1991. Sorption of divalent metals on calcite. *Geochimica et Cosmochimica Acta* 55, 1549-1562.

Zeest, I.B., 1960. Keramicheskaya tara Bospora. Izd-vo Akademii nauk SSSR, Moscow (in Russian).